NOTE TO USERS

A MODEL FOR COLLECTOR-STORAGE WALL WITH AND WITHOUT PHASE CHANGE MATERIAL

Jian Zhang

A Thesis

in

the Department

of

Building, Civil and Environmental Engineering

Presented in Partial Fulfillment of the Requirements
For the Degree of Master of Applied Science at
Concordia University
Montreal, Quebec, Canada

February 2005

Your file Votre référence
ISBN: 0-494-04351-2
Our file Notre référence
ISBN: 0-494-04351-2

ABSTRACT

A MODEL FOR COLLECTOR-STORAGE WALL WITH AND WITHOUT PHASE CHANGE MATERIAL

Jian Zhang

A collector-storage wall (CSW) is an effective system for solar energy utilization in buildings. The CSW is usually combined with fenestration to form a south-facing façade, which has an important effect on the indoor environment. This thesis presents a numerical model to analyze the thermal performance of the CSWs, and simulations based on this model are carried out for the following cases: a traditional heat storage wall with natural convective flow, integrated photovoltaic (PV) CSWs with forced convective flow, a wall with controlled blinds, and several cases with a phase change material (PCM). For the traditional masonry CSW, simulation results indicate that optimal room temperature occurs when the thickness of the heat storage wall is 0.35 ~ 0.40m and the width of the air gap in the cavity is 0.20 ~ 0.25m. The blinds used in CSWs can reduce direct solar gain and enhance room comfort by lowering the temperature swing by up to 2 °C. Experiments are performed to determine the thermal properties of the PCM gypsum board, to verify the simulation results and to evaluate the energy performance of the CSWs for the different cases. The tests with a differential scanning calorimeter and a guarded heat flow meter indicate that the PCM gypsum board used as heat storage material is stable in thermal properties and can be used as a building material. Further, another test with an outdoor test facility indicates that for a system with photovoltaic panels installed in the middle of a wall cavity, the overall solar energy utilization

efficiency of this wall system is more than 70%. The use of PCM can significantly reduce the use of traditional construction materials as heat storage material and make the structure of the CSW compact. The validation results show significant agreement with the experimental results. The numerical model developed can be used as a design tool to analyze the thermal performance of CSWs.

ACKNOWLEDGEMENTS

I would like to express my deepest gratitude to my supervisor, Dr. A. K. Athienitis for his expert guidance, encouragement, and support during my graduate studies.

I thank Dr. D. Feldman and D. Banu for providing me with useful information during my study.

I would like to extend my appreciation to Mr. Qou Kai, Ms. Ning Ming and to all my friends at Concordia University for their sincere help and good company throughout these years.

Special thanks and appreciation also go to my whole family, especially to my wife Fengxia Li, my son Zijing Zhang and my parents for their unconditional love, patience, understanding, encouragement and moral support.

CONTENTS

LIST OF FIGURES

LIST OF TABLES

NOMENCLATURE

A	Area (m^2)
Al	Altitude (km)
C	Thermal capacitance (J/°C)
C_{eff}	Effective specific heat (J/ (kg °C))
CSW	Collector-storage wall.
D	Damper.
E	Electrical output (W).
F	Velocity factor.
Gr	Grashof number
H	Wall height (m)
Hd	Time delay (hour)
Hl	Latent heat (J/kg)
I	Solar intensity (W/m^2).
L	Thickness (m) or Latitude (degree)
M	Mass (kg)
Nu	Nusselt number
P	Pressure, Pa, subscript o presents outside air pressure, m presents pressure in wall cavity.
PCM	Phase change material
Pr	Prandtl number
Q	Heat energy (W)
R	Thermal resistance (m^2°C/W)

Ra	Rayleigh number
Re	Reynolds number
S	Solar radiation (W/m^2)
CSW	Collector-storage wall
T(x, t)	Temperature, ℃, subscript r represents room air, o represents outside air. s stands for surface, g represents glazing, w represents wall, in represents inlet air, out represents outlet air, a represents air, a_i, represents air in inside cavity, a_o represents air in outside cavity.
U	Component conductance (W/ ℃), subscript win represents window, wal represents wall, inf represents infiltration.
V	Air velocity (m/s), subscript m represents mean velocity, fix represents fixed-point velocity.
W	width (m)
Ach	Air change per hour
p	Material density, (kg/m^3).
c	Specific heat, [J/ ($kg\,^{o}C$)]
e	Roughness factor
f	Friction loss factor
g	Local acceleration due to gravity (m/s^2)
i,j	Node number
k	Thermal conductivity, ($W/m\,^{o}C$). subscript s and l present solid phase and liquid phase respectively, eff presents effective thermal conductivity.
hi	Inside film heat transfer coefficient, ($W/m^2\,^{o}C$)

ho	Outside film heat transfer coefficient, (W/m^2 °C)
q_l	Latent heat flux (W)
q_s	Absorbed solar radiation (W/m^2)
t	Time, (s)
x	Distance, (m)
a	Solar altitude (degree)
a_t	Thermal diffusivity (m^2/s)
β	Tilt angle (degree)
β_t	Expansion coefficient (1/K)
γ	Surface solar azimuth (degree)
δ	Declination angle (degree)
ϵ	Surface emmisscity
θ	Angle of incidence (degree)
ν	Kinematical viscosity, (cm^2s^{-1})
σ	Stefan-Boatman constant, $5.67 \cdot 10^{-8} \cdot W/m^2 \cdot K^4$
τ	Transmittance
ϕ	Solar azimuth (degree)
ψ	Surface azimuth (degree)

Chapter 1 INTRODUCTION

1.1 Background

The energy consumed in buildings is about a third of total energy consumption and 50% of electricity consumption. It is also one of the main sources of pollution in the environment. In Canada, it accounts for approximately 29.5% of the total energy used and 12% of greenhouse gas emissions (Cox, 2000). So it is of great importance to improve building energy efficiency, to reduce the impact on the environment, and to meet the requirements of indoor comfort as well.

As it is known that building envelope components are the main source of heat loss/gain, great efforts have been made in recent years to make them more energy efficient and cost effective. Among these components, the south-facing façade* has a significant influence on the indoor environment because of the solar radiation. Overheating and overcooling are usually caused by too much heat gain/loss through the south wall. Therefore, the design of a south-facing façade has become an important approach in the design of energy-efficient buildings. In this study, a collector-storage wall, which is a south-facing façade with and without phase change material as a thermal storage material, is studied.

1.2 Collector-storage wall (CSW)

South-facing façades have been studied by many researchers and have developed from an early simple heat storage wall (called the Trombe wall) to the modern multi-technology integrated wall. For the early heat storage wall, researchers focused

The term south-facing facade generally describes all surfaces which are near to south facing, i.e. $\pm 30^{\circ}$ azimuth from due south.

studying the effect of the thickness of the storage wall. The basic principle in the design of this structure is to use a glazing to cover a high mass, dark coloured wall with an air space. The air gap is connected to the room and/or the outside by three or four vents. The main advantage of this wall is to keep the room temperature swing small, so that the thermal comfort in the room is more enhanced than that without a heat storage wall. Although there is a low heat capacity in such an air system, it is the simplest and least expensive way to allow installation during construction. Integrated multi-technology walls, such as walls with photovoltaic (PV) panels, blind control walls, present numerous advantages in application, since they have high overall efficiency. However, the room with such wall usually undergoes a significant temperature swing, and the cost of manufacture and installation of these structures is high as well, thereby limiting the wide application of these walls. There are two practical approaches to increasing the cost effectiveness: one is to reduce the overall cost of the system by reducing each component's cost; another is to raise the overall efficiency of the system by increasing the comprehensive application, including heat extraction, daylighting, electricity generation, air quality, thermal comfort, etc. In order to improve room thermal comfort, the use of phase change materials in the CSW is attractive because they have a high ability to store/release heat at a small range of temperature. Therefore, it is necessary to study the CSW with phase change material.

1.3 Phase change material

Phase change materials (PCMs) are divided into two categories: organic and inorganic. Inorganic PCMs have the advantages of having a low cost and a high ability to

store heat, but mostly a special container is needed because of easy corrosion, which offsets the cost advantage of the PCMs. Organic PCMs have more advantages as building heat storage materials, such as low cost, wide selection, good compatibility with other building materials, though they also have some shortcomings, such as flammability, oily exudation, etc. The main advantage of the PCMs is their marked ability to release and/or to absorb heat at ideal transition temperatures. This characteristic, used to even out the mismatch between energy supply and energy demand, can enhance thermal comfort and thermal efficiency. In this thesis, a PCM gypsum board with butyl stearate is employed.

1.4 Motivation

CSWs have been studied for many years, and several models have been developed to investigate their performance. However, most of the researches focused on specific topics such as the effect of the thickness of the storage walls on the room temperature, the effects of transmittance, the effects of inlet and outlet conditions, etc. Up to now, little work has been done to provide general design guidelines for using CSWs with PCMs that can be used by designers to optimize overall performance. Due to the complexity of the problems that arise in the CSWs, it is suggested that direct simulation is necessary for specific applications (Ramachandran, 2003).

Indeed, a CSW is a complex system, especially in the case of a system with PCMs. Because this system involves not only a complex airflow, in which the airflow may be dominated by one of natural flow and forced flow, or of mixed flow, it also includes different heat exchange rates during the transition process. It is known that the convective heat transfer coefficient is not easy to determine accurately for natural flow, and so far there are few articles that discuss the introduction of airflow into the CSW. Furthermore,

PCMs have a more complex latent heat transfer than do sensible heat materials. When PCMs are used in the CSW, the complexity of the wall system is increased. However, the high ability of PCMs to store thermal energy and to increase thermal comfort makes it possible to improve the performance of the CSWs. With more theoretical and experimental studies for such CSWs with PCMs, some key parameters may be identified to help us learn how they affect the overall performance of the wall system.

1.5 Objectives

The major objective of this thesis is to develop a numerical model to study the CSW with and without the PCM. The numerical model is also to be used as a design tool to size the main components in a CSW.

1.6 Thesis organization

In this thesis, Chapter 2 reviews the development and current studies of CSWs and PCMs and the related theoretical analysis of CSWs. Chapter 3 presents the methodology that will be used in later simulations. It mainly deals with how to calculate the solar radiation, the buoyancy effect, and the heat exchange within the wall cavity. It also presents explicit a finite difference method to solve a few typical cases with the aid of thermal networks. Chapter 4 presents simulation and validation. Using a few cases of test rooms, simulations are carried out on the influence of a simple heat-storage wall, the effect of blinds in the CSW on room temperature, and the effect of PCM on the thermal response of the room. Some conclusions are drawn from the results. The validation is performed by comparing these results with outdoor test results. Chapter 5 presents the experimental results and the performance of the CSWs. The determination of two key

parameters that are used in one-dimensional analysis is also depicted. Chapter 6 summarizes the main conclusions of this study and gives recommendations for future work.

Chapter 2 LITERATURE REVIEW

2.1 Introduction

This chapter presents a literature review of collector storage walls (CSWs), the current application of phase change materials (PCMs), and related knowledge about heat transfer in the cases of natural convective flow and forced convective flow in vertical wall cavities. Emphasis is placed on the development of the CSWs and the PCMs, and on the establishment of an explicit finite deference model that will be used to analyze thermal performance of the CSWs.

2.2 Development of CSWs

The CSW is an important approach to designing an energy efficient building, in which solar energy is collected and stored in a wall. Moreover, the CSW blocks the sunlight after solar radiation passes through the glazing. The wall is usually painted with black or a dark color so that it works as a good absorber. The wall can consist of masonry, water held in containers, or other complex forms. The most well-known structure is the Trombe wall that was first proposed by Morse (1881) (Figure 2.1). The following three features characterize this CSW:

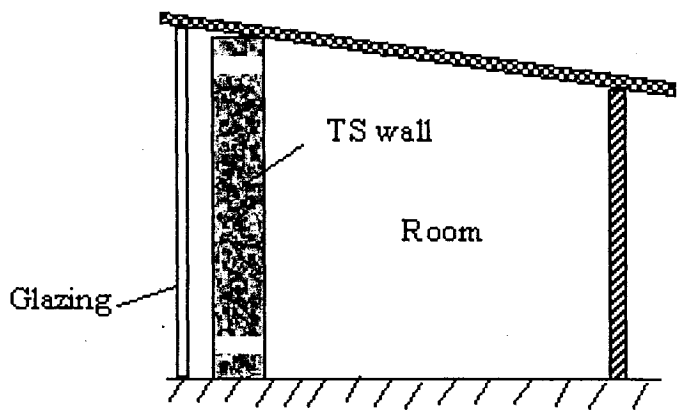

Figure 2.1 Tombe wall structure

First, due to a simple structure and easy operation, it is possible to foresee the effectiveness of the wall in different climates, of wall material properties, of certain glazing treatments, of varying wall thickness and possible variations in the degree of thermo circulation. Therefore, it has a popular application in solar houses.

The second major advantage of this wall system is the ability of the wall to reduce temperature fluctuations by interposing a capacity effect between the solar gain and the living zone. Data taken from the Los Alamos Scientific Laboratory test rooms that operated without auxiliary heat on sunny February day indicated the impact of such walls (shown in Table 2, 1).

Table 2.1 Thermal storage walls and its performance (Franta, 1978)

Type of wall	Heat capacity (KJ)	Thermal storage surface/Glazing area (m^2)	Inside daily temperature swing (°C)	Time of Inside wall temperature peak (hour)
Direct gain room	70.2	2.8	21	15:00
40cm heat storage wall (without vents)	60.7	0.84	14.4	16:00
40cm heat storage wall (with vents)	60.7	0.84	5	22:00
Water wall	66.4	1.01	13.9	16:00

These test results reveal that room temperature swings in rooms with heat storage walls (14.4°C and 5°C respectively) are much smaller than those in direct-gain rooms (21°C). These results are more extreme than those that would be observed in a passive building since the test rooms have a large ratio of collector area to load [~13.7m^2/W], and

consequently the inside temperature averages about 10°C above the outside temperature on sunny mid-winter days. The results clearly show the action of a heat storage wall in a solar building.

Another advantage of this thermal storage wall is that it provides a time delay between the absorption of solar energy on the outside wall and the delivery of the energy to the interior of the building. Characteristically, this time delay is of the order of 6 to 12 hours so that the maximum heating can generally occur in the evening at a time when it is most needed in a residential application. This time delay effect allows for flexibility in thermal design. The building can be heated by direct gain or thermo circulation during the day and by wall at night. The fluctuation of room air temperature will be small, and the comfort that occupants feel will increase. The following table lists the characteristics, on sunny days, of a solid concrete wall with double-glazing on the outside.

Table 2.2 Time delay in passive house with CSW (Franta, 1978)

Thickness (cm)	Inside surface temperature swing (°C)	Time delay of peak temperature (hours)
20	22	6.8
30	11	9.3
40	5.6	11.9
50	2.8	14.5
60	1.1	17.1

The thickness of a solid wall that gives the maximum annual energy yield to the

building is reported to be about 30 centimeters and is independent of local climate (Franta, 1978). However, a building with such a wall would be cold and uncomfortable during long cloudy periods. Thus, the designers are led to consider thicker walls that provide more heat storage and more stable inside surface temperatures. Paul (1979) has summarized the rules of thumb used in the design of a solar house:

- 0.6 to1.0 square meters of south-facing double-glazing should be used for each watt of additional thermal load (i.e., exclusive of the glazing). This will give 70 to 80% solar heating in northern New Mexico for a building kept within the range of 18 to 24°C.

- A thermal storage capacity of at least 146 kg of water, or 732 kg of masonry or rock should be used for each square meter of south-facing glass. This storage should be located in direct sunshine.

- A shading of a south window should be used to reduce summer and fall overheating. An effective geometry can be found in a roof overhang that will just shade the top of the window at a noon sun elevation of 45 ^{o} and will fully shade the window at a noon sun elevation of 78^{o}.

- The best thickness of such a CSW is from 30 to 40 cm, for it can yield a time delay of from 9 to 12 hours, it can reduce room temperature swings, and it can enhance inside comfort. Thermo circulation vents can be used to increase daytime heating but will not increase the nighttime minimum. Vents should have lightweight passive back draft dampers to provide a means of preventing reverse flow at night.

However, a structure like the Trombe wall has three major shortcomings: the cost of construction is high, it has to use some precious space inside the building, and this wall system has low energy efficiency. Therefore, many researchers have studied other

approaches.

South-facing façades are becoming increasingly sophisticated and complex, particularly in commercial buildings. New materials and new technologies are often considered in the design of the south-facing wall. This wall not only functions as one component of building enclosure, but it also presents the characteristic of energy efficiency. It becomes an effective way to attain clean, abundant solar energy when it combines with windows to work as a building enclosure, and it realizes a maximum of energy saving in all kinds of buildings. Therefore, various configurations of the new type of south walls have been developed. The Mataro library in Barcelona (1996) uses a photovoltaic (PV) technology in the south wall, in which the PV cells are sandwiched between two glazings to form a semi-transparent façade, providing the building with electricity and shading at same time. Charron (2003) presented a double façade with an integrated photovoltaic (PV) panel or controlled blinds, in which electricity, heat, daylighting, and indoor comfort are comprehensively considered. The overall performance and construction cost effectiveness of a south-facing wall are therefore improved (refer to Figure 2.2). However, it is found that these new façades lack the advantages of early heat storage walls, such as a large time delay and low temperature variation. So people are led to search for other solutions. Although there are many new approaches that have been used with great interest, at the present time, there are few articles or books that give the general design guidelines for the CSW with PCM. This is the case because the performance of a double façade wall depends on the geometric, thermo-physical, optical and aerodynamic properties of the various components. It is difficult to analyze the wall in a simple way. Therefore, it is suggested

that it is practically impossible to obtain general design guidelines, and simulations should be performed for each individual design (Dincer, 2001).

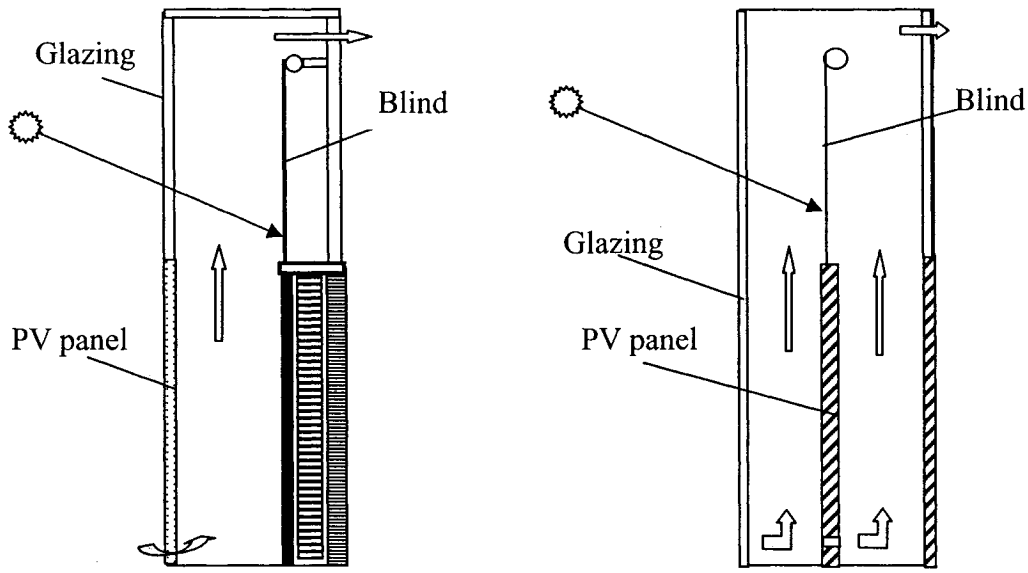

Figure 2.2 Configurations of airflow window (Charron, 2003)

2.3 The development of phase change materials (PCMs)

PCMs are well known for the great latent heat released or gained at their transition temperatures. Interest in PCMs can probably be traced back to early work on solar thermal storage. In 1940, Telkes reported the application of heat storage by fusion-solidification of Glauber's salt (Na_2SO_4 $10H_2O$). The system ran for three years. However, there were problems with corrosion, and water loss took place. The experiment had to be interrupted.

Subsequently, there have been numerous research articles reporting energy storage materials, most of them are inorganic salt. Many authors, such as Abhat (1982, Germany), Feldman, (1983, Canada), Lane, Salyer (1983, 1985, USA), Shibasaki and Fukuda (1985, Japan), et al., studied and analyzed the thermal features of inorganic PCMs. Their research and analysis showed the main problems with such materials. These

materials usually require special containers due to their susceptibility to corrosion. The extra cost of the containers offsets the cost advantage of PCMs. However, inorganic PCMs are not suitable for use in building materials principally because of corrosion and because of their tendencies to super cool and melt incongruently (Feldman et al, 1986).

The value of organic materials as thermal storage media has been known for a long time, but it is only since 1970 that general interest has been shown in their incorporation into building materials (Lane, 1983).

Organic storage materials, some of them much more than others, exhibit a better compatibility with building materials, and can be directly impregnated with construction materials (Hawes, 1992, Feldman, 1992). Feldman has presented alkaline (paraffin) concrete and butyl stearate gypsum board as building thermal storage materials and shown that these PCMs yield a good performance and long stability. However, both of these materials are used only in early test stages, and some of their properties need further study.

Both inorganic and organic materials have advantages and disadvantages when they are chosen as energy storage materials.

2.3.1 Inorganic PCMs

These PCMs have the following attractive properties:

- High latent heat value;
- Inflammability;
- Useful transition temperature range;
- Inexpensive cost and readily available use.

However, they also have some unwanted characteristics:

- They are corrosive and therefore incompatible with many other materials used in buildings;
- They need special containers to prevent their corrosion and they therefore require support and take up a certain space;
- They have a tendency to super cool;
- Components do not melt congruently and segregation may occur;
- They may lose hydration water after many freeze-thaw cycles and they may consequently change their thermal properties.

These materials are characterized by $X(Y)_n\ m\ H_2O$, where $X(Y)_n$ is an inorganic compound. When a salt hydrate, $X(Y)_n\ m\ H_2O$, is heated up to the transition temperature, one of the following reactions will occur:

$$X(Y)_n\ m\ H_2O \rightleftharpoons X(Y)_n + m\ H_2O \quad (2.1)$$

$$X(Y)\ m\ H_2O \rightleftharpoons X(Y)_n\ p\ H_2O + (m-p)\ H_2O \quad (2.2)$$

Thus, at the melting temperature, the hydrate crystals break up into anhydrous salt and water or into a low hydrate and water; when the temperature drops below the freezing point, the liquid components continuously take the form of the original hydration salt.

To prevent these shortcomings and to use the features of high latent heat of inorganic PCMs, some companies, such as Teap Energy, Inc., in Australia, PCM Thermal Solution, Inc., in USA, etc., attempt, in the application, to encapsulate the inorganic PCMs, thereby making a successful application in buildings. However, the problem is that the cost is so high and the life span of the component is so limited that the technique cannot be used on a large scale in the building industry in the future.

2.3.2 Organic PCMs

In order to avoid some of the problems inherent in inorganic PCMs, an interest has developed in the use of organic PCMs because they have a number of important advantages:

- There is a wide variety to choose from;
- The components melt congruently and do not segregate;
- They are chemically stable;
- They can be incorporated into the building materials without containment;
- They are compatible with various building materials;
- The installation cost is low;
- They may be tailored for melting and freezing at the desired temperature

Table 2.3 Typical PCM materials and their latent heat

PCM	Melting point (℃)	Latent heat (kJ/kg)
$CH_3(CH_2)_{16}COO(CH_2)_3CH_3$ Butyl stearate	21	140
CH3(CH2)11OH 1-dodecanol	25	200
CH3(CH2)nCH Paraffin	49-60	200
45/55 capric-lauric acid	21	143
CH3(CH2)12COOC3H7 propyl palmitate	20	190

However, organic PCMs also have some disadvantages:

- They are capable of flammability and smoke generation;
- Some have a strong odor;
- Some present oily exudation;
- A few have appreciable volume changes during phase change.

However, a careful, appropriate selection can eliminate the shortcomings of some organic PCMs. Some potential organic phase change materials are shown in Table 2.3 (Feldman, et al, 1993).

2.3.3 PCM's selection criteria

The selection of an appropriate PCM depends on the relevant combination of its thermal, physical, chemical, kinetic, economical and environmental properties (Feldman, et al. 1993, Dincer, 2001).

Thermodynamic consideration. A good PCM should have a higher latent heat and a higher conductivity so that the heat transfer of the system with the PCM is more efficient. As the PCM changes from one phase to another, it is desirable that the equilibrium should be maintained in both phases. That is to say, the composition of the PCM in liquid form should be identical to that in solid form. The phase transition temperature range must be appropriate, and usually the PCMs are selected so that heat will be released or absorbed in a comfort zone. For indoor conditions, the transition temperature should be in the range of from 18 to 28℃ in most cases. The initial melting and freezing temperatures should be within 4℃ to prevent excursions outside the comfort range.

Physical Properties. The PCM must remain within the host material in both states and must not cause color changes, oily exudation or crystalline formation. The density

affects the storage efficiency per unit volume. It is usually desirable to select material with the greatest density so that the heat storage per unit volume will reach maximum.

Chemical properties. An ideal PCM should be stable in chemical properties. Oxidation or thermal decomposition must not occur during the operation. Such a PCM must be compatible with other building materials. Moreover, there must be no toxic or fire hazard.

Kinetic properties. In order to achieve solidification at a satisfactory rate, the rate of crystal growth is important. Usually a high rate of crystal growth is required so that heat exchange takes place within an acceptable period of time. Moreover, super cooling should also be avoided since some materials remain in the liquid state even when the temperature drops below the freezing point. This phenomenon will decrease the transfer efficiency of this material.

Economic and environmental consideration. The annual capital and the operation cost for the thermal storage system should be low, and the selected material should preferably not excessively impact on public health or natural ecology and environment during the manufacture, distribution, installation or operation of the system

2.4 PCM gypsum board

On the basis of the foregoing criteria, from the results of previous work done in the Department of Building Civil & Environment Engineering, Concordia University, the principle PCM candidates are presented in Table 2.4. It can be seen from this table that the selected phase change material is a commercial mixture of 50% butyl stearate, 48% butyl palmitate and 2% other fatty esters (EMEREST 2326). This PCM gypsum wallboard is made by incorporating this PCM into standard gypsum wallboard.

There are a number of reasons for choosing this PCM gypsum wallboard as a building heat-storage material.

(i) The use of wallboard is widespread and is found in every type of building in Canada and North America;

(ii) The surface area is very large, allowing effective heat exchange.

(iii) As a function of its geometry, structure and location, PCM wallboard serves as a heat reservoir, a heat exchanger and a building element;

Table 2.4 Final selection of PCM candidates (Feldman et al., 1993)

Candidate	Freezing point (°C)	Latent heat (k/kg)	Disposition	Reason for rejection
Carbowax	20	130	Rejected	Melting range too large
Dodecane	25	200	Rejected	Too flammable
Mixture of Capric Acid (67%) Lauric Acid (33%)	20	137	Rejected	Oily exudation
Mixture of Capric Acid (45%) Lauric Acid (55%)	21	143	Rejected	Cannot directly introduced into gypsum paste
Mixture of Capric Acid (85%) Palmitic Acid	21	150	Rejected	strong odor
Coconut Fatty Acid (Emery 626)	19	120	Rejected	Melting range too large
Propyl Palmitate	20	190	Rejected	Not on market
Mixture of Butyl Stearate (50%) Butyl Palmitate	17	140	Accepted	

(iv) Its porous structure is such that even in the liquid state the PCM will be retained

in the matrix of the gypsum board due to surface tension.

(v) The addition of the PCM to the wallboard can easily be achieved in three ways:

- Immersion of the wallboard for a short time in a bath of liquid PCM;
- Direct incorporation of PCM into the gypsum paste, a procedure that can be achieved in small and large-scale production.
- Encapsulation of the PCM in a small plastic container when the components of the building material are blended (gypsum, concrete, etc.).

(vi)The stability and performance of this PCM board will be inspected to see whether or not they have changed after 10 years of operation.

A recent study performed by Feldman et al in the Department of Building, Civil & Environmental Engineering, Concordia University, has shown that this PCM board, by comparison with regular wallboard, has the following features:

- Flexural strengths are comparable;
- Durability after a few annual freeze-thaw cycles is satisfactory;
- Compatibility with fasteners and representative paints and wall covers is very good;
- Moisture absorption is about one third lower than that of ordinary wallboard.

2.5 Thermal analysis of the CSW

There are two main methods of dealing with the variety of heat transfer problems: the experimental approach and the mathematical approach. The first is mainly used in the early stage of research, in which no standard reference can be used. It is usually limited by the knowledge of the operator, but it is the basis of all kinds of work. The mathematical solution is developed on the basis of experiments and/or previous

knowledge. In some instances, it can be used to predict or simulate before the operations. The experimental approach and mathematical analysis are important tools in the research field, and they work together to find out whether or not a theoretical analysis is reasonable. Therefore, they are widely used in building thermal analysis.

The mathematical solution can be subdivided into two categories. One is the analytical solution and the other is the numerical solution. The analytical solution usually solves only relatively simple heat transfer problems with first kind and second kind boundary conditions. Ozisik (1979) has dealt with an infinite medium with cylindrical symmetry and gave a temperature distribution and change trend of phase change material using an analytical method. Athienitis (1986) has presented a thermal network solution with the delta-to-star transformation to analyze heat transfer in a direct gain solar room. However, in practice, many of the problems are related to third class boundary conditions that usually involve time variables. The analytical approach for this situation is very complicated. It includes an analysis of components such as the heat transfer process in the PCM wallboard exposed to the boundary condition with transient convective and radiant heat sources that are often involved in a CSW in a solar house. The equations used in analysis containing variable λ and η (the ratio of liquid-mushy and mushy-solid boundary location to time (Ozisik, 1979)) are found with a time variable involved explicitly. It is hard to determine the values of these components, and therefore it is difficult to get accurate results.

The numerical solution, however, has been successfully applied even to very complicated heat and mass transfer problems in which the substance may involve phase transition within a given temperature range. Morgan (1981) has presented an explicit

finite element algorithm for the solution of the basic equations describing combined conductive and convective transfer with phase change involved.

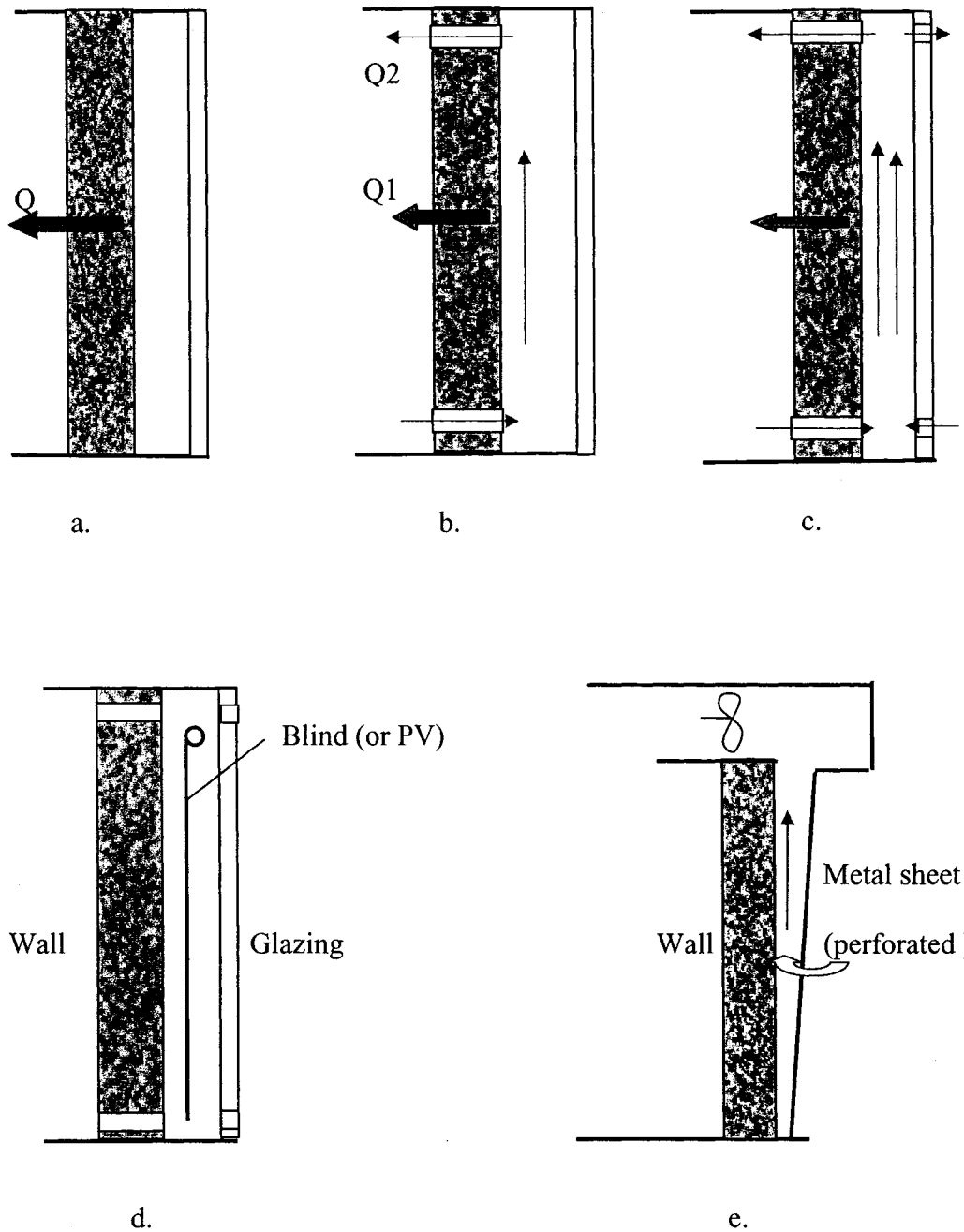

Figure 2.3 Five forms of CSWs

The earlier thermal analysis of the wall focuses on the determination of the thickness

of the storage wall and the width of the cavity by using one-dimensional steady state heat transfer. The wall structure is relatively simple. There are mainly two forms of walls: walls with vents and walls without vents. Later, to simulate the real process of heat transfer, transient analysis has become available due to the evolution of IT technology. In addition, the structures have also changed with the development of the building industry. There are mainly five types of CSWs referred to in Figure 2.3. Two types of cavity (closed cavity and open cavity) and two statuses of airflow (natural convective flow and forced convective flow) are usually involved in the CSWs.

2.5.1 Heat transfer in a closed cavity

The governing equations of heat exchange in a closed cavity with steady, two-dimensional, incompressible, buoyancy-induced flow are obtained for a rectangular configuration in the following manner when neglecting viscous dissipation (Dincer, 2001):

$$\frac{\partial V}{\partial x} + \frac{\partial V}{\partial y} = 0 \tag{2.3}$$

$$V\frac{\partial V}{\partial x} + V\frac{\partial V}{\partial y} = -\frac{1}{\rho}\frac{\partial P}{\partial x} + g\beta_t(T - Tc) + \nu\nabla^2 V \tag{2.4}$$

$$V\frac{\partial V}{\partial x} + V\frac{\partial V}{\partial y} = -\frac{1}{\rho}\frac{\partial P}{\partial Y} + \nu\nabla^2 V \tag{2.5}$$

$$V\frac{\partial T}{\partial x} + V\frac{\partial T}{\partial y} = \alpha_t\nabla^2 T \tag{2.6}$$

where Tc and Th are the temperatures of the cold surface and the hot surface respectively. The boundary conditions for the equations above are:

$$Vx = Vy = 0, \quad T = Th \quad \text{at } y = 0 \tag{2.7}$$

$$Vx = Vy = 0, \qquad T = Tc \quad \text{at } y = L \tag{2.8}$$

$$Vx = Vy = 0, \qquad \text{at } x = 0, \text{ and } H \tag{2.9}$$

The thermal condition at the horizontal surface is specified as:

$$\frac{\partial T}{\partial X} = 0 \ , \qquad \text{at } x = 0, \text{ and } H \tag{2.10}$$

As can be seen from the equations above, it is difficult to solve this problem theoretically. F.L. Sherbiny et al (1982) have developed equations to calculate the convective heat transfer coefficient in a closed cavity. They state that the convective coefficient is determined by the larger value of the following Nusselt numbers:

$$Nu = 0.0605 \cdot Ra^{1/3} \tag{2.11}$$

$$Nu = [1 + \frac{0.104 \cdot Ra^{0.293}}{[1 + (6310/Ra)^{1.36}]^3}]^{1/3} \tag{2.12}$$

where Ra is Rayleigh number.

2.5.2 Natural convective flow in an open cavity

An open cavity is a common feature of CSWs in solar houses. Due to lack of theoretical or experimental equations available describing the natural convective flow in such a cavity, efforts should be taken to obtain some pertinent information that would allow the exploration of the thermal phenomena in the CSW. Rohenow et al (1998) have presented the Nusselt numbers and their conditions in a fully developed regime with Aung's results for the natural cooling between two vertical plates as follows:

$$Nu_{fd} = \frac{4T^{*2} + 7T^{*} + 4}{90(1 + T^{*})^2} \cdot Ra \approx \frac{Ra}{24} \qquad Ra \le 10 \tag{2.13}$$

$$Nu = c \cdot Ce \cdot Ra^{1/4} \qquad 10 < Ra \le 10^5 \tag{2.14}$$

$$Nu = [Nu_{fd}{}^{m} + (c \cdot Ce \cdot Ra^{1/4})^{m}]^{1/4} \qquad \text{Ra} > 10^5 \qquad (2.15)$$

$$T^* = (Tc\text{-}To) / (Th\text{-}To), \qquad 0 \le T^* \le 1 \qquad (2.16)$$

However, it is found that these equations are not always suitable for the analysis of heat transfer in the CSW because the parameter T^* is not always in the range of 0~1 in the summer mode. During that period it is required to have natural cooling for an open vertical wall. These empirical equations should be modified before it can be used in the thermal analysis of buildings.

Charron et al (2003) have presented a control volume-based finite difference model, which is used to study a double façade wall. The thermal performance is analyzed by using the energy balance on each control volume in the cavity. Each equation is expressed as the sum of all incoming heat flows, minus the sum of all outgoing heat flows acting on the control volume, which is set to zero by the conservation of energy. The temperature change of each component can be predicted by solving a set of equations. However, a steady state condition is considered in the paper, and the situation of having an inner heat source is not taken into account, either. So, more effort needs to be done in more complicated cases such as CSW with thermal storage.

2.5.3 Forced convective flow in a cavity

For a CSW with forced convective flow, it is important to determine whether the airflow falls in forced, natural, or mixed convective regimes. The following relationships between Grashoffs number and Reynolds number are used to determine the flowing status (Incropera et al, 1990):

$Gr << Re^2$ forced convection (2.17)

$Gr >> Re^2$ natural convection (2.18)

$Gr \sim Re^2$ mixed convection (2.19)

For each status of airflow, there are several kinds of empirical formulas to describe heat transfer. In this thesis study, Dincer's (1997) correlation is used and will be discussed in more detail in a later chapter.

2.5.4 Mixed natural and forced convection

The CSW wall is a south-facing wall and is often exposed to solar radiation. Therefore, in most cases, airflow in this wall is a combination of natural and forced flow. When natural convection is dominant, even a small externally forced flow can play an appreciable role in fluid motion near the heated surface; when the externally forced flow is large, forced convection is dominant, but the natural convection will contribute to it. The relationship between them can be described by Churchill's empirical equation as follows (Jaluria, 1980):

When the directions of natural flow and forced flow are parallel, the resultant Nusselt number Nu is related to that Nu_f from purely forced convection correlations and that Nu_n from purely natural convection correlations by

$$Nu^3 = Nu_f^3 + Nu_n^3 \tag{2.20}$$

When the direction of natural flow and forced flow are anti-parallel, the relationship between them is depicted as

$$Nu^3 = Nu_f^3 - Nu_n^3 \tag{2.21}$$

2.6 Thermal analysis on the PCM wall

The heat transfer of PCMs is very complex, especially when the PCMs are at their transition stage. Figure 2.4 shows the temperature transition profile across a PCM

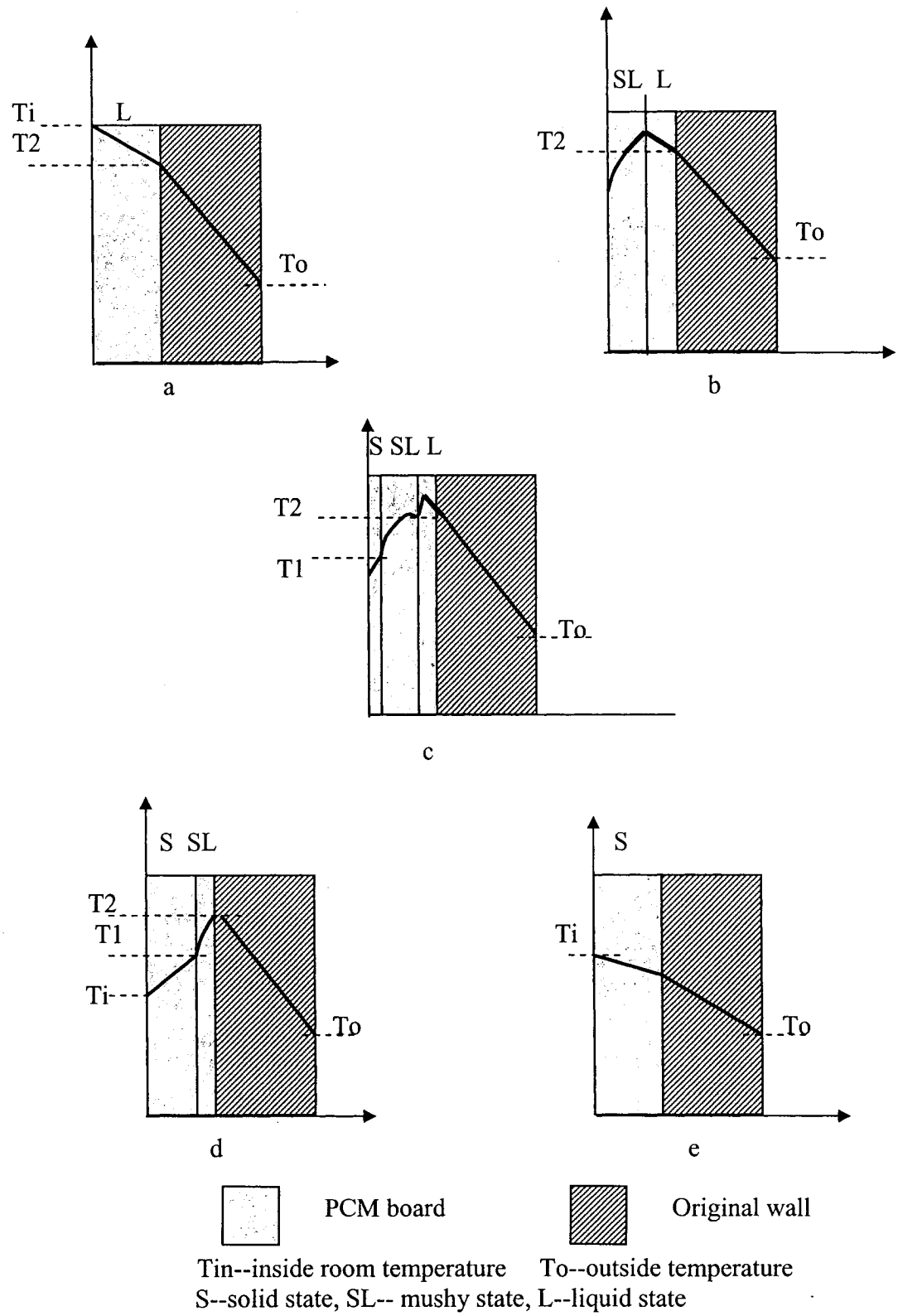

Figure 2.4 Conceptual temperature distributions across PCM during freezing process (Chunyuan, 1996)

board when it freezes. In the initial condition, the behavior of the heat transfer of the PCM looks like that of uniform materials because all of the PCM is in the liquid stage. As the temperature drops, the solidification process starts from the cooler edge of the PCM board, and the PCM presents two phases: liquid and mushy. Then three phases exist at the same time: solid, mushy and liquid. With further development, the liquid phase disappears as it totally changes into the solid state. During the process of phase change, the density and properties of the three states are different. These differences will cause internal convection heat exchange, which will result in the appearance of non-uniform thermal properties. Therefore, the mechanism of heat transfer that takes place in PCMs is so complicated that simplification has to be made before modeling the heat exchange in PCMs.

Kaushik et al (1981) have developed an approximate analytical model for estimating the behavior of time-dependent phase change processes. The main ideas are presented as follows:

- Use effective thermal properties to represent the overall characteristics when phase change takes place. The effective specific heat and thermal conductivity are respectively:

$$C_{eff} = C + \frac{Hl}{T - Ta} \times \frac{x_o}{L} \tag{2.23}$$

$$K_{eff} = K \cdot (1 - \frac{x_o}{L}) + K_l \cdot \frac{x_o}{L} \tag{2.24}$$

where K and K_l represent the thermal conductivity of the PCM at solid phase and liquid phase respectively, C is the specific heat of the solid phase of PCM, Hl is the latent heat of fusion, x_o is the average melting depth or liquid thickness in the PCM, L is the

thickness of the PCM slab, T and To are the average steady state temperature over the thickness of the slab and the ambient temperature respectively.

- Treat the process of heat transfer as heat conduction without phase change, and then analyze the temperature distribution using the following governing equation and boundary conditions:

$$\rho \cdot C_{eff} \cdot \frac{\partial T(x,t)}{\partial t} = K_{eff} \cdot \frac{\partial^2 T(x,t)}{\partial x^2} \tag{2.25}$$

$$-K_{eff} \frac{\partial T}{\partial x}\Big|_{x=0} = h_o[T_s(t) - T(x_{=0},t)] \tag{2.26}$$

$$-K_{eff} \frac{\partial T}{\partial x}\Big|_{x=L} = h_i[T(L,t) - To] \tag{2.27}$$

where h_o and h_i are outside and inside convective coefficients respectively, ρ stands for the density of the PCM.

However, this method is too rough to estimate the heat transfer mechanism in the PCM. First, it is very difficult to decide the effective specific heat and conductivity; second, this simplification is quite different from the actual process of heat transfer. So it is difficult to obtain satisfactory results.

Some researchers use experimental techniques to analyze the heat transfer in the PCM. Scalat (1995), Banu (1998) have presented an analysis method that is based on numerous experiments. The average latent heat and the transition temperature for the considered PCMs are depicted. Simona (1996) have investigated the full-scale thermal performance of a PCM board under laboratory conditions. However, how the latent heat flux changes with temperature in solar conditions is not described so far.

To describe the heat transfer that takes place in phase change material, Athienitis

(1997) uses a finite difference thermal network model as in the following equation:

$$T_{i,p+1} = \frac{\Delta t}{C_i} \cdot (q + \Sigma \frac{T_{j,p} - T_{i,p}}{R_{i,j}}) + T_{i,p} \tag{2.28}$$

where the subscript i indicates the node for which the energy balance is written and all nodes j are connected to node i, p is the time step, $R_{i,j}$ is the thermal resistance between nodes i and j, C_i is the thermal capacitance associated with node i, q represents a heat source at node i such as absorbed solar radiation or internal heat generation (e.g. due to latent heat flow).

The latent heat flux is modeled by the combination of the enthalpy method and the results of the Differential Scanning Calorimeter test, and is written as follows:

$$q = 2 \cdot Hl \cdot R \cdot \frac{T - T_1}{(T_2 - T_1)^2} \tag{2.29}$$

where *Hl* is the latent heat for the temperature range T_1 to T_2, at which the freezing or melting process starts and ends, R is the heating or cooling rate, °C/s.

The problem is that the equation of latent heat flow is based on Differential Scanning Calorimeter test results; it cannot be completely suitable for use in the CSW because the heating rate R is dependent on the intensity of solar radiation for a specific material, which changes with time.

2.7 PCM in CSW

CSWs are an important approach in the improvement of the energy efficiency of buildings. They have developed from the early simple form of the Trombe wall to today's versatile structures using modern technology. The mechanism of heat transfer and airflow in the wall cavity is complex and so is its control. PCMs have been studied for many

years and show an attractive feature in storing energy. They can be used as part of building materials, such as floor heating material (TEAP Energy, Austrian), building lining material (Feldman 1998) and sunspace heat-storage material. A PCM may be used in CSWs for the following three reasons: first, it can save precious space; second, it can store a larger amount of heat in a specific volume than a normal concrete wall does; third, it can improve the overall thermal performance of the CSW and enhance room comfort by enlarging its heat capacity.

2.8 Objectives

As a consequence of the literature review above, efforts in this present research will be put on the following aspects:

- Developing a model that can be used to describe heat transfer under the following conditions:
  1. Natural convective airflow in the CSW,
  2. Forced convective flow in the wall cavity.
- Using the model developed to simulate several cases, so that it can help to determine the thickness of the storage wall and the depth of the cavity, and to analyze the effect of blinds on room temperature swing;
- Doing experiments to verify the simulation results;
- Analyzing data and summarizing the results.

Chapter 3 MATHEMATICAL MODEL

3.1 Introduction

As mentioned in Chapter 2, numerical solutions have been successfully applied even to very complicated heat and mass transfer problems because of the following characteristics:

- They are applicable to all kinds of boundary conditions.
- It is not difficult to solve the equations with various parameters related to time variables.
- They are easily modified to simulate the thermal performance of other building materials, such as PCMs.

This chapter presents an explicit finite difference model for a CSW with PCM.

3.2 Major factors that affect room comfort

Before establishing a mathematical model, it is necessary to analyze the heat transfer process involved in a CSW with a PCM. As shown in Figure 3.1, factors that may affect indoor comfort (including indoor temperature, air humidity, and visible factor) mainly consist of the following parameters:

Solar radiation is one of the most important factors affecting indoor temperature variation. There are usually two ways to collect solar energy when sunlight is incident on a south-facing façade with a CSW. One is that sunlight passes through windows, and is absorbed by an internal floor and /or wall. It is then transferred to the air and the furniture in the room and the walls themselves. Another way is through CSW (see Figure 3.2). In the wall, solar radiation affects the room temperature in two ways: one is that the

PCM board absorbs solar heat during the daytime and then releases its warmth to the interior by conduction through the wall during the day and night hours. The other way occurs when there is convective heat exchange between two surfaces (glazing and PCM board) and air in the cavity. The air in the cavity is delivered into the room. In the cavity, a complicated heat transfer takes place when the air flows along the channel and through the vents located at the top and bottom of the wall respectively. The ambient air temperature is another major factor that affects room comfort. Its influence changes from time to time in two possible ways: conduction through a building enclosure and air infiltration. Wind speed and wind direction affect heat exchange markedly and increase the instability of the heat flow.

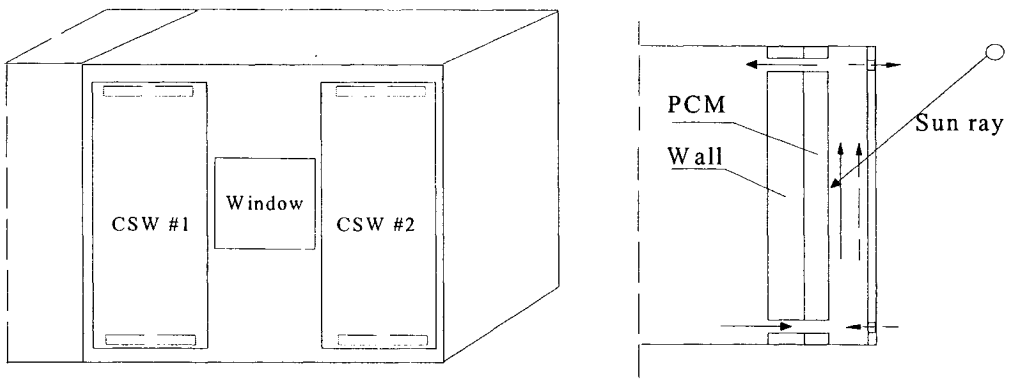

a. Example room with CSW wall

b. Cross-view of CSW

Figure 3.1 Configurations of example room with CSW

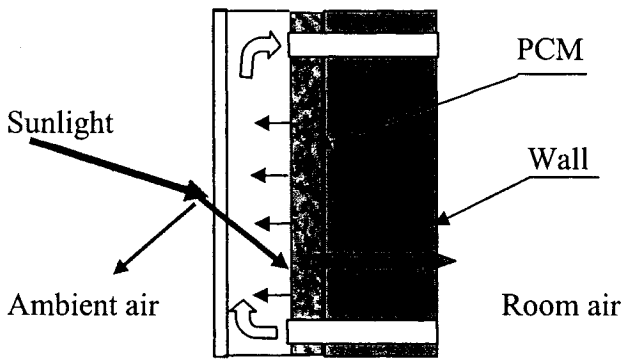

Figure 3.2 Heat exchange in a CSW

3.3 Modeling assumptions and governing equations

The following assumptions are made to model the heat transfer in CSWs:

- The heat transfer process is treated as one-dimensional.
- The natural convection between two phases in the PCM is neglected because the density difference between the mushy and liquid phases is small, and the convective effect is significantly reduced due to the flow resistance caused by gypsum pores.
- The PCM and gypsum matrix are treated as a uniform body with the same physical and thermal properties. For example, they have unique specific heat, density, thermal conductivity and latent heat. Although the individual properties of the PCM and the gypsum matrix differ significantly in some cases, their overall property does not change too much because the small particles of the PCM are evenly disposed in the matrix pores. In practice, these integrated properties could be obtained by using the Differential Scanning Calorimeter (DSC) test and the heat flux test.
- Isothermal surfaces.
- The end and edge effects of the surface and the air cavity are neglected.

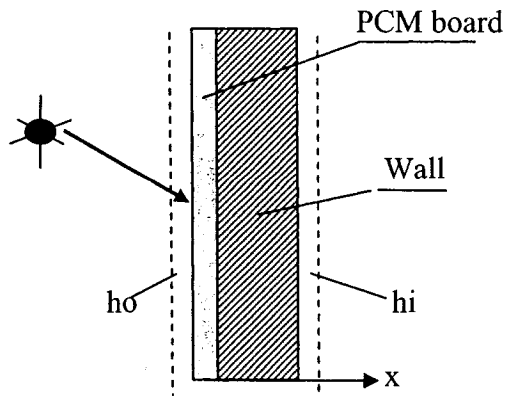

Figure 3.3 Wall section schematic for heat transfer model

Based on the assumptions above, the heat transfer of a wall with a PCM can be treated as a one-dimensional, transient heat diffusion problem with uniform physical and thermal properties. The heat diffusion through the compound wall is described by the following one-dimensional heat diffusion equation.

$$\rho \cdot c \cdot \frac{dT(x,t)}{dt} = k \cdot \frac{d^2T(x,t)}{dx^2} + q_l \tag{3.1}$$

with boundary conditions:

$$-k \cdot \frac{dT(x,t)}{dx} = ho \cdot [To - T(0,t)] + q_s \qquad \text{at} \quad x = 0 \tag{3.2}$$

$$-k \cdot \frac{dT(x,t)}{dx} = hi \cdot [T(x,t) - Tr] \qquad \text{at inner surface of room} \tag{3.3}$$

where q_l is latent heat flux when phase change occurs, in watt; q_s represents the absorbed solar radiation, W/m^2, and it can be described as follows:

$$q_s = \begin{cases} 0 \cdot \dfrac{\text{watt}}{\text{m}^2} & \text{if } t < t_{sr} \\ S(t) & \text{if } t_{sr} \le t \le t_{ss} \\ 0 \cdot \dfrac{\text{watt}}{\text{m}^2} & \text{if } t > t_{ss} \end{cases} \tag{3.4}$$

where t_{sr} is the time of sunrise; t_{ss} is the time of sunset. The calculation of instantaneous solar radiation on a vertical wall is based on the Clear Sky Hottle's model (Athienitis, 2002), given in Appendix A.

3.4 Determination of latent heat flow

For the PCM gypsum board, according to previous work done at Concordia University, the latent heat transfer can be described as follows (Athienitis 2002):

$$q = 2 \cdot Hl \cdot R \cdot \frac{T - T_1}{(T_i - T_f)^2} \tag{3.5}$$

where q is latent heat flow, watt, Hl is latent heat, J/kg, R is heating/cooling rate, °C/s, T_i, T_f are the initial melting and freezing points, respectively.

3.5 Convective coefficient in a vertical cavity

The natural convection flow enclosed between two parallel plates has been studied extensively by many researchers due to its relevance to many practical problems, such as thermal insulation by double walls as solar collectors.

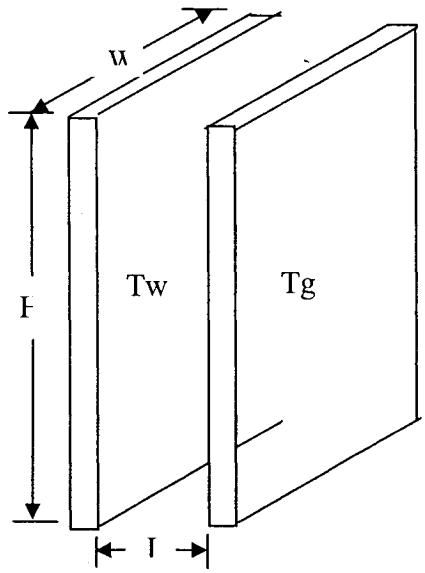

$$Ra = \frac{g\beta(Tm - To)L^3}{\gamma\alpha} \cdot \frac{L}{H}$$

$$Tm = \frac{Tw + Tg}{2}$$

$$Tre = \frac{Tg - To}{Tw - To} \tag{3.6}$$

Figure 3.4 Geometry and nomenclature for natural convective heat transfer between vertical walls

Figure 3.4 shows a configuration of airflow between two vertical walls. The important variables in the problem are the temperature difference between the vertical walls ΔT, the horizontal distance L, and the height H. The depth of the cavity is considered much larger than L and H. The temperatures of vertical walls are Tw and Tg respectively. The

ambient air temperature is presented by To. A one-dimensional convective motion, which is induced by the buoyancy force due to the temperature difference and the resulting heat transfer, is considered in this study on the basis of the analytical and experimental information available.

In a closed cavity, the convective coefficient *hc* is determined by a larger Nusselt number according to the following equations (Sherbiny et al. (1982)):

$$Nu = 0.0605 \cdot Ra^{1/3} \tag{3.7}$$

$$Nu = [1 + \frac{0.104 \cdot Ra^{0.293}}{[1 + (6310/Ra)^{1.36}]^3}]^{1/3} \tag{3.8}$$

In an open cavity with a parallel isothermal wall, when airflow is in a natural condition, the Nusselt number in the developed regime is determined by Aung's empirical equation (Rohsenow 1998), as referred to Figure 3.4:

$$Nu_{fd} = \frac{4Tre^2 + 7Tre + 4}{90(1 + Tre)^2} Ra \qquad Ra \le 10 \tag{3.9}$$

$$Nu = cCeRa^{0.25} \qquad 10 < Ra \le 10^5 \tag{3.10}$$

$$Nu = [Nu_{fd}{}^m + (cCeRa^{0.25})^m]^{\frac{1}{m}} \qquad Ra \ge 10^5 \tag{3.11}$$

where the subscript *fd* stands for a fully developed flow, c, Ce and m are empirical constants. For air, c = 1.20, Ce = 0.515, m = -1.9.

In vertical CSWs, the forced convective coefficient can be described by Dincer's (1997) correlation as follows:

$$Nu = 0.332 \cdot \mathrm{Re}^{1/2} \cdot \mathrm{Pr}^{1/3} \qquad \text{For laminar flow} \tag{3.12}$$

$$Nu = 0.0296 \cdot \mathrm{Re}^{4/5} \cdot \mathrm{Pr}^{1/3} \qquad \text{For turbulent flow} \tag{3.13}$$

$$Nu = (0.037 \cdot \mathrm{Re}^{4/5} - 871) \cdot \mathrm{Pr}^{1/3} \qquad \text{For mixed flow} \tag{3.14}$$

The convective coefficient is determined by the Nusselt number as follows:

$$h = Nu \cdot ka / H \tag{3.15}$$

where ka is air conductivity.

3.6 Radiation coefficient in a cavity

Heat transfer in an air cavity usually consists of convection and radiation. In some cases, the heat transfer coefficient is considered as a combination of radiant and convective heat transfer coefficients, while in other cases they are kept separate.

$$h_t = h_c + h_r \tag{3.16}$$

where h_c is the convective coefficient, it is calculated by equation 3.15; h_r is the linearized radiation coefficient and can be expressed as the following correlation:

$$h_r = \frac{4 \cdot \sigma \cdot T_m^{\,3}}{1/\varepsilon_1 + 1/\varepsilon_2 - 1} \tag{3.17}$$

where ϵ is the surface emissivity, σ is the Stefan-Boltzman constant (σ = 5.67 x 10^{-8} W/m^2K^4), and T_m is the mean temperature between the glazing and inside wall surface in Kelvin.

3.7 Buoyancy effect and induced velocity in an open cavity

In the cavity of a CSW, the wall temperature $T0$ and /or Tg is usually higher than the outside air temperature To. So the air temperature in the cavity Tm is correspondingly higher than the outside air temperature due to heat transfer. This phenomenon will cause a density difference between the cavity air and the outside air, which further results in a natural convective airflow in the cavity (due to buoyancy).

The buoyancy pressure difference is approximately equal to the pressure difference

between two columns: the inside column with air temperature T_m and the outside one with ambient air temperature T_o.

$$dP_{buoyancy} = (\rho_0 - \rho_m)H \cdot g = d\rho \cdot H \cdot g \tag{3.18}$$

For ideal gas, $P = \rho RT$

Therefore, $$d\rho = \frac{1}{R}(\frac{P_0 \cdot T_m - P_m T_0}{T_0 \cdot T_m}) \tag{3.19}$$

The equation above is approximately equal to

$$d\rho = \rho(\frac{T_m - T_0}{T_m}) \tag{3.20}$$

So the buoyancy pressure difference can be expressed as follows

$$dP = \rho(\frac{T_m - T_0}{T_m})H \cdot g \tag{3.21}$$

Meanwhile, the pressure difference due to buoyancy is also equal to pressure loss at entrance and exit plus friction loss in the cavity,

$$\rho(\frac{T_m - T_0}{T_m}) \cdot H \cdot g = C_i \frac{\rho V^2}{2} + C_O \frac{\rho V^2}{2} + f \cdot \frac{H}{L} \cdot \frac{\rho V^2}{2} \tag{3.22}$$

where C_i and C_o are pressure loss coefficients at the entrance and exit, usually for rectangular and perpendicular channels, these coefficients are $C_i = C_o = 2.5$ (Long, 1979), f is friction loss factor in cavity, the value of which depends on the airflow status.

For laminar flow, i.e. $\mathrm{Re} < 2500$, $$f = \frac{64}{\mathrm{Re}} \tag{3.23}$$

For turbulent flow, i.e. $\mathrm{Re} > 10^4$ $$f = 0.11 \cdot (\frac{e}{L} + \frac{68}{\mathrm{Re}})^{0.25} \tag{3.24}$$

where e is the roughness factor, about 0.03 for smooth surfaces (e.g. glass, PVC pipe), 0.09 for medium-smooth surfaces such as steel ducts with seams, 0.15 for average surfaces and 3 for rough surfaces such as concrete (see in ASHRAE).

So from the equations above, the induced air speed is the following:

$$V_{in} = \sqrt{\frac{2(\frac{T_m - T_o}{T_m}) \cdot H \cdot g}{(C_i + C_o + f \cdot \frac{H}{L})}} \tag{3.25}$$

3.8 Heat transfer in the CSW and system efficiency

Convection heat transfer takes place between the component's surface (glazing and inner wall) and the air (air within cavity, outside ambient air and inside room air). It can be calculated according to the following equation,

$$Q_c = h_c \cdot A \cdot (Ts - Tair) \tag{3.26}$$

Radiation heat transfer can be expressed by a linearized equation (3.27),

$$Q_r = h_r \cdot A \cdot (Tw - Tg) \tag{3.27}$$

where h_r is the linearized radiation heat transfer coefficient referred to the equation 3.17.

Conductive heat transfer takes place in a component. It can be expressed as follows:

$$Q_c = \frac{k \cdot A}{\Delta X} \cdot (T_2 - T_1) \tag{3.28}$$

where k is the conductivity of the component, ΔX is distance. No conductive heat transfer is assumed to occur through the component boundaries.

Heat transferred to the air in the cavity occurs through convection and advection; the enthalpy gained in the cavity elements is obtained using equation 3.29.

$$Q_{air} = M_a \cdot \rho_a \cdot c_a \cdot (T_{out} - T_{in}) \tag{3.29}$$

where M_a is an airflow rate of air (m^3/s), ρ_a represents the air density (kg/m^3), and c_a is the specific heat capacity of air (J/kg.℃).

The efficiency of the CSW system with a PCM and photovoltaic panels can generally be expressed with the following equation:

$$\eta = \frac{E_{pv} + Q_{air} + Q_{sto} - E_{fan}}{S \cdot A} \tag{3.30}$$

where E_{pv} is the electrical output of photovoltaic(PV) panels integrated with the CSW, Q_{air} is the heat absorbed by flowing air in the CSW, Q_{sto} is heat stored in the PCM in this cavity, E_{fan} is electrical fan power.

3.9 Thermal network and energy equations

After the analysis of thermal transfer processes, the thermal networks are established for the selected room in the winter case and the summer case respectively as shown in Figure 3.5. Ucw represents the air thermal conductance of the heat transfer between the air cavity and the room in winter. Ucs represents the air thermal conductance between the air cavity and the outside in summer. In the winter case, there is no Ucs appearing in the network; in the summer case, there is no Ucw in the network. Ug is the conductance of the double-layer glazing; the heat storage wall is divided into four equivalent layers represented by nodes 1, 2, 3 and 4, and their capacities are represented by C1, C2, C3, and C4. U_{inf}, Uwin, and Uwall represent the conductance of the infiltration, the window and the wall (including the roof). Qaux is the auxiliary heat source. Sg, Ss and Sf represent the solar energy absorbed by glazing, the PCM board and

the indoor floor. Um1 and Um2 are the two thermal conductances of the floor with thermal capacity C5. Ua and Ub are convective conductances in the wall cavity, Ui and Uii are indoor convective conductances that occur between the CSW and room air, and between floor and room air. Based on this network, an equation is established for every node, denoted as i, as follows:

$$C_i \cdot \frac{T_{p+1} - T_p}{Dt} = \sum U_{i,j} \cdot (T_{j,p} - T_{i,p}) + q \tag{3.31}$$

where the subscript j denotes the nodes that are connected to the node i , p is the time step, $U_{i,j}$ is the thermal conductance between nodes i and j, C_i is the thermal capacitance associated with node i , q represents heat source at node i (the source could be solar radiation, latent heat or auxiliary heat). During the freezing phase of the PCM, heat is released, q is positive; during the thawing phase, heat is absorbed and q is negative. To ensure numerical stability, the time interval Dt is selected based on the following condition:

$$Dt \leq \min[\frac{C_i}{\sum_j (1/R_{i,j})}] \qquad \text{for all nodes i} \tag{3.32}$$

Simulations are also carried out to study the blind effects, which are classified into three cases, (1) airflow in front of the blind, (2) airflow behind the blind, and (3) airflow in both cavities. The west wall of the simulation room is connected to other rooms, as shown in Figure 3.6. Ucon represents the thermal conductance of the west wall. Ua, Ub, Ud and Ue are the air convective thermal conductances in the two cavities respectively. Node b stands for the blind. When the airflow passes only through the cavity in front of the blind, there is no flowing air conductance Uba in the network; when the air flows behind the blind, there is no flowing air conductance Ufr appearing in the figure. In the

situation where air flows through both sides of the blind, the thermal network is referred to Figure 3.6 below.

Figure 3.7 shows the thermal network for a CSW with a PCM gypsum board. The PCM gypsum board is divided equally into four layers. Each layer is represented by capacity C11, C12, C13, and C14. The conductance representing heat transfer due to air that passes through the CSW is represented with Uin. All variations of these conditions will be discussed in Chapter 4.

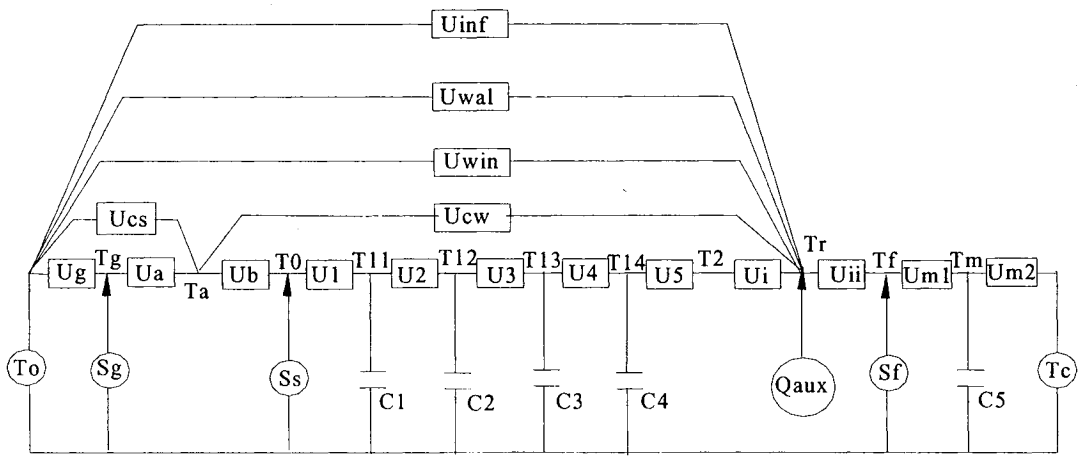

Figure 3.5 Thermal network for an example room

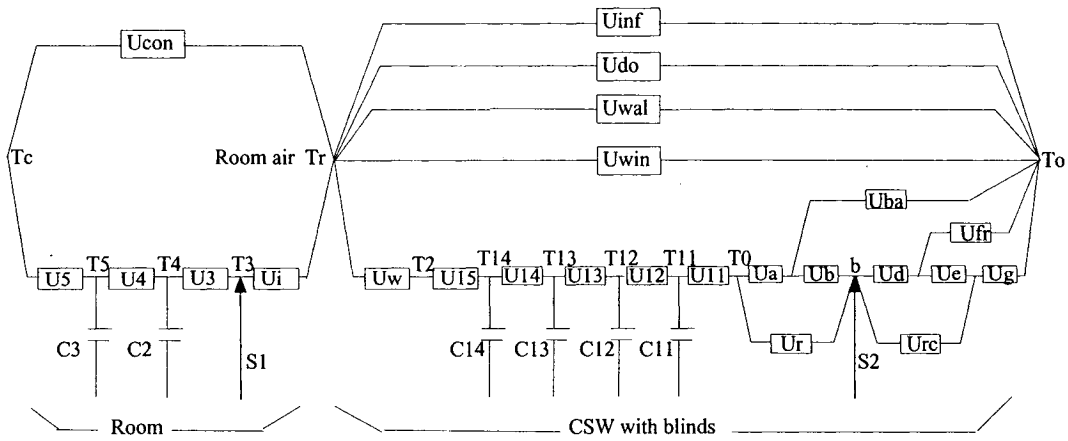

Figure 3.6 Thermal network for a room having a CSW with blind

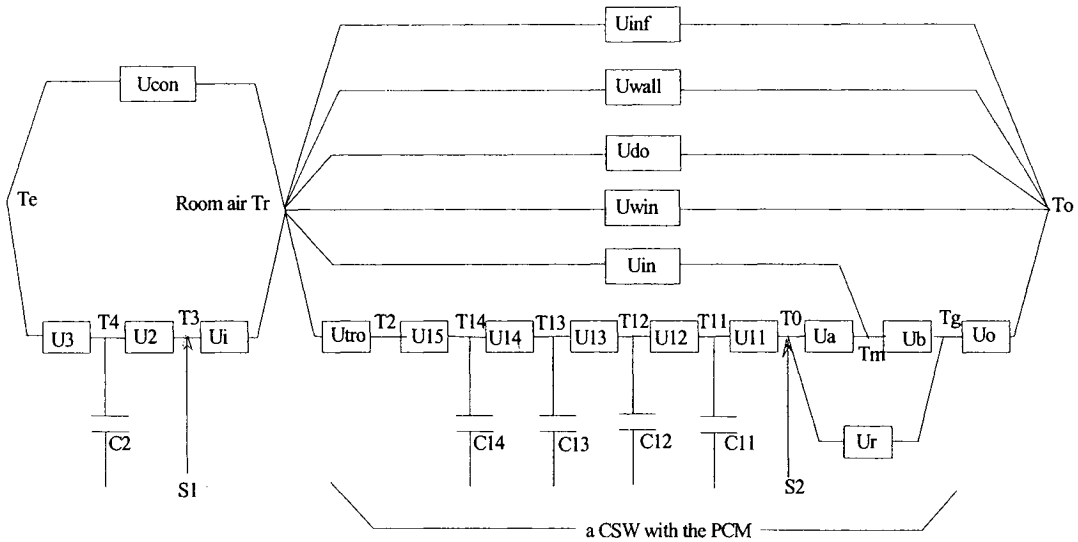

Figure 3.7 Thermal network for a room having a CSW with PCM

Chapter 4 SIMULATION AND VALIDATION

4.1 Introduction

This chapter mainly presents simulation results and model validation. Simulation is performed with previous established models for the following cases: application of a CSW in a simulation room, the effects of blinds in the CSW on the thermal response of the room, and the PCM effect on the room temperature. The simulations are verified by the experimental results. Validation is carried out on a CSW with Photowatt PV panels and a CSW with PCM gypsum board.

4.2 Test room with CSW and optimum characteristic dimensions

A room is chosen for the investigation in the simulation, as shown in Figure 4.1. It has the following dimensions: 3.5m x 3.5m x 3.5m, with a 1.5m x 1.5m window. The CSW consists of two parts with equivalent dimensions: 3.0m x1.5m, the floor is 0.2m thick concrete. The thickness of the heat storage material in the CSW is initially set to 0.1m (concrete). This room is connected to another room by the west wall.

For each specific surface temperature of the CSW, there would be specific radiating heat transfer (Ur), air velocity (Vcir), Rayleigh number (Ra), etc. Among these interrelated parameters, air velocity is the dominant factor that affects the other parameters such as the Reynolds number (Re) and the average air temperature (Tm). However, the value of the velocity is also dependent on other parameters, such as the resistance factor of the airflow. A program was developed to calculate these interrelated parameters (see Appendix C).

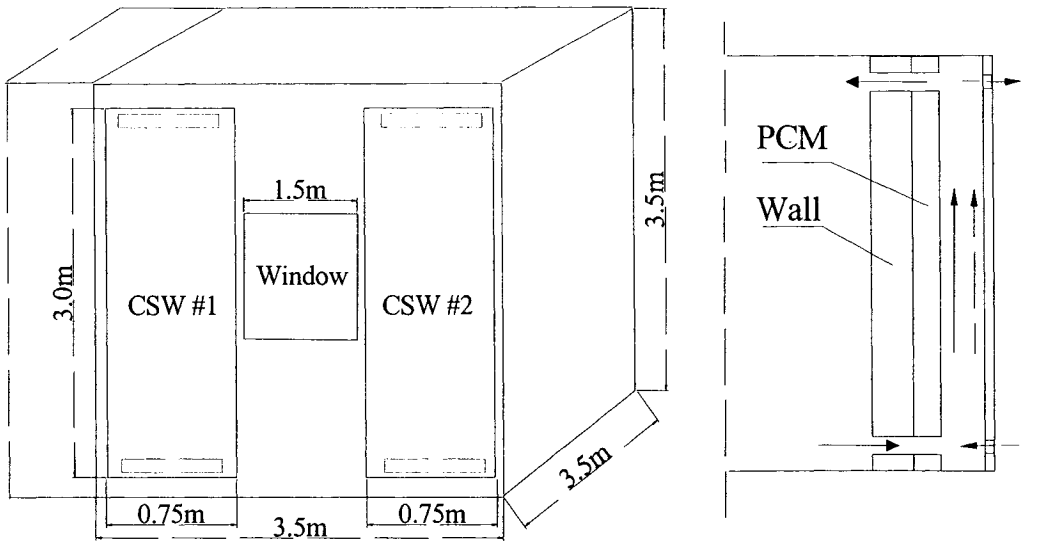

a. Example room sketches with CSW wall

b. Cross-view of CSW

Figure 4.1 CSW in simulation room

The algorithm is as follows: first, assume the air velocity to be a small value, for example, Va = 0.1m/sec, and use the given condition, T_{hot}, T_{cold}, To, and other known parameters, such as, the width of the wall (W) and air gap (L), and air properties (ρ, c), etc., to determine the induced air velocity (Vin). If the velocity difference Vin -Va > 0.1 m/s, then increase Va =Va + 0.1m/sec. Repeat the calculation until the difference of (Vin-Va) is in the range of 0~0.1 m/sec. If the value of (Vin-Va) is already in the range of 0 ~ 0.1m/sec, the computation is assumed to have converged.

Table 4.1 shows the variation of the major parameters, such as the inner surface temperature T2, the room air temperature Tr, the maximum fluctuation of the room air temperature ΔTr, and the time delay of the CSW Hd (Hd is the time difference between the occurrence of peak temperatures of the outside surface and the inner surface), as a function of storage mass thickness.

Table 4.1 Variation of major parameters with storage wall thickness

Thermal mass thickness Lg (m)	Temperature of inner surface T2 (℃)	Variation of room temperature ΔTr (℃)	Time delay Hd (hours)
0.1	39.6	15.0	3.4
0.15	38.7	13.5	3.9
0.20	38.0	11.7	4.5
0.25	32.0	9.3	5.2
0.30	27.8	7.5	6.5
0.35	24.7	6.4	7.5
0.40	22.3	6.0	8.8
0.45	20.5	6.2	9.5

The variation of the air temperature in the room and the time delay of heat conduction through the storage wall can be seen in Figure 4.2 and Figure 4.3. As can be seen from Figure 4.2, the indoor air temperature swing decreases as the thickness of the wall increases, and has a minimum value when the thickness is equal to 0.4m. That is because solar radiation affects the room temperature in two ways: one through the CSW, another through the window. The window is the major source of a large temperature oscillation. The CSW acts as a "heat buffer", which reduces the oscillating effect by delaying the entrance of heat into the room, and needs a longer time to transfer its warmth to the room, as the CSW is thicker. Thus the wall will result in a smaller temperature swing in the room, referred to Chapter 2. Meanwhile, the wall delivers less heat to the room when the wall is thicker. The wall cannot reduce the temperature swing

when the thickness is beyond a certain value. Therefore, the room temperature swing will again grow.

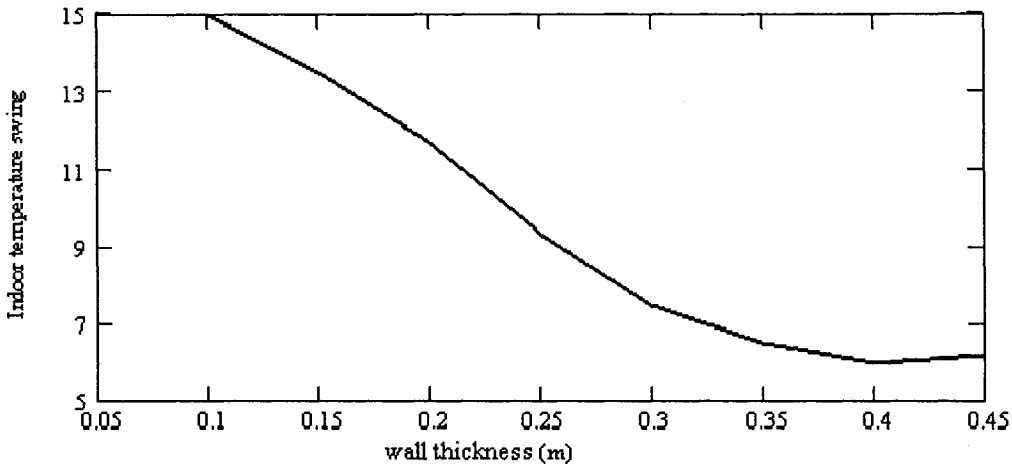

Figure 4.2 Indoor temperature difference as a function of mass thickness

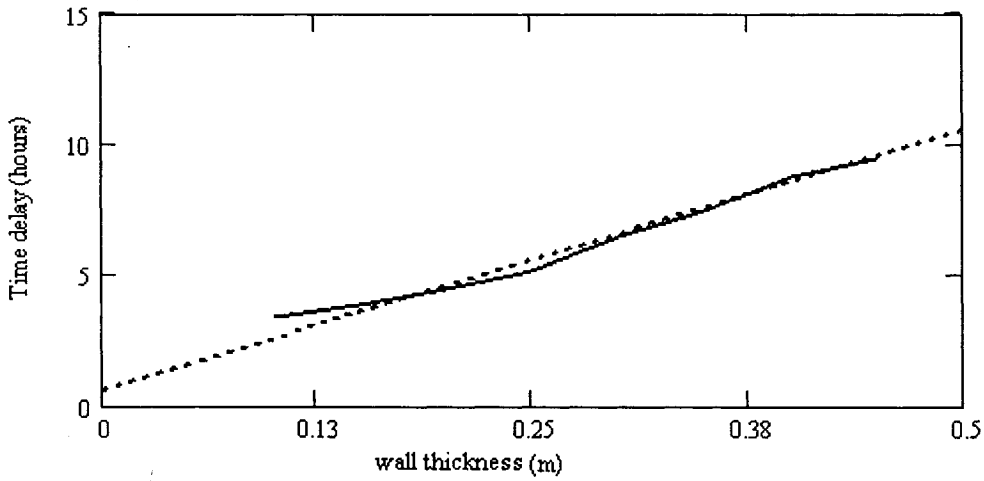

Figure 4.3 Time delay of the wall as a function of mass thickness

As can be seen in Figure 4.3, the time delay approximately changes linearly with the thickness of the wall and the relationship can be expressed as follows:

$$Hd = 20.47 \cdot L_w + 0.40 \qquad \text{(hours)} \qquad (4.1)$$

The correlation coefficient is 0.998, where L_w is the thickness of the storage wall, m; Hd is the time delay, in hours. Figure 4.2 and 4.3 can be used to predict the effect of the

mass thickness of the heat storage wall on the thermal response because the optimal wall thickness and linear relationship exist in any passive solar house without PCM.

Using Figure 4.4, it is observed that heat delivery by air passing though the cavity of the CSW and by the wall itself reaches a maximum when the gap thickness is 0.2 ~ 0.25m. As the air gap becomes thicker, the natural convective coefficient also becomes higher based on the relationship between natural convective coefficient and Rayleigh number. So there is more heat flow into the room. However, the heat delivered to the room will decrease rather than increase, after the thickness is beyond 0.25m. This occurs because the convective coefficient in the cavity within such a wide gap does not keep increasing (Bejan, 1993), but the conduction heat through the wall into the room significantly decreases when the air gap thickness continuously increases. This will cause less heat to enter the room.

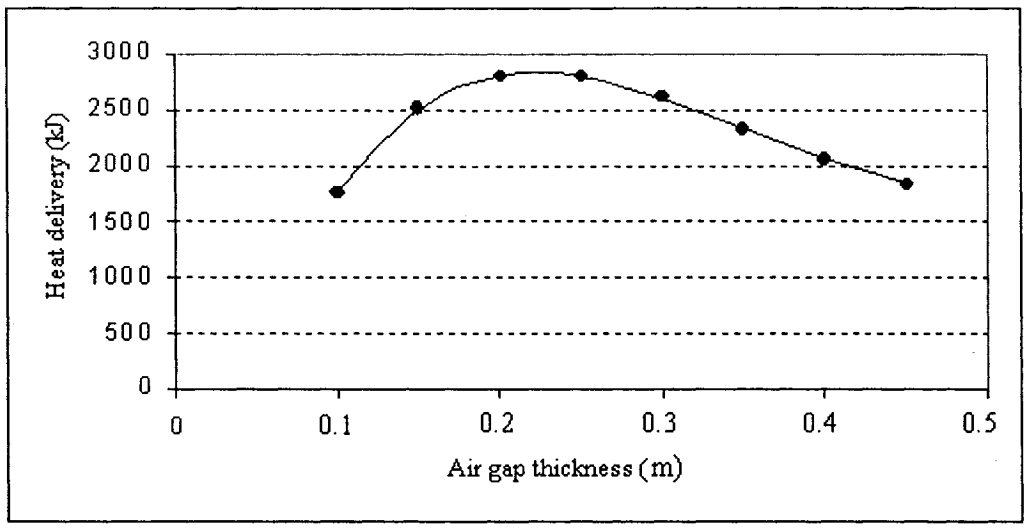

Figure 4.4 Heat delivered to room as a function of air gap thickness

The room temperature swing is an important factor that affects room comfort. The smaller it is, the better the room comfort. Meanwhile, as the room receives more solar

heat; the less traditional energy is consumed. A passive solar house with a masonry heat storage wall reaches a comfortable condition with the following parameters:

- The thickness of the storage wall is in the range of 0.35 ~ 0.40m,
- The width of the air gap is around 0.2 ~ 0.25m.

4.3 Simulation of the effect of blinds in a CSW

In a room with the same structure as the previous test room, a roll-blind is installed in the cavity. Airflow can pass through the cavity in the following three ways: airflow in front of the blinds, airflow behind the blinds and airflow on both sides of the blinds. To see how the blinds affect the thermal response of the room, the following assumptions are made: when the airflow passes only through the front cavity, the back cavity is considered as a closed cavity; when the airflow passes through the back cavity, the front cavity is considered as a closed cavity. Simulations are taken on a sunny day, July 15. The thermal network is referred to in Figure 3.6 in Chapter 3.

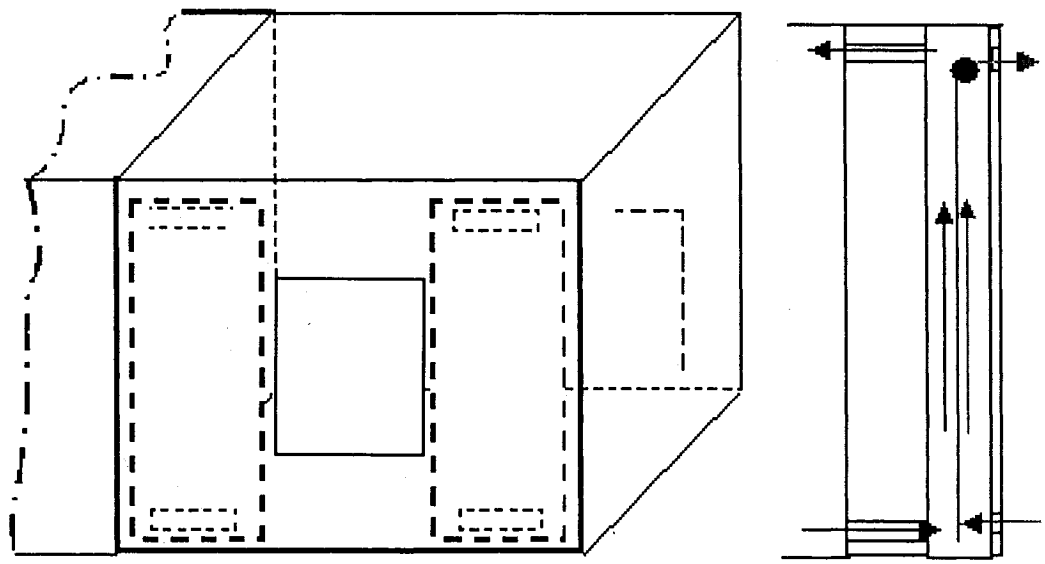

Figure 4.5 Simulation room with blind

Figure 4.6 shows the changes of the natural air velocity generated by the buoyancy that occurs on both sides of the blinds. The air velocities in the inner cavity are always higher than those in the outer cavity. During sunshine hours, the velocities in these two cavities are very close, and are 0.22~0.35m/s and 0.2~ 0.33m/s respectively. However they have significant difference during the rest of the time and have average velocities of 0.20 and 0.13 m/s respectively. Figure 4.7 shows the same general trend for the natural convective coefficient as for variation of air velocities with time. The natural convective coefficients in these two cavities have average values of 4.6 W/m^2 ℃ and 4.5 W/m^2℃ respectively during sunshine hours, and have 3.4 W/m^2℃ and 2.5 W/m^2 ℃ at sunless time individually. There are two peaks in a day for both the air velocities and convective coefficients. The explanation for this phenomenon is as follows:

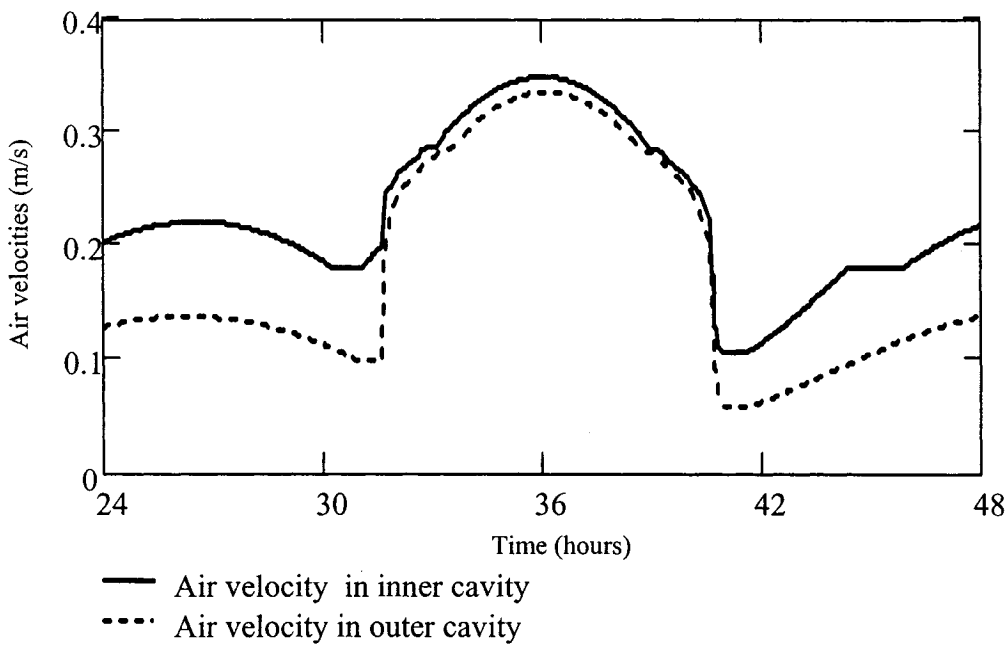

Figure 4.6 Air velocities induced by buoyancy effect in two cavities

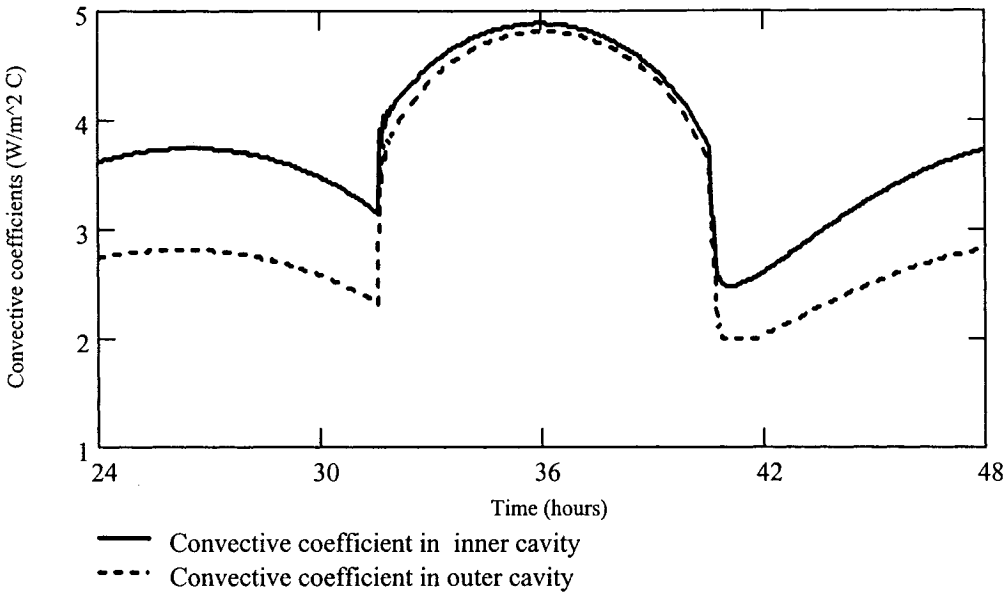

Figure 4.7 Natural convective coefficients in two cavities

In the cavity, the natural convection airflow is dependent on the temperature difference between the cavity air and the outside air due to buoyancy. The air temperature inside the cavity is also related to the wall temperature. When the difference between the wall temperature and the outside air temperature is at the highest value, the velocity of natural convective flow will be highest. In the morning, the blind in the cavity absorbs solar radiation, and the temperature difference between the walls and the outside air becomes larger and larger. The natural convective flow, therefore, gradually increases until the solar radiation reaches a maximum at noon. Then, the temperature difference becomes smaller with the decrease of radiation. The airflow velocity tends to diminish as the buoyancy becomes weaker. After sunset, the ambient air temperature drops quickly; the inner wall in the cavity is still warm due to the high thermal capacity of the wall. As a result, the temperature difference again becomes high. The air velocity continues to increase until the ambient air reaches the lowest temperature during the night. After that,

the airflow again decreases, as the ambient air becomes warmer and warmer until sunrise. The cycle is repeated the next day.

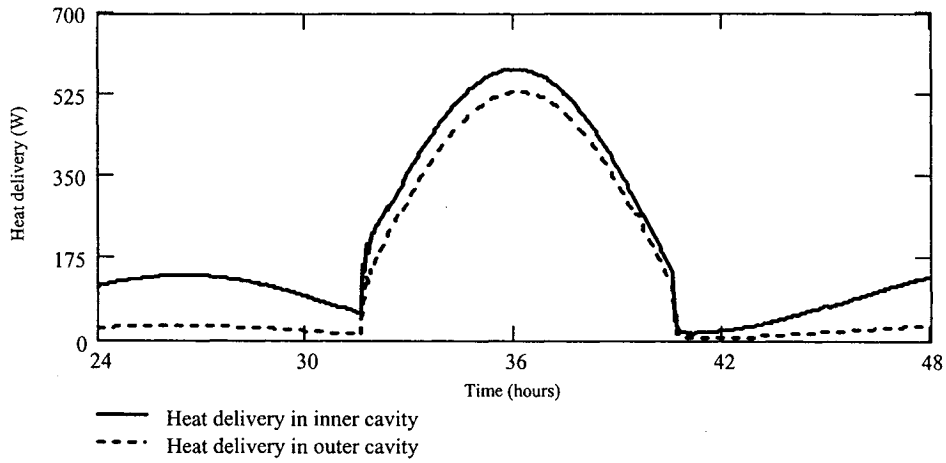

Figure 4.8 Heat delivered to outside

Figure 4.8 shows the heat delivery from the air cavity to the outside. It indicates that the heat that is delivered changes with the intensity of the solar radiation, and more heat is delivered by the inside cavity than by the outside cavity because the temperature of the interior wall surface is higher than that of the exterior glazing.

The effects of the blind on the room temperature in the different cases can be seen in Figures 4.9 and 4.10 below. Two conclusions can be drawn from them:

- The application of the blind can reduce the room temperature by 1.0 to 2.0°C in this simulation. For an airflow that passes only through one side of the blind, it is better if the air flows through the back of the blind rather than if the air passes through the front cavity.
- Airflow on both sides of the blind is better than either type of single airflow. This is of great importance in practice. First, it is simple for the designer to design blinds in the CSW; second, it is also easy for the user to operate.

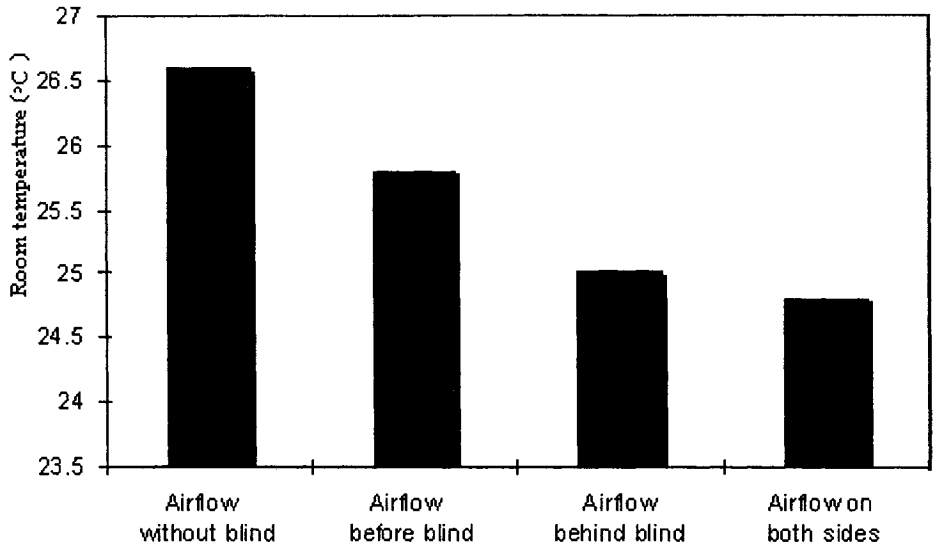

Figure 4.9 Blind effects on room temperature in different cases

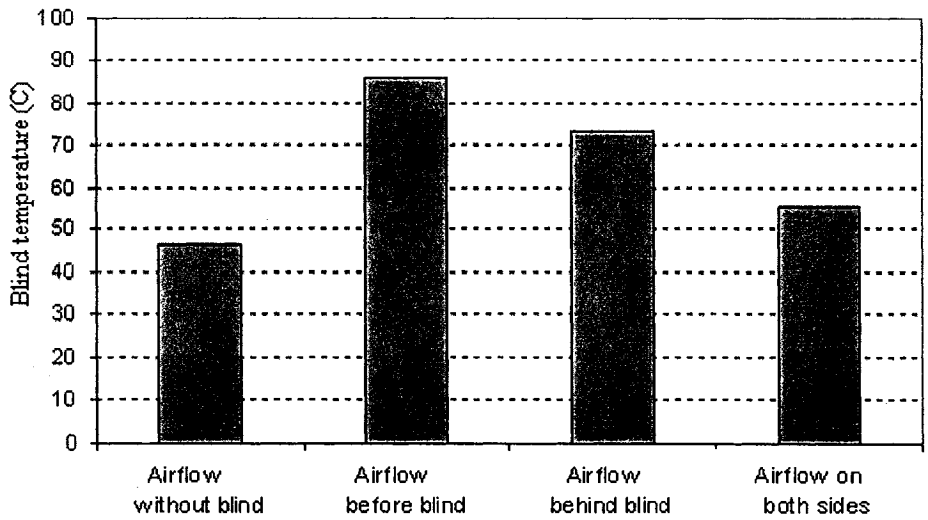

Figure 4.10 Temperature of the blind in different cases

4.4 A CSW with phase change material (PCM)

To see the effect of phase change material (PCM gypsum board) on the thermal response of the room, a simulation was performed on the previous simulation room in Montreal in February (see Figure 4.1), in which the heat storage wall consists of a PCM with the same properties as the PCM gypsum board.

Table 4.2 Variation of major parameters with PCM thickness

PCM wall thickness (m)	Temperature of inner surface (℃)	Time delay Hd (hours)	Variation of room temp ΔTr (℃)
0.02	72.5	0.6	51.5
0.04	43.6	1.5	29.5
0.06	31.8	2.2	20
0.08	24.9	3.2	16
0.1	19.8	4	15.1
0.12	18.8	4.5	15.2
0.13	18.8	3.2	15.3
0.14	18.8	1.5	15.5
0.16	18.8	2	15.8
0.18	18.7	3	16.1

Table 4.2 indicates the variation of inner surface temperature, indoor temperature and the time delay caused by PCM wall, as a function of PCM thickness. Figure 4.11 shows the response of PCM thickness. It is observed that the indoor temperature swing and the inner surface temperature both decrease as the thickness of the PCM wall increases. The variation of indoor temperature reaches minimum when the thickness is equal to 0.1m, then it slowly changes big. That is because that the amount of heat stored in PCM does not change large under present solar radiation due to its enough heat capacity when the thickness of the PCM continues to increase, though the capacity

becomes big when the PCM wall is thicker. On the contrary, the balance ability of the PCM will be weak when the wall is too thick. This phenomenon can be also observed in the curve of time delay in Figure 4.11.

The time delay has two increasing sections because the first one is caused by the effect of releasing and/ absorbing latent heat of the PCM. The second one is caused by sensible heat transfer of the PCM because no phase change takes place in the inner part of the PCM, in such situation, heat transfer takes place as conduction. The conduction relation between heat delivery and the wall thickness is shown in section 4.2 in this chapter.

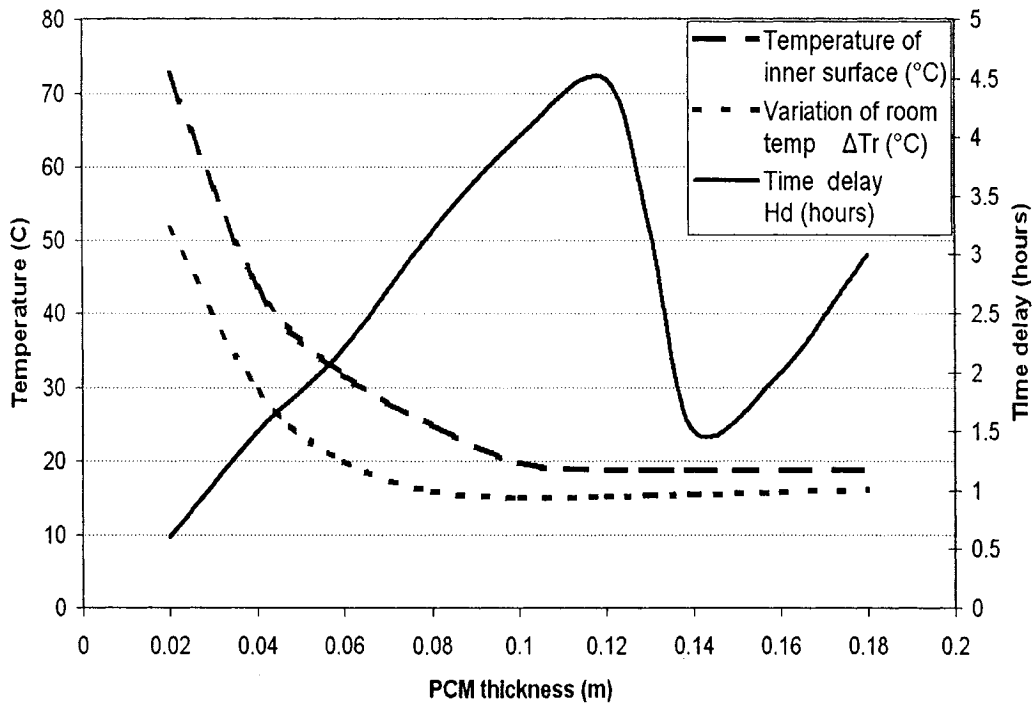

Figure 4.11 Influence of PCM thicknesses on indoor parameters

Figure 4.12 shows the variations of temperatures at different points in the PCM wall when the wall thickness is equal to 0.14. It can be observed that no phase change takes place in the inner part of the PCM wall during the procedure. In other wards, this part of

PCM works like traditional sensible materials in the CSWs. Compared to the previous masonry heat storage wall, it is found:

- The PCM can save much traditional sensible heat storage material. In this case, the PCM wall with thickness of 0.1m can attain the optimum indoor temperature; the masonry wall thickness is 0.4m so that the room temperature is in optimum situation. It can save as much as 75 percent of masonry material in volume.
- The PCM releases stored heat at stable transition range. So the room comfort is enhanced.

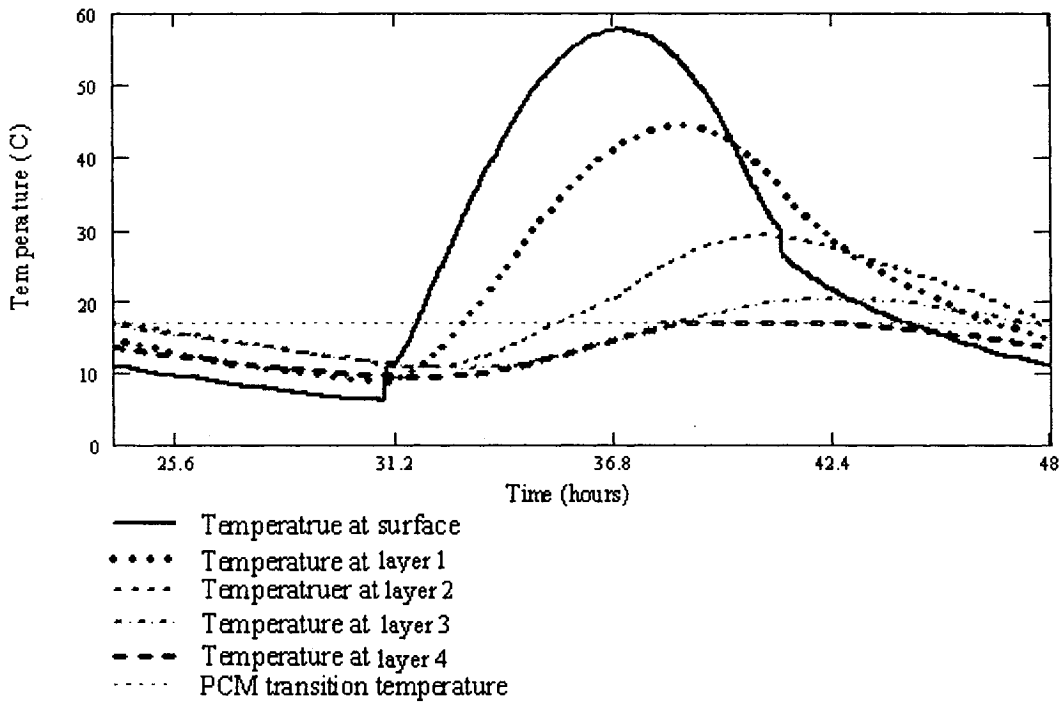

Figure 4.12 Temperature variations at different points in PCM wall

4.5 Model validation

A test room was built at Concordia University to investigate the application of the CSW (see Chapter 5). Two types of CSWs are used to yield simulation results: One CSW integrated with Photowatt PV panels and other CSW with a PCM gypsum board.

4.5.1 A CSW with Photowatt PV panels

Two Photowatt PV panels are installed on the exterior of the façade forming a 0.091m airflow channel; the room side of the cavity is an insulated wall (plywood + Polyethylene). Some issues need to be addressed with the experimental setup. The apparatus used to measure the exterior heat transfer coefficient was not calibrated and the readings obtained in its current state seem to be higher than expected. The days that were chosen for the simulation had low wind so that an exterior heat transfer coefficient was assumed to be 15 W/m^2K, which corresponds to values obtained from empirical relations. The inlet air temperatures of the CSW are assumed to be equal to the outdoor temperature.

In the simulation procedure, the effect of the wind is not taken into account in the airflow. In the air cavity, there are also more than 20 thermocouples used to measure the surface temperatures of the PV panels, the insulation wall and the air temperatures. All of these factors affect airflow status and would decrease air velocity below what is calculated and probably increase the heat transfer coefficient beyond the calculated value.

In natural convective flow, buoyancy is the driving force. This force is greater near the heat sources, thus, near the PV surface and the insulation wall, leading to non-symmetric velocity profiles. In a 1-D model, an average velocity for each case must be assumed to represent a specific air speed. The determination of air velocity and air temperature is referred to in section 5.4 of Chapter 5. The experiment for the CSW with a natural convective flow started at 8:00 A.M on October 13, 2003. It was a cloudy day in the early morning. It became clear as of 9:30. Figure 4.13 indicates the major parameters of the experiment in time from 10:00 to 11:15.

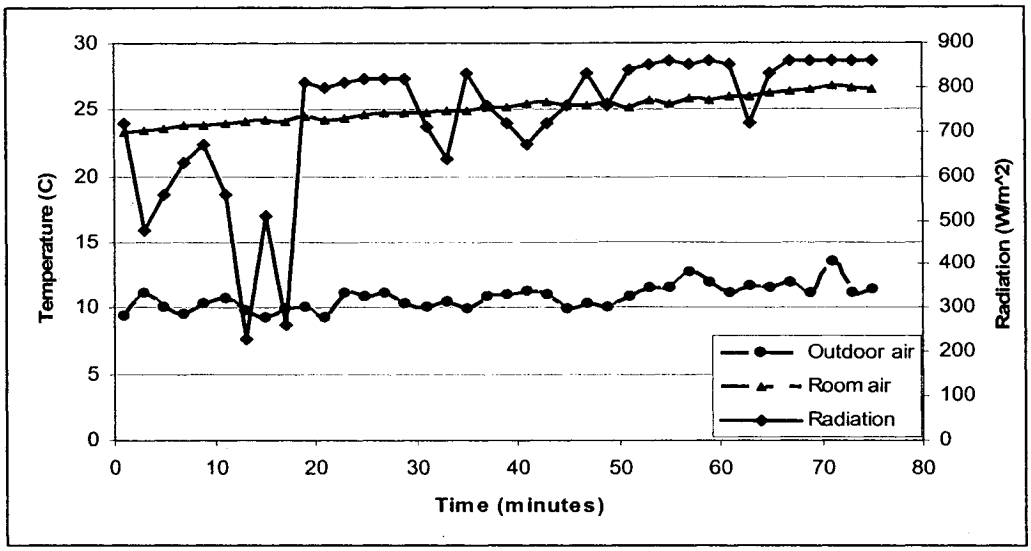

Figure 4.13 Solar radiation and temperatures of room air and outdoor air in test

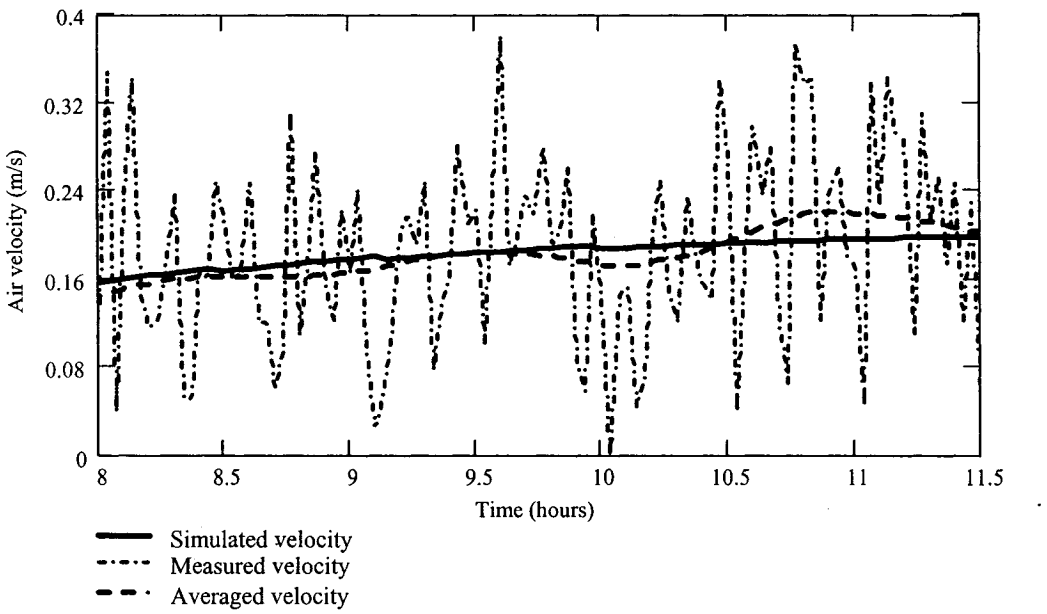

Figure 4.14 Comparison of air velocity in natural flow

Figure 4.14 shows the instantaneous velocities that are measured, averaged (every 15 minutes) and the theoretically calculated velocity. Due to the effect of the outside wind and the small buoyancy, the measured velocity vacillates so much that it is difficult to find a relation between the calculated value and experimental result until the data is averaged. However, the averaged velocities that were derived from measurements are

close to the simulation results. The temperatures of the PV panels match quite well those of simulation and experiment (Figure 4.15). That is because during the period from 9:30 to 11:30 a.m., the weather condition is similar to the case of the simulation. The fluid air temperatures at the outlet of the CSW oscillate, but they change around the simulated values.

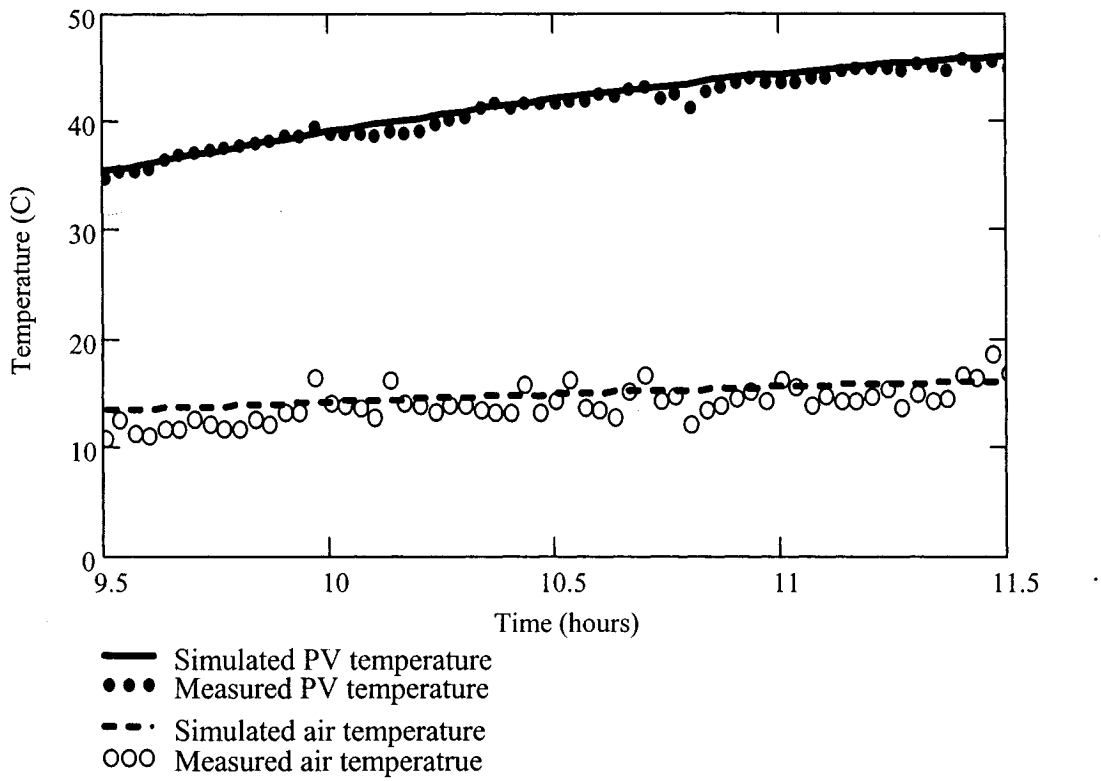

Figure 4.15 Temperatures of PV panel and air at the CSW outlet

In forced convective flow, air velocity is a dominant factor in heat transfer, and the variation of the air velocity changes in a relatively small range. In this investigation, experimental data were recorded during the time period from 8:00 to 12:00 A.M on March 30, 2004. The average air velocity was 0.34 m/s. Figure 4.16 shows the major parameters used in the experimental investigation.

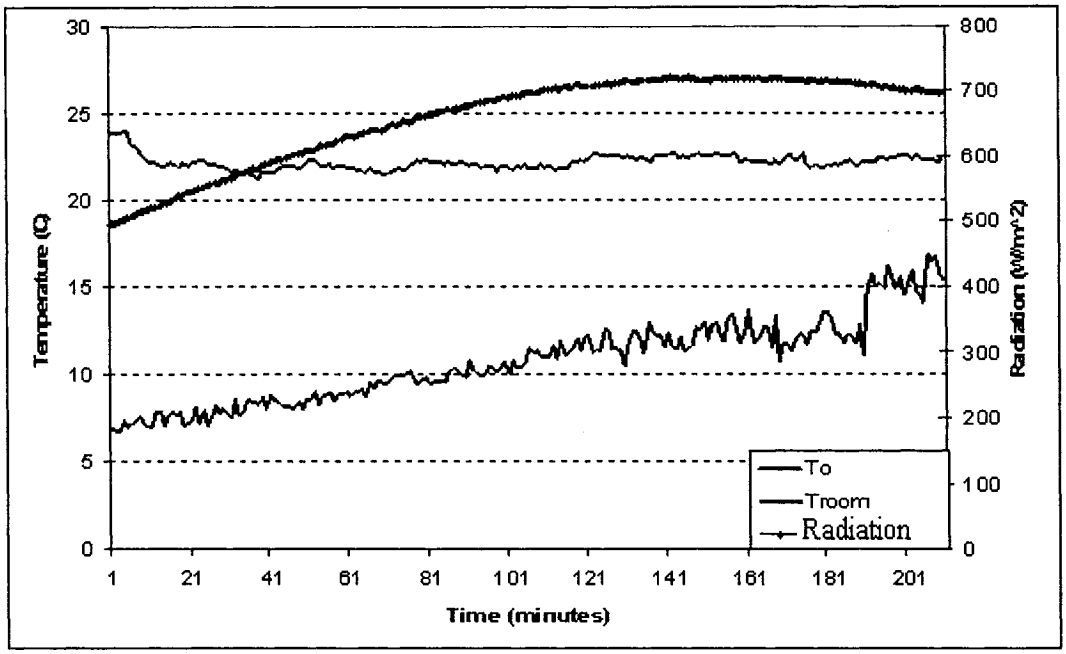

Figure 4.16 Solar radiation and the temperatures in a case of forced flow

The calculation results of PV panel temperature in forced convective flow fit well with the experimental results (Figure 4.17). However, the outlet air temperature of the CSW (see Figure 4.18) fits well only when the calculated convective coefficient is multiplied by a factor 1.6. The following two effects could cause the experimental results to be beyond the theoretical computation value: 1. The air inlet is in a 90°-bent shape and there are many wires of measure sensors in the cavity, which cause a strong turbulent airflow with a high convective coefficient. 2. The air velocity actually changes from time to time. In simulation, an average air velocity (constant) is assumed due to a relatively small change in the air cavity. However, during the actual operation of the CSW, the air velocity in the cavity changes from time to time. This unsteady flow continually enhances the heat exchange between the surfaces and the flowing air. These two factors result in a convective coefficient beyond what is used in the theoretical simulation.

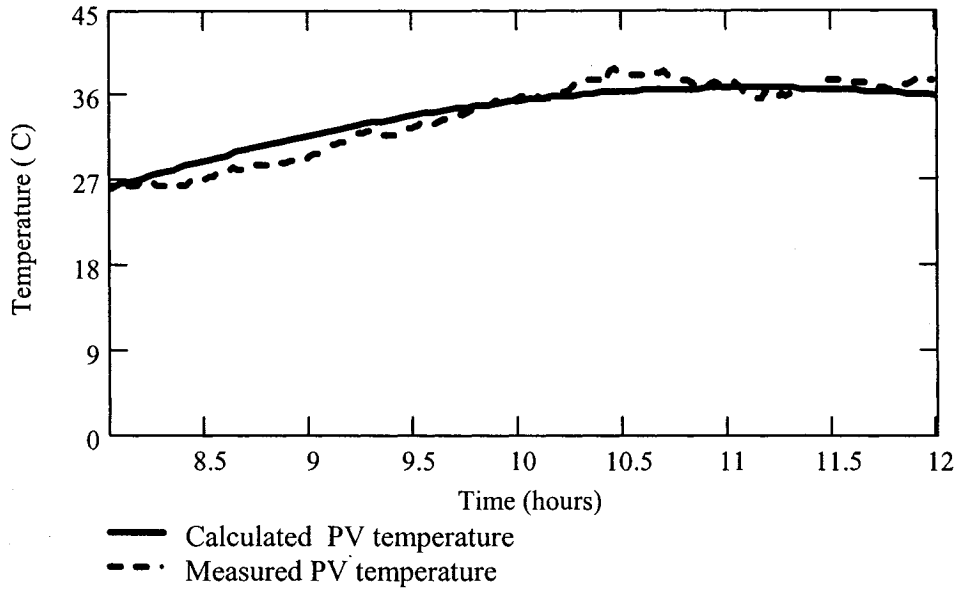

Figure 4.17 Comparison of the PV panel temperature in forced airflow

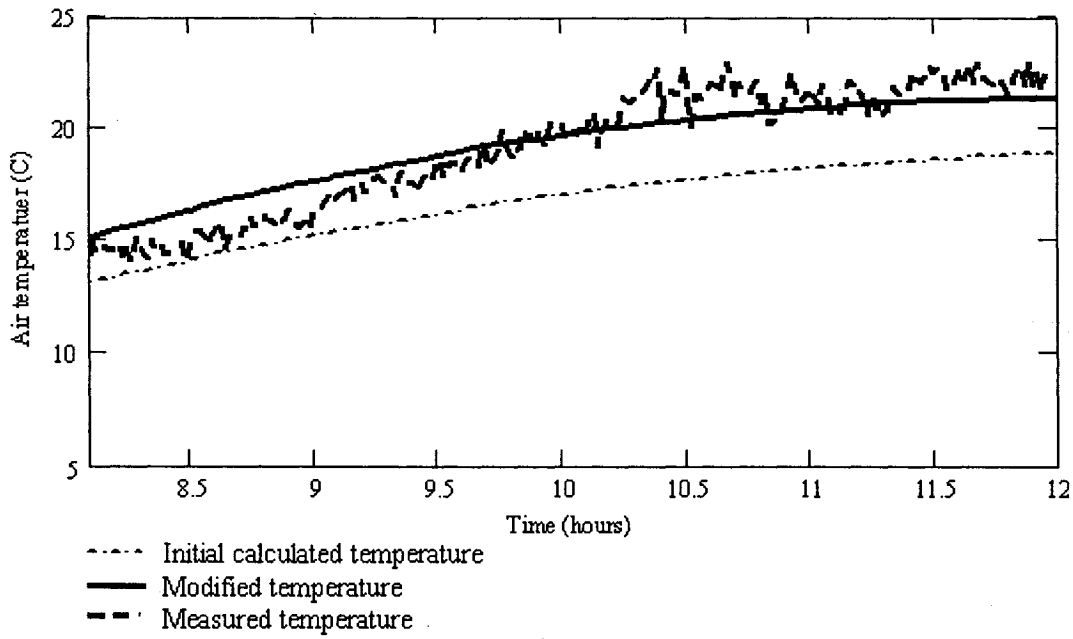

Figure 4.18 Air temperatures at the outlet of the CSW

4.5.2 A CSW with a PCM gypsum board

To validate the temperature variation of PCM, the experimental data were recorded during the time period from 9:47 to 11:47 on November 10, 2003 for forced convective airflow in the wall cavity. The average air velocity is 0.65 m/s. The PCM board is

installed to leave an air space of 0.09m from the outside glazing. The inner surface of this board faces room air. Figure 4.19 shows the major parameters in the test.

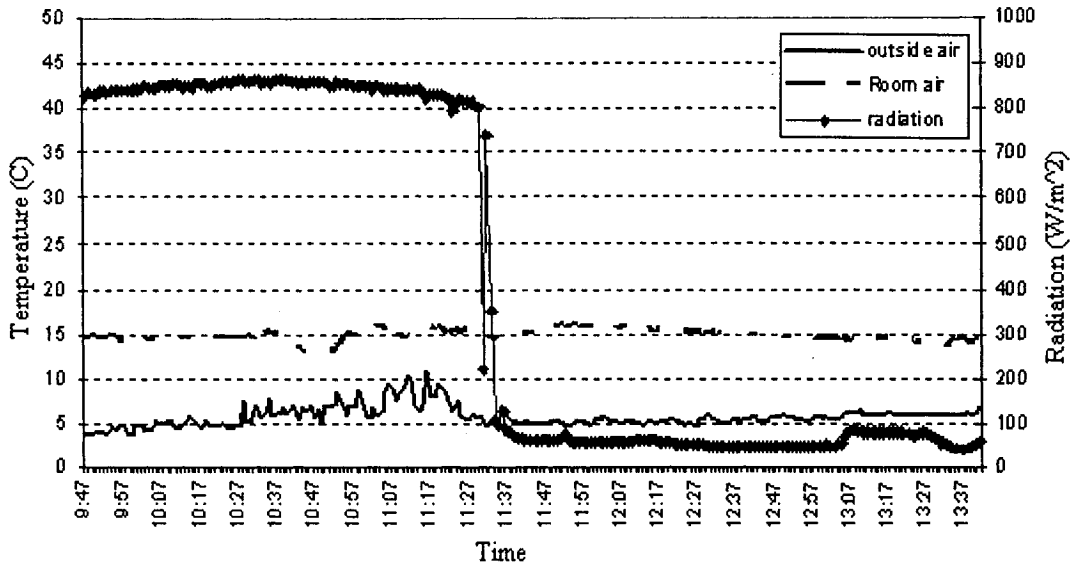

Figure 4.19 Solar radiation and the temperatures of room air and ambient air

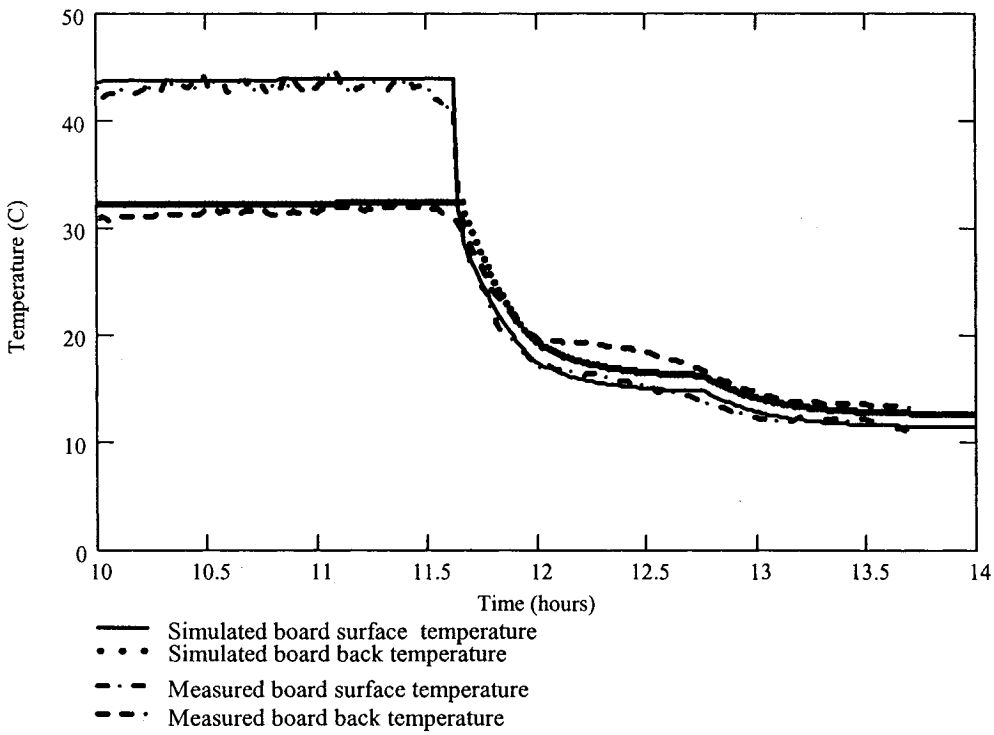

Figure 4.20 Temperatures of PCM board surface (inside and outside)

Figure 4.20 indicates that the simulation for the PCM board has a good agreement with experimental results after convective heat transfer coefficient is multiplied by a factor 1.2. This factor is appropriate because of specific inlet structure and wiring plus other obstruction in the wall cavity, which would cause more strong turbulent airflow with high convective coefficient. In high speed forced airflow, the influence of inlet and wiring plus other obstructions on heat transfer is relatively smaller than that in low speed forced airflow. Therefore, it is reasonable that the factor of 1.2 in this case is smaller than the previous factor of 1.6.

Chapter 5 EXPERIMENT AND RESULTS

5.1 Introduction

As mentioned in Chapter 2, a PCM gypsum board would be used as the heat storage material in CSWs, but its properties need to be clarified before it is installed in experimental CSWs. Because it was made in 1995, its properties, such as latent heat, transition temperature, and conductivity, may have changed after such a long storage time. Meanwhile, in order to explore the performance of the CSWs and to validate the previous simulations, it is necessary to take measurements on the CSWs. Consequently, this chapter addresses the following: PCM property test in laboratory, the performance of the CSWs in an outdoor test facility, and the determination of the average air velocity and the average air temperature in the wall cavity.

5.2 PCM property tests

The latent heat L and the transition temperatures T_{in} and T_{fa} are the most important parameters for phase change materials. They are the basis of the thermal analysis of phase change materials. In the present study, a DuPont 910 Differential Scanning Calorimeter (DSC) is used to measure these parameters (calibration was finished before the test). The mechanism is shown in Figure 5.1. A weighed sample is placed in a sample pan in an insulated chamber. It is then heated or cooled together with a reference by same rate. When heat exchange related to the material phase change takes place in the sample, but not in the empty reference pan, the resulting difference in the temperature between the sample and the reference is directly related to the heat flow to or from the sample.

The difference in the heat flow can be quantitatively measured and plotted in the form of a DSC curve as shown in Appendix B. The latent heat can be calculated by automatic peak integration of the related heat flow versus time curves. The melting point and the freezing point are the calculated temperatures at the intersection of the base line with the tangent to the infection point in the curve of heat flow versus temperature.

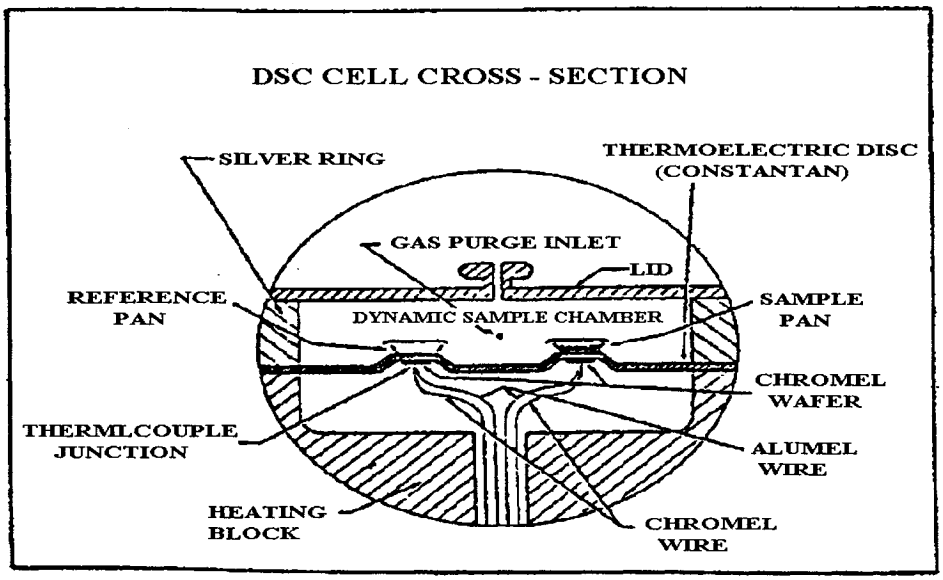

Figure 5.1 DSC test schematic (apparatus manual)

The results of the DSC test conducted on the PCM gypsum board, in which different parts of the board were selected, are summarized in Table 5.1. It is observed that the variation of the latent heat is 1.0% in comparison to that which was measured in 1995. The variation is within a standard deviation of 2.18 J/g. The melting interval and the freezing interval are also found to be almost the same between these two tests

Results of the test indicate that:

1. The PCM gypsum board is stable in thermal properties. Its latent heat and transition temperature remain almost the same as 10 years before.

2. This board is suitable for use in the present study as building thermal storage material.

Table 5.1 Comparison on PCM gypsum board Properties

Time	Latent heat	Melting interval	Freezing interval	Number of specimens
1995	28.8 J/g	17.0~20.9 °C	19.3~17.3 °C	20 specimens
2003	29.1J/g	16.8~20.9 °C	19.2~17.0 °C	4 specimens

To measure the thermal conductivity and the resistance of the related material that would be used in this study, a Lambda 2000 Heat Flow Thermal Conductivity Instrument is used to perform the test. A cross-sectional view of this equipment is given in Figure 5.2.

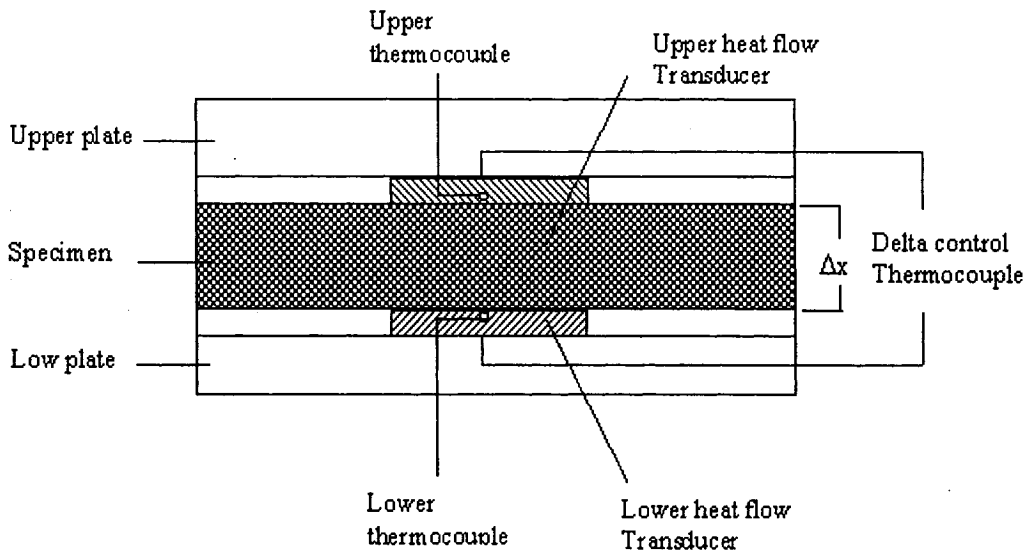

Figure 5.2 Cross-sectional view of heat flow instrument

The test is conducted under atmospheric pressure and ambient room temperature at 24°C (+/-1℃) and the relative humidity at 50% (+/-2%). The instrument is calibrated just

before the test. The accuracy of the equipment is 1~3%. Control parameters (usually mean temperature and temperature difference) are set with respect to material property after the power is switched on.

Each sample is placed in a test chamber; the chamber separation is adjusted by moving the upper plate downward to ensure a good fit of the specimen between the two plates. The operation program of the instrument is reset, and the inner metering system is then activated to monitor the thermal state of the sample until a steady-state condition is reached. The main parameters, such as thermal conductivity, sample thickness, sample surface temperature, and heat fluxes, are recorded. When the instrument reaches thermal equilibrium, the following values are constant:

- Temperature of each plate
- Temperature gradient across the specimen
- Heat flow through the specimen

When these values do not change, the Heat Flow Meter determines the thermal conductivity of the specimen according to Fourier's law of heat conduction. The following table shows the change of this PCM gypsum board. It is observed that the conductivity change is small. Its maximum change is only 6.9%. Therefore, it could be assumed to be a constant in the theoretical analysis. It is of great importance to simplify the complicated characteristics of the phase change material during the simulation procedure.

Figure 5.3 shows the difference between the PCM gypsum board and regular gypsum board under the same conditions of setting T_{mean} =14℃, ΔT =6℃. It is observed that there are significant differences in heat flux between these two materials, even though the same

test condition is maintained. In the regular board, because there are no inner heat sources in the board, the top plate heat flux and the low plate heat flux in the test chamber will maintain relatively small differences at the beginning of the test, and the test reaches steady state quickly. In the PCM gypsum board, however, during the process of phase change, the PCM releases the latent heat so that the test equipment needs to absorb more heat to cool down the low surface temperature of the specimen until no more latent heat is released. Meanwhile, the top surface of the specimen absorbs some heat and requires more heat to maintain the measuring temperature. Therefore, the difference between the heat fluxes of the top and the low plates is significant, and more time is needed to reach steady state.

Table 5.2 Thermal conductivity of the PCM under different conditions

Test condition	Tmean=30 ΔT=6	Tmean=19 ΔT=2	Tmean=10 ΔT=6	Maximum change rate
Conductivity	0.174	0.173	0.185	6.90%

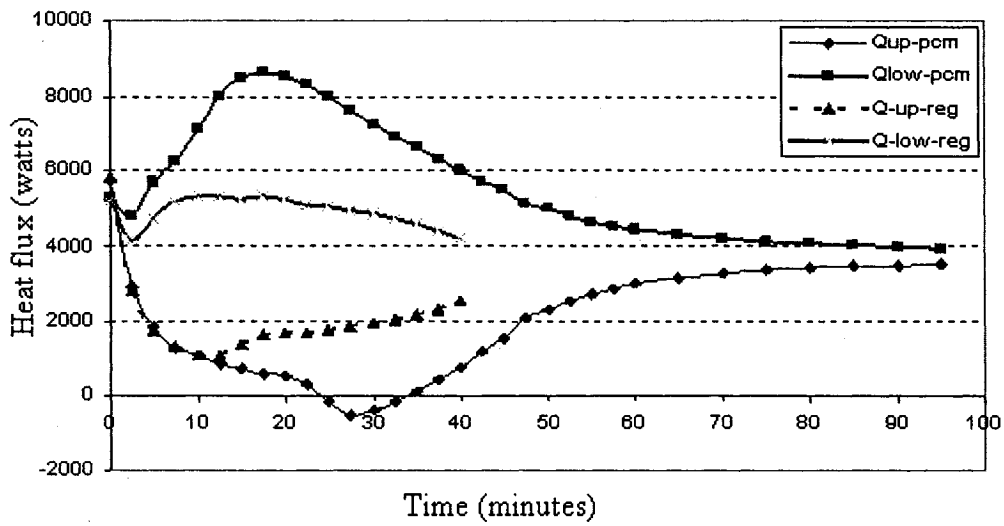

Figure 5.3 Variation of heat flux at condition of T_{mean}=14°C, ΔT=6°C.

Table 5.3 shows the characteristics of the materials that would be used in later tests. It is found that the thermal conductivities of common materials, such as regular gypsum board and polyethylene foam remain almost the same when the accuracy of the instrument (2%) is taken into account.

Table 5.3 Thermal properties of related materials

Material	Conductivity (W/ m°C)		Thickness (cm)	R-value (m^2°C /W)	
	T_{mean}=24 ΔT=20	T_{mean}=14 ΔT=6		T_{mean}=24 ΔT=20	T_{mean} =14 ΔT=6
PCM gypsum board	0.174	0.185	1.261	0.073	0.068
Regular gypsum board	0.145	0.148	1.243	0.086	0.084
Polyethylene foam	0.0286	0.0288	2.544	0.89	0.88

5.3 Outdoor test facility

To investigate the application of the CSW, a new test room, which was a prefabricated housing unit, was built on the roof of the BE building at Concordia University. The chamber has an interior dimension of 2.972m x 2.896m x 3.045 m, with a total floor area of 8.61 m^2. There are two double-layer windows that are located separately on the east wall and the west wall. CSWs are located in the wall facing south 10° to east.

Photovoltaic (PV) is a very useful technology in a solar field, which converts abundant, clean solar energy into electricity. As well, the application of PV panels has no impact of pollution on the environment, so its use has received significant attention (Wade, 2003). However, its electrical efficiency is usually quite low, generally less than 15% in practice. In other words, more than 80% absorbed energy is lost to the

surroundings by different forms of heat transfer: conduction, convection and radiation. It is deplorable to waste so much energy if no more effective measure is taken. Hence, one of the motivations in the use of PV panels in CSWs is to improve the performance of the CSWs, which have the following characteristics:

- Provide heat and electrical energy at same time,
- Reduce the cost of PV application,
- Enhance overall efficiency.

There are two kinds of PV panels used in the present study: Photowatt PV panels and Spheral Solar PV panels. They are integrated into the south-facing façade to make several types of CSWs. These CSWs, moreover, also work as an electrical generator, an air ventilator, a light source, a heat exchanger, etc., because there are four photovoltaic panels (two are Photowatt panels; the others are Spheral Solar PV panels), low emit windows, and two pieces of PCM gypsum board, which are used to store heat in the CSWs.

The Photowatt PV panels are installed on the exterior of the left façade forming a 91mm-wide airflow channel; in addition, they are connected in series to provide electricity on sunny days. On the right side of the façade, there are two Spheral Solar PV panels located in the middle of the cavity forming two airflow channels; they are also connected in series. The inside walls of the CSWs are insulated (plywood plus polyethylene foam) so that heat transfer to or from the room is negligible. Figure 5.4 is a photo of the test room showing the configuration of the façade.

Four configurations of the CSWs are considered in this test study:

1. Two cavities (one with Photowatt PV panels in the bottom and the other with a

PCM gypsum board on the top) are connected and have the same airflow channel (cross section dimension: 91mm x 930 mm), as shown in Figure 5.5 a. The main test is taken with the following statuses: damper 1 and 4 are closed; damper 2 and 3 are open.

2. A low-e double-glazed window replaces the PCM gypsum board of case 1. The test is focused on the integrated PV CSW shown in Figure 5.5 b.
3. In the double façade cavity, there is only a PCM gypsum board attached to the insulation wall. The airflow is controlled in two states: natural convective flow and forced convective flow. Seen in Figure 5.6 a.
4. In case 3, two Spheral Solar PV panels connected in series and installed in the middle of the cavity separate the original cavity into two airflow channels. The width of the outside channel is 35mm; that of the inner channel is 56mm. So the air can flow through both sides of the Spheral Solar PV panels.

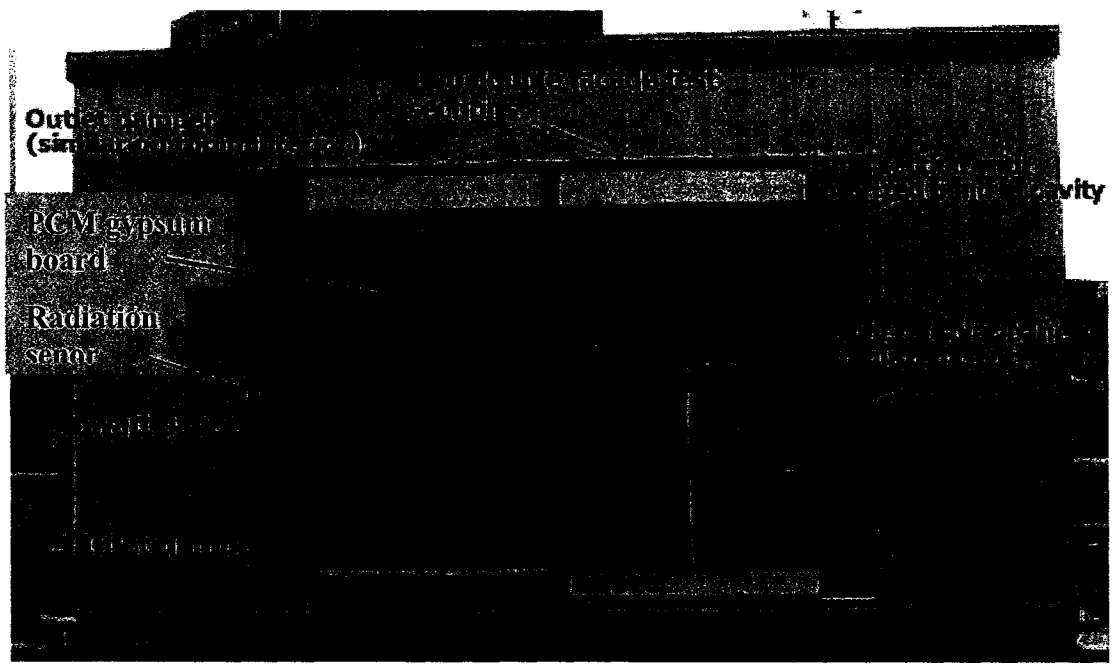

Figure 5.4 Photo of south façade of test room

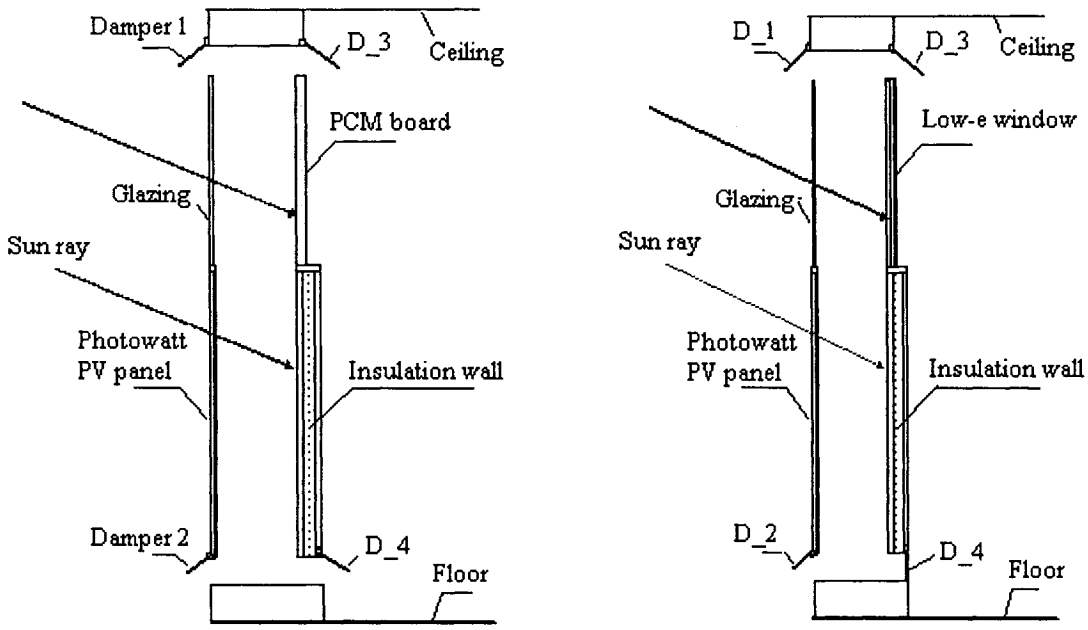

Figure 5.5 Configuration of CSW with Photowatt PV panels

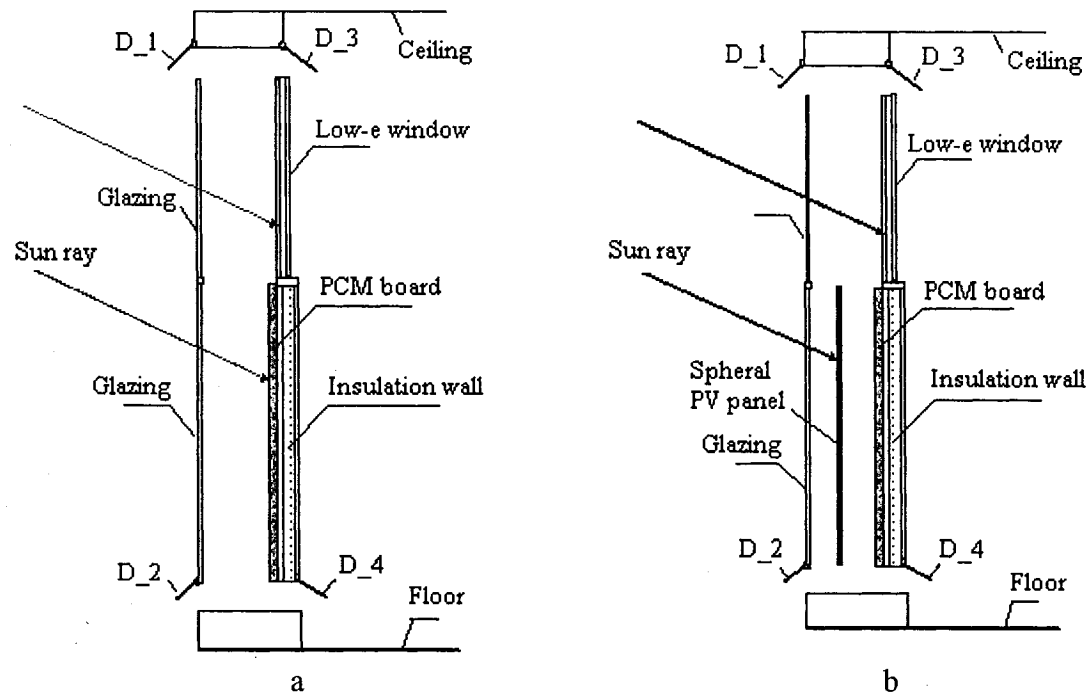

Figure 5.6 Configurations for CSWs with a PCM or Spheral Solar PV panels

The parameters that are measured in the present study include solar radiation, the temperatures of each component, the air velocity in cavity, the PV output voltage, et al. The signals that measure these parameters are connected to a data acquisition system and are automatically recorded by a VEE control program.

5.4 Determination of average air temperature and air velocity

In this thesis study, airflow is treated as 1-D thermal dynamical airflow, which means that the air temperature in the CSW is considered as having the same value at horizontal level. However, in practice, the temperature distribution is usually quite different from this assumption, especially for depth direction. To ensure the calculation accuracy when a 1-D equation is used, a representative temperature must be found. A measurement is taken in the test by setting several thermal couples in the airflow channel.

Take the data obtained on November 10, 2003 as an example to show the actual measured temperature profile in the Photowatt cavity ($B_{j,10}$ in Figure 5.7). The representative temperature can be calculated by least-squares fitting function:

$$T(x) = F(x) \cdot G \tag{5.1}$$

where F(x) is a fitting vector, and G is a linear function,

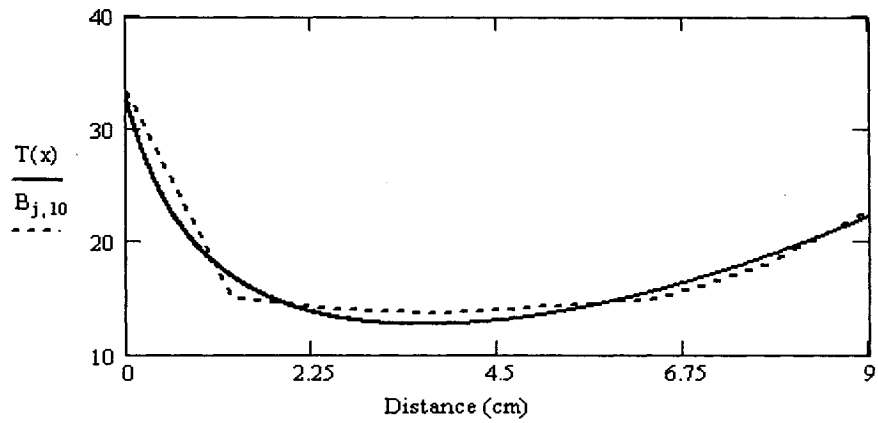

Figure 5.7 Temperature profiles of measured points and fitting function.

$$F(x) = \left[1, 1/(1+x), x^2\right]^T \qquad G = linefit(L, B, F) \tag{5.2}$$

where L is distance from glazing, B is the measured temperature, So the representative temperature can be expressed as

$$Tave = \frac{1}{8.8}\int_{0.1}^{8.9} T(x)\,dx \qquad Tave = 16.3 \cdot \deg C \quad \text{(In this case)} \tag{5.3}$$

When a 1-D model is used in numerical thermal analysis, the air velocity is another parameter that needs to be fixed since it is influenced by many factors, such as the cavity geometry, the air pressure, the outside wind, etc. It is thus necessary to find an average value as the representative air velocity in each horizontal level along the vertical CSW. One approach is to install a velocity transducer in the middle of the airflow channel to measure a velocity. Then, a portable air velocity meter is used to measure the instantaneous velocity profile; finally, a relationship between the instantaneous value and the fixed one would be determined. It would be used in experimental analysis.

Figure 5.8 shows the change of the measured value and the fitting function in a CSW with Photowatt panels on one sunny day: March 30, 2004.

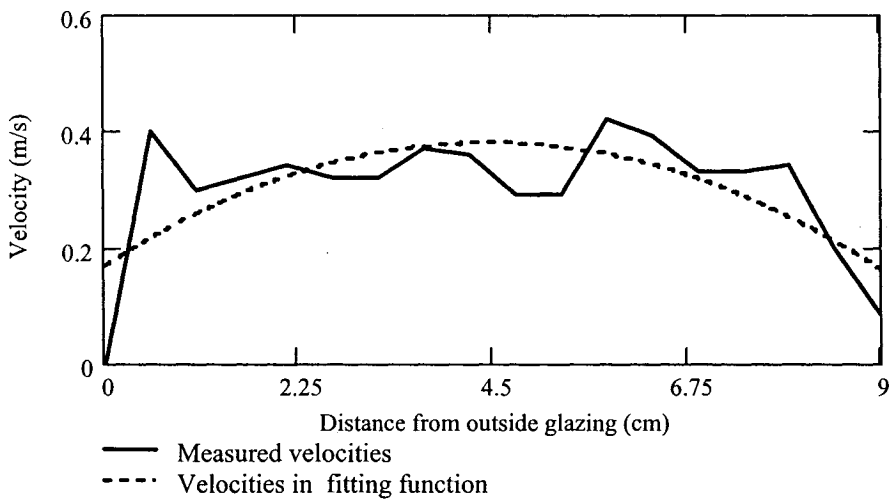

Figure 5.8 Velocity profile in Photowatt cavity

The fitting function of the measured velocity profile is as follows

$$V(x) = -0.011x^2 + 0.094x + 0.17 \tag{5.4}$$

where x is the distance from the external PV panel.

The average velocity can be calculated by integrating this fitting function:

$$Vm = \frac{1}{9} \cdot \int_0^9 V(x)dx \qquad Vm = 0.31 \cdot m/s \text{ (In this case)} \tag{5.5}$$

Moreover, the velocity at the fixed point is $V_{fix} = 0.33$ m/s

So the factor between the average velocity and the velocity at fixed point has

$$F = \frac{Vm}{V_{fix}} \qquad F = 0.93 \tag{5.6}$$

With the aid of a data acquisition system, the velocity at each moment can be derived from the velocity at fixed point as the follows,

$$V = F \cdot V_{fix} \tag{5.7}$$

5.5 Performance of a CSW with Photowatt PV panels

In this structure, two Photowatt PV panels and insulation wall make a rectangular airflow channel (Figure 5.9). The two PV panels functioning in series are connected to a load of 24.1 ohms to provide electricity.

An energy balance was set on the cavity with PV panels on November 10, 2003; the time period was from 10:30 to 10:40 AM. The characteristic is shown in Figure 5.9. In the cavity, the heat transfer through the back wall can be considered negligible because the wall is well insulated. The average air temperature *Tav* at the top level of the wall cavity can be obtained using the equation 5.5 according to the measured profile temperatures: 15.6, 114.6, 14.0, 14.8, 15.3, and 17.9 ℃.

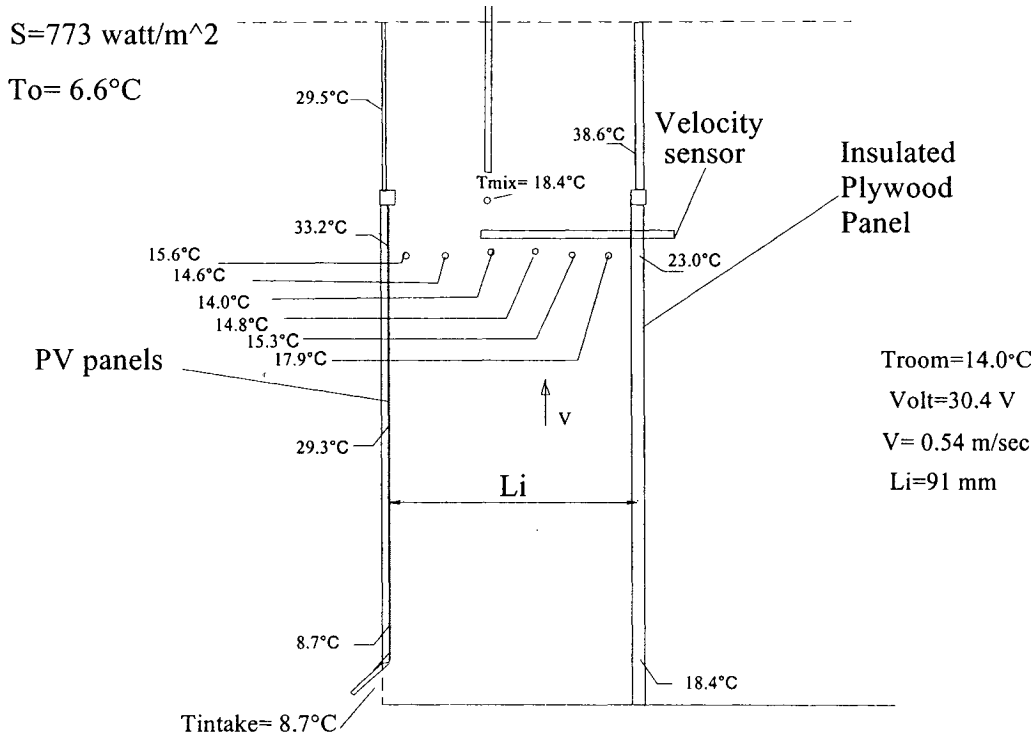

Figure 5.9 Structure schematic and specific parameters in a CSW with Photowatt PV panels

The thermal energy that is absorbed in flowing air is

$$Q_{thermo} = Li \cdot W \cdot V \cdot \rho \cdot c \cdot (Ta - Tin) \qquad Q_{thermo} = 342.2 \text{ W}$$

where W is width of the CSW, Li is thickness of the air gap. The power of Photowatt PV panels is (the voltage U = 30.4 volt, the resistance R = 24.1 ohm)

$$Pe = \frac{U^2}{R} \qquad Pe = 38.35 \text{ W}$$

The overall efficiency is

$$\eta = \frac{Q_{thermo} + Pe}{S \cdot A} \qquad \eta = 0.62$$

It is observed that the CSW with Photowatt PV panels is effective; it can not only produce electricity with up to 10.7% efficiency, but can also provide the room with heat

at about 51.5% efficiency.

The convective coefficient in the cavity can be obtained by using energy balance on the air control volume in the wall, which is

$$Qthermo = h \cdot W \cdot H \cdot [Tpv + Tw - (Ta + Tin)]$$

So the convective coefficient is

$$h = \frac{Qthermo}{W \cdot H \cdot [Tpv + Tw - (Ta - Tin)]} \qquad h = 13.5 \text{ W/m}^2\text{℃}$$

5.6 Performance of a CSW with Spheral Solar PV panels

This structure consists of Spheral Solar PV panels and an insulation wall. There are two Spheral Solar PV panels connected together in series, providing electricity to an instrument (27.3 ohms). These PV panels are located in the middle of the left cavity at a distance of 0.035 m from the outside glazing, 0.055m from the insulation wall, referred to in Figure 5.10.

An energy analysis is carried out on January 26, 2004, the time period being from 11:20 to 11:50. The measured average air velocities and the top air temperatures in the wall are as follows:

$Vo = 0.15$ m/s $\qquad\qquad$ $Vi = 0.35$ m/s

$Ta\_o = 21.6$ ℃ $\qquad\qquad$ $Ta\_i = 2.0$ ℃

So the thermal energy absorbed from flowing air is given by

$$Qtherm\_o = Lo \cdot W \cdot Vo \cdot \rho \cdot c \cdot (Ta\_o - Tin) \qquad \text{Qtherm\_o} = 236.8 \text{ W}$$

$$Qtherm\_i = Li \cdot W \cdot Vi \cdot \rho \cdot c \cdot (Ta\_i - Tin) \qquad \text{Qtherm\_i} = 427.3 \text{ W}$$

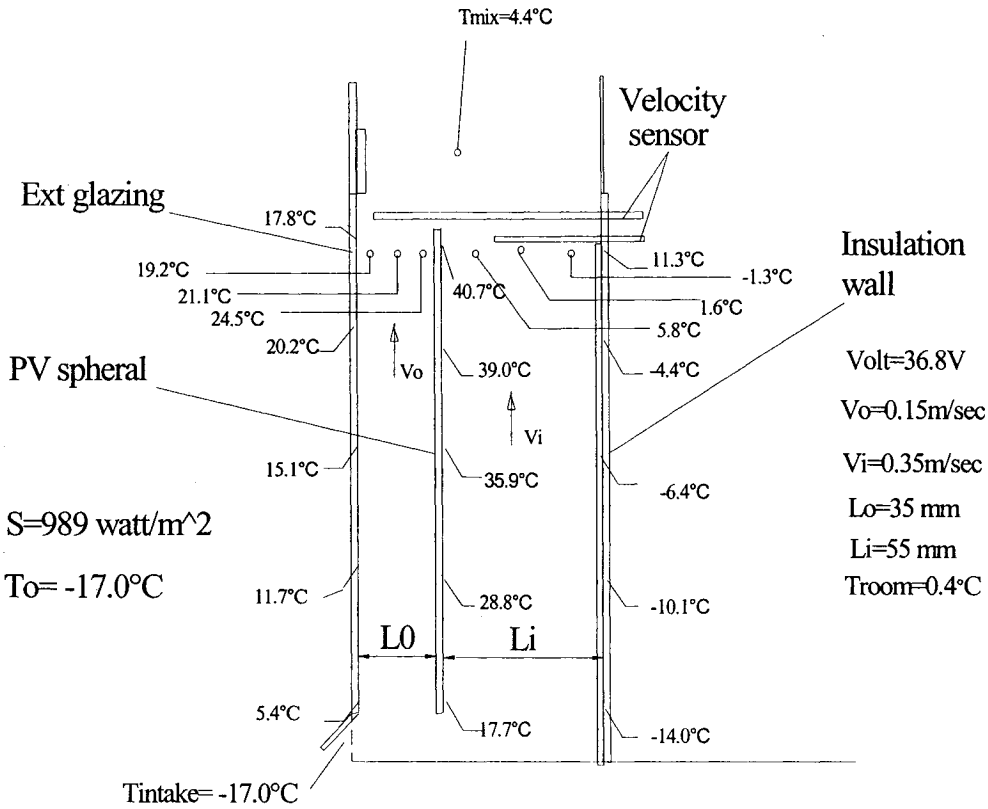

Figure 5.10 Schematic and parameters in Spheral Solar cavity

The power output of the Spheral Solar PV panels (that were connected to a load with a resistance of 27.3 ohms) is measured with the voltage being 36.8 V.

$$Pe = \frac{U^2}{R} \qquad \text{Pe} = 49.5 \text{ W}$$

So the overall efficiency of this collector wall is

$$\eta s = \frac{Qtherm\_o + Qtherm\_i + Pe}{S \cdot A} \qquad \eta_s = 0.709$$

Compared with the previous Photowatt cavity, it is found that the CSW with the Spheral Solar PV panels has higher overall energy efficiency than that with Photowatt PV panels, although the Spheral Solar PV panels in this cavity have low electrical efficiency. That is because

- Photowatt panels are directly exposed to the outside atmosphere, which inevitably loses some heat to the outside; moreover, Spheral Solar PV panels are set in a cavity, and flowing air passes through both sides of these panels.
- Spheral Solar PV panels have low efficiency so they transfer more absorbed solar energy into heat.

The convective coefficients in these cavities can be calculated by setting energy balances on air control volumes as follows,

$$Qtherm\_i = hi \cdot W \cdot H \cdot [Ts + Twall - (Ta\_i + Tin)]$$

$$Qtherm\_o = ho \cdot W \cdot H \cdot [Ts + Tg - (Ta\_o + Tin)]$$

So the convective coefficient in the inner cavity is

$$hi = \frac{Qtherm\_i}{W \cdot H \cdot [Ts + Twall - (Ta\_i + Tin)]} \qquad \text{hi} = 9.7 \text{ W/m}^2\text{℃}$$

The convective coefficient in the outer cavity is

$$ho = \frac{Qtherm\_o}{W \cdot H \cdot [Ts + Tg - (Ta\_o + Tin)]} \qquad \text{ho} = 5.5 \text{ W/m}^2\text{℃}$$

5.7 Performance of a CSW with a PCM board

Figure 5.11 shows the configuration of a cavity with PCM gypsum board. At the bottom of this CSW, a piece of PCM board is attached to the back of the insulation wall. It has a dimension of 1.12m x 0.9m. A single layer of glazing covers the cavity, forming a 0.09m air gap.

Figure 5.12 shows the temperature variation of the PCM board, the room air and the ambient air on the sunny day of November 10, 2003. The solar radiation is 848 W/m^2. Air flows through the CSW by a forced flow with an average velocity of 0.65 m/s. At

about 11:30 AM, a high building shades the test room, so the effect of the PCM gypsum board can be observed. It is found that the temperatures of the outside surface and the inner surface of this PCM board change slowly at the transition point (16.7 ~ 20.0) due to heat released from the PCM board.

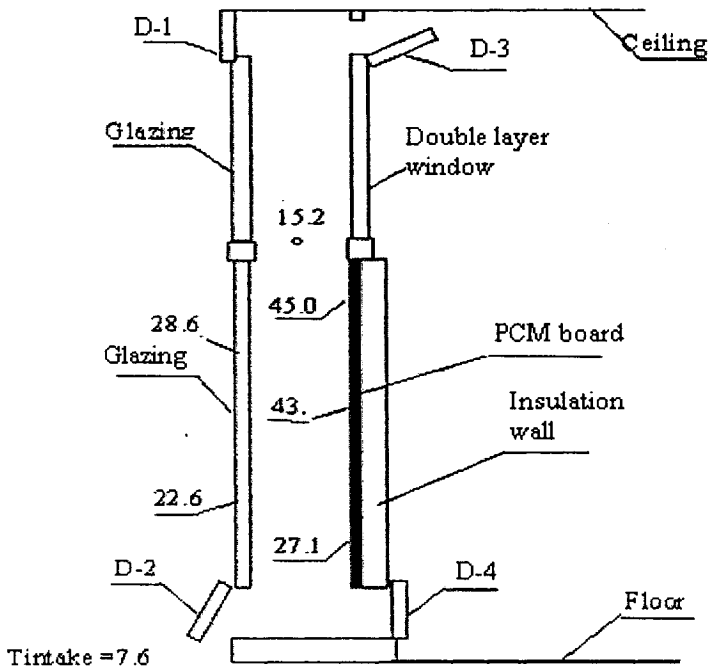

Figure 5.11 Schematic of a cavity with PCM board

The heat transfer through the insulation wall is negligible; an energy balance is performed for the PCM gypsum board as follows:

$$Qs = Si - (Qo + Qair + Qg)$$

where Si represents incident solar energy, Qo represents heat loss to the outside of CSW, Qair represents the heat delivered by air, Qg represents the heat absorbed by glazing and Q_s represents the heat exchanged with PCM gypsum board. The variation of

energy storage in PCM gypsum is shown in Figure 5.13, according to energy conservation principle.

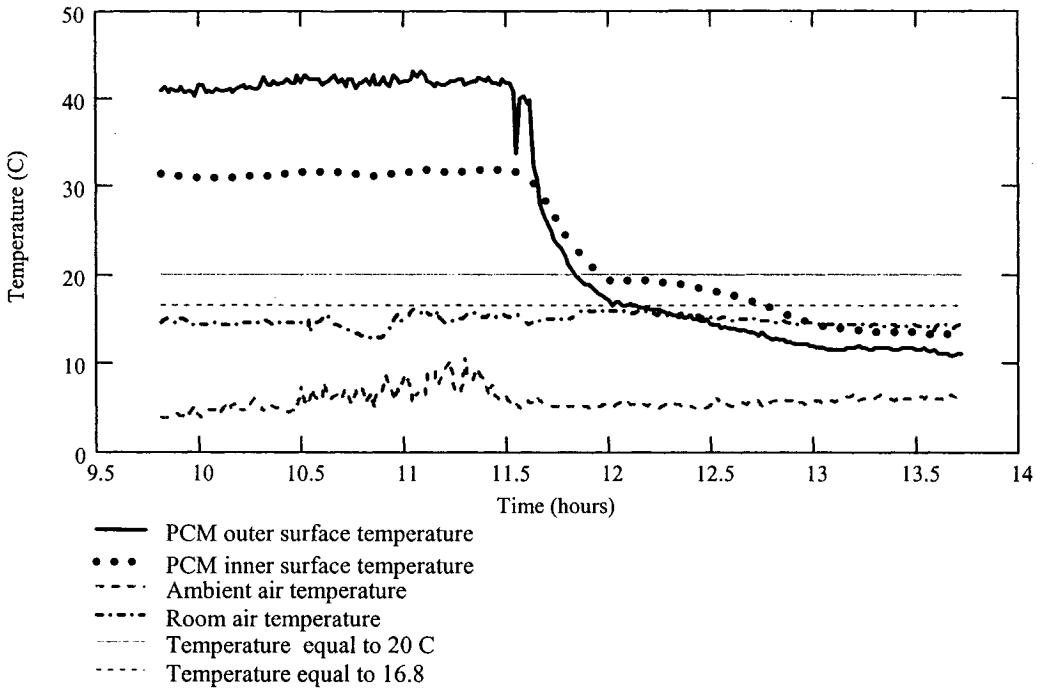

Figure 5.12 Temperature characteristics of PCM gypsum board

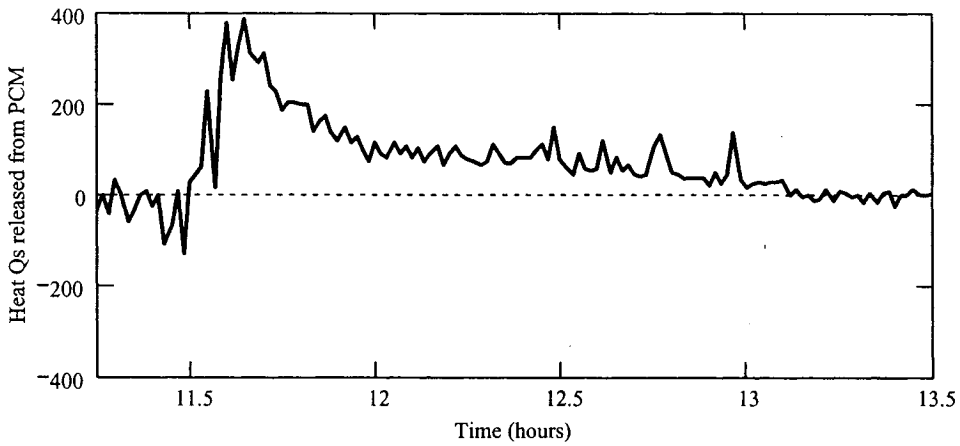

Figure 5.13 Energy release from PCM board

Since the back wall is well insulated, air convection is the only way to affect the room temperature. This air convection determines the thermal performance of this wall

system. During the sunny period around 11:00 AM, no phase change occurred in the PCM gypsum board. The heat delivered to room is

$$Qair = L \cdot W \cdot Vair \cdot \rho \cdot c \cdot (Tout - Tin) \qquad Q_{air} = 480 \text{ W}$$

The efficiency of the wall at this moment is

$$\eta = \frac{Qair}{S \cdot Apcm} \qquad \eta = 0.66$$

When there is no direct sunlight on the CSW and the temperature of the fluid air is continuously dropping and below the PCM transition temperature, the PCM gypsum board begins to release heat until its total latent heat is released. The performance of the PCM gypsum board during this process is attractive, though it cannot be described by an accurate equation. It is just a unique feature of phase change material which absorbs solar thermal energy in the morning and releases it at a time when the surrounding temperature is below the freezing temperature of PCM, thereby further reducing the temperature swing in the room.

Chapter 6 CONCLUSIONS AND RECOMMENDATIONS

6.1 Conclusions

A one-dimensional model has been developed to study the CSWs on the basis of two kinds of airflow: natural convective flow and forced convective flow, focusing on the natural convective flow that has wide application in the design of a passive solar house. Thermal analysis and simulations are carried out mainly for three cases: a traditional masonry CSW, a double façade wall with blinds, and a CSW with a phase change material named PCM gypsum board. The thermal properties of such a PCM are stable compared to those from previous tests. The CSWs that are considered in present study have high thermal performance.

6.1.1 Traditional masonry CSW

The design of a CSW is a necessary step in building a passive solar house with good thermal properties. Some papers have presented general rules for the design of these CSWs (Paul, 1979). This thesis develops more detailed models that can consider combinations with advanced technologies such as PV.

The variation of room temperature decreases as the thickness of the CSW increases. For a CSW that uses concrete as heat storage material, the room temperature swing has a minimum value when the thickness is in a range of 0.35 ~ 0.40m.

A large quantity of thermal mass in the CSW would cause a long heating time-delay in winter and would resist overheating in summer, which is one of the characteristics of the CSW. The time delay approximately changes linearly with the thickness of the wall.

The room gets heat from the CSW wall in two ways: conduction through the wall

and airflow in the cavity of the CSW. The effect of airflow in the gap on room temperature depends upon the gap thickness. Simulations undertaken for this study have shown that the CSW delivers maximum heat when the gap thickness is 0.2 ~ 0.25m.

6.1.2 The effect of PCM in CSW

Tests have shown that the PCM gypsum board (that was developed by Feldman et al. 1995) has the potential to be used as building heat storage material for the following reasons:

- The thermo-physical properties even after an approximate 10-year freeze-thaw cycle are stable,
- It is easy to process and install wherever it is needed,
- It is a good heat storage material because it has appropriate latent heat, high conductivity, and proper transition temperature.
- PCM gypsum board can save precious space that a traditional heat storage wall usually needs. In this study, the PCM can save 75% of traditional masonry material as heat storage material.
- Most importantly, the PCM used in CSWs can enhance the thermal capacity of the wall, thereby avoiding overheating and overcooling which often occur in buildings with large fenestration.

6.1.3 Effect of blind in cavity

When a blind is used in the CSW cavity, three forms of airflow are possible: airflow in front of the blind, airflow behind the blind and airflow on both sides of the blind. Each airflow status has a different effect on the room temperature. In the simulated room, the

maximum decrease of room temperature is 2.0 °C. When the airflow passes through both sides of the cavities, the effect of decreasing the temperature is the most obvious compared with airflow passing through only one side of the cavity. Furthermore, airflow that passes behind the blind has better effect than airflow in front of the blind.

6.1.4 Comparison with test results

Both the natural convective coefficient and the air velocity change with the intensity of solar radiation under conditions of natural convective flow. The air velocity varies in the range of 0.2 ~ 0.35m/s during the sunshine hours; the convective coefficient changes accordingly in the range of 4.0 ~ 4.8 W/m^2 °C. The test results reveal the effects of these two items and prove that the air velocity is close to the calculated value.

In forced convective flow, model validation shows that there is a significant agreement between the simulation and the actually measured value only when the theoretically calculated convective coefficient is multiplied by a constant of 1.6. This factor of 1.6 is appropriate for the following two factors: the wall's specific structure (such as an air inlet with 90° bent and signal wires) and the actual variable velocity, which would cause a strong turbulent flow with a high convective coefficient.

6.1.5 Integrated PV collector storage walls

The integration of photovoltaic panels into the CSW presents advantages for future applications:

- Low overall cost. Such a set-up does not need a large frame and complex outdoor control system, which a PV system usually requires. PV integrated with a building façade will improve the cost effectiveness of the system.

• High and stable efficiency. PV panels not only produce useful electricity, but are also a good heat collector (absorptance around 96%). In winter, the CSW system with Photowatt panels has an overall efficiency of 62%, and the system with Spheral Solar panels reaches 71% efficiency.

6.2 Recommendations for future work

As mentioned in Chapter 2, a CSW is a complex system with many interrelated parameters. When phase change material is integrated into this system, considerable uncertainty arises due to its inherent complexity. Therefore, modeling such a system accurately is a challenging process. The following is a list of research areas that have been only briefly touched upon in this study but will benefit future work.

- A detailed investigation into CSW is needed. This wall system relies solely on thermal buoyancy as the driving force. It is easily affected by many factors.
- The influence of inlet/outlet configurations on parameters such as the convective heat transfer coefficient, mass-flow rate, should be taken into account.
- The role played by the fact that a part of the air in the room circulates through a CSW wall on the wall system should be studied, though a few tests in this study have briefly proved that it benefits thermal performance of a room in the heating season.
- The wind effect on the wall system should be investigated. The tests that were carried out in this study have shown that the wind has a large effect on airflow in the cavity of the CSW, especially in the case of the natural convective flow.

- Control strategies should be investigated for the CSW system. The performance of the CSW system with the PCM relies on indoor air requirements. The appropriate controls enable the CSW system to work efficiently. For example, the opening position of a damper affects the airflow significantly in the cavity with Spheral Solar PV panels. Using the control, the CSW system could always make an useful contribution to the room.
- Exploration of the PCM transition mechanism is needed. One important aspect in this field is to investigate the effect of solar radiation on the heat transfer of PCM gypsum board.
- The optimization of CSW system parameters such as airflow rate, geometric dimensions, should be investigated.

With the completion of the work listed above, a new detailed model can be developed, and the performance of the CSW will be improved.

REFERENCES

Athienitis. A. K. and Santamouris. M, 2002, Thermal Analysis and Design of Passive Solar Buildings. James and James, London UK.

Athenitis. A. K and Tzempelikos. A, 2002, A Methodology for Simulation of Daylight Room Illumination and Light Dimming for a Room with a Controlled Shading Device, Solar Energy Vol. 72, No 4, pp.271-281

Athenitis. A. K, 1999, Building Thermal Analysis, Electronic MathCAD Book, second edition, Mathsoft Inc., Boston, U.S.A

Athienitis, A. K., 1999, Thermal Analysis of Buildings in a Mathematical Programming Environment and Applications, Building and Environment, Vol. 34, pp.401-415

Athienitis. A. K, Liu. C. et al, 1997, Investigation of The Thermal Performance of A Passive Solar Test with Wall Latent Heat Storage, Building and Environment, Vol. 32, No.5, pp.405-410.

Athienitis, A. K., 1994, A Numerical Model of a Floor Heating System, ASHRAE Trans., Vol. 100, Part 1, pp.1024 1030.

Athenitis. A. K, 1993, A Methodology for Integrated Building-HVAC System Thermal Analysis. Building and Environment, Vol.20, pp. 483 496.

Athienitis.A.K and Shou. J, 1991, Control of a Radiant Heating System Based on the Operative Temperature, ASHRAE Trans. Vol.97, part 1, pp.787-798.

Anderson. B, Riordan. M et al. 1976, Solar Home Book: heating, cooling, and designing with the sun, Brick House Publishing.

Bejan, A, 1995, Convective Heat Transfer. Second edition, New York, J. Wiley, U.S.A.

Bourdeau, L. E. 1980, Study of Two Passive Solar Systems Containing Phase Change Material for Thermal Storage. The 5th National Passive Solar Conference.

Banu. D, Feldman. D, 1998, Evaluation of Thermal Storage as Latent Heat in Phase Change Material Wallboard by Differential Scanning Calorimetry in Large Scale Thermal Testing, Thermochimica Acta, Vol. 3926, pp. 1-7.

Bajnoczy. G.et al, 2001, Heat Storage by Two-grade Phase Change Material, Periodic polytechnic ser. Chemical Engineering. Vol.43

Cao.Y, Faghri.A and Juhasz. A, 1991, A PCM/forced Convection Conjugate Transient Analysis of Energy Storage Systems with Annular and Countercurrent Flows, Journal of Heat Transfer, Feb,Vol.113, pp.37-42.

Cox. J.E. 2000, Canada's Energy Assessment. ASHRAE Journal, Vol. 42, No. 7, pp 22.

Charron, R and Athienitis. A.K, 2003. A Two-dimensional Model of a PV-integrated Double Façade. SESCI 2003 conference.

Chunyan L.1996, Thermal Performance of a Room with Wall Latent Heat Storage, Master Thesis, Concordia University.

Darkwa. K, Kim, J. S, 2003, Dynamics of Energy Storage in Phase Change Drywall Systems, Energy Research, Vol.27, No.3, pp.215-223

Douglas. W. H, 1991, Latent Heat Storage in Concrete, PhD Thesis, Concordia University;

Dincer. I, Rosen. M. A, 2001, Thermal Energy Storage System and Applications. Wiley, New York. U.S.A.

Feldman. D, Khan. M. A, and Banu. D, 1989, Energy Storage Composite with Organic PCM, Solar Energy Materials, Vol.18, pp.333-341

Feldman.D, et al, 1995, Development and Application of Organic Phase Change Mixtures in Thermal Storage Gypsum Wallboard, Solar Energy Materials and Solar Cells, Vol. 36, pp.147-157.

Franta, G.E , 1978, Solar Architecture, Ann Arbor Science, pp. 83-110

Garg. H.P, Muilick. S.C, Bhargava. A.K, 1985, Solar thermal Energy Storage, USA.

Holman. J. P, 2002, Heat Transfer, ninth edition, New York, McGraw-Hill, U.S.A.

Hensen. J, Bartak. M., et al, 2002, Modeling and Simulation of A Double-skin Façade System, ASHRAE Transactions, Vol.108, part2, pp.1251-1258

Heinrich Manz, 2003, Numerical Simulation of Heat Transfers by Natural Convection in Cavities of Façade Elements, Energy and Buildings. Vol.35, No.3, pp.305-311

Hawes. D.W and Feldman. D, 1992, Absorption of Phase Change Materials in Concrete, Solar Energy Materials and Solar Cells. Vol. 27, No.2, pp.91-101.

Hawes. D.W, Banu. D and Feldman. D, 1992, The Stability of Phase Change Materials in Concrete, Solar Energy Materials and Solar Cells Vol.27. No.2, pp.102-118.

Incropera F, et al, 1985, Fundamentals of Heat and Mass Transfer, second edition, Wiley, U.S.A.

Jaluria.Y, 1980, Natural Convection: Heat and Mass Transfer, Pergamon Press, Oxford.

Long. K, et al, 1979, Fluid Mechanics in Engineering Application, Industry publisher, Beijing, China.

Kaushik. S.C et al, 2000, Periodic Heat Transfer and Load Leveling of Heat Flux Through A PCM Thermal Storage Wall/roof in An Air-conditioned Building, Building and Environment, Vol.16 (2), pp.99-108.

Kedl. R.J, 1990, Conventional Wallboard with Latent Heat Storage for Passive Solar Applications, Proceedings of the Intersociety Energy Conversion Engineering Conference, Vol.4, pp.222-225.

Mei L, et al, 2003, Thermal Modeling of A Building with an Integrated Ventilated PV Façade, Energy and Buildings, Vol. 35, No.6, pp. 605-617.

Morgan. K, A, 1981, Numerical Analysis of Freezing and Melting with Convection, Computer Method in Applied Mechanics and Engineering, 8th IBPSA conference, North Holland.

Muneer. T, Kubie. J and Grassie. T, 2003, Heat transfer –A Problem Solving Approach, Taylor & Francis, U.S.A.

Neeper.D.A, 2000, Thermal Dynamics of Wallboard with Latent Heat Storage, Solar Energy, Vol. 68, No. 5, pp. 393-403.

Ozisik. M.N and Uzzell. J.C, 1979, Exact Solution for Freezing in Cylindrical Symmetry with Extended Freezing Temperature Range, Journal of Heat Transfer, Vol.101, No. 2, pp.331-334

Paul. J.K, Passive Solar Energy Design and Materials, Noyes Data Corp. U.S.A.

Ramachandran.V.S, etc, 2003, Handbook of Thermal Analysis of Construction Materials. Noyes Publications, U.S.A.

Reddy.J.N, Gartling.D.K, 2001, The Finite Element Method in Heat Transfer and Fluid Dynamics, second edition, CRC Press.

Reddy. B.V and Jagadish. K.S, 2003, Embodied Energy of Common and Alternative Building materials and Technologies, Energy and Buildings, Vol.35, No.2, pp.129-137.

Rohsenow. W, Hartnett. J. P, Cho.Y. I, 1998, Handbook of heat transfer, third edition, McGraw-Hill, U.S.A.

Scalat. S, Banu. D, et al, 1996, Full scale thermal testing of latent heat storage in wallboard, solar energy material and solar cells, Vol.44, No.1, pp 49-61.

Scalat. S, Banu. D, et al, 1995, Energy Consumption and Thermal Comfort Conditions in Buildings Using Phase Change Materials, the second international thermal energy congress.

Wade, H, 2003, Solar Photovoltaic Project Development, Paris, French.

APPENDIX A

1. Simultaneously solar radiation on vertical wall

There are two models that can be adopted to calculate solar radiation when theoretical analysis is taken on studies related to solar energy applications: Clear Sky Hottle's model and Average Cleanness Index model. In this study, the Clear Sky Hottle's model is used because of its relative simplicity, directness and accuracy.

Solar time is the basis of calculating solar radiation and is calculated by the following equation:

$$ST = LST + ET + 4 \cdot (STM - LNG) \tag{1}$$

where ST is solar time, LST is local standard time, STM is local standard time meridian, LNG is local longitude, and the ET is time equation that is function of date n_d, which is day number counted from January 1.

$$ET = \left[9.87\sin(4\pi \frac{n_d - 81}{364}) - 7.53\cos(2\pi \frac{n_d - 81}{364}) - 1.5\sin(2\pi \frac{n_d - 81}{364}) \right] \tag{2}$$

The position of the sun and geometric relationship between solar incidence and a plane can be shown in following angles (Figure 3.4):

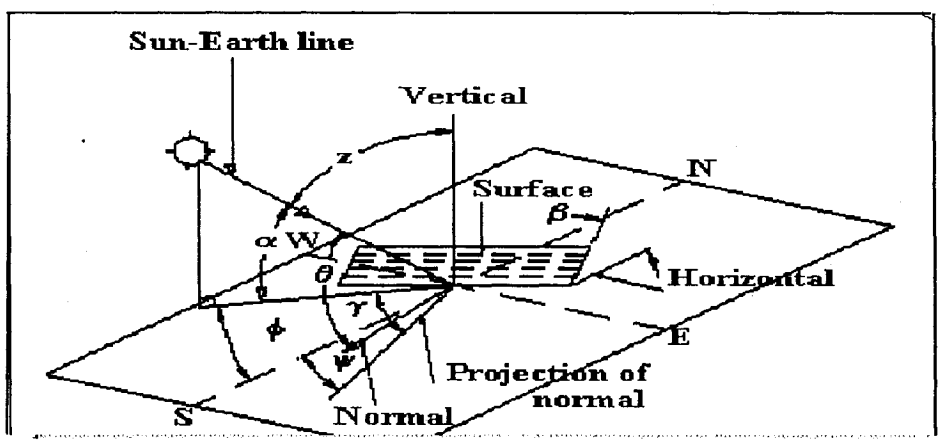

Figure 3.4 Solar radiation geometry for inclined surface

The angle of solar declination δ

$$\delta = 23.45\sin(360\frac{284+n_d}{365}) \tag{3}$$

The hourly angle of sun, h

$$h = 15(ST-12) \tag{4}$$

Solar altitude α

$$\alpha = a\sin(\cos L\cos\delta\cosh + \sin L\sin\delta) \tag{5}$$

Solar azimuth

$$\phi = a\cos(\frac{\sin\alpha\sin L - \sin\delta}{\cos\alpha\cos L}) \tag{6}$$

Surface solar azimuth γ

$$\gamma = \phi - \psi \tag{7}$$

After the surface azimuth ψ and surface tilt angle β are known, so far the incidence angle θ between sunray and plate is

$$\theta = a\cos(\cos\alpha\sin\beta\cos\gamma + \sin\alpha\cos\beta) \tag{8}$$

Transmittance of solar radiation

Solar beam transmittance

$$\tau_b = a_0 + a_1\exp(-\frac{k}{\sin\alpha}) \tag{9}$$

Where the constant a, k depend on climate and altitude A (km)

$$a_0 = r_0[0.4327 - 0.00821(6-A)^2]$$

$$a_1 = r_1[0.5055 - 0.00595(6.5-A)^2]$$

$$k = r_k[0.2711 + 0.01858(2.5-A)^2] \tag{10}$$

Where the correction constants are given in table 3.1

Table 3.1 Correction factors for Hottl's clear sky model (Athienitis, 2002)

Climate type	r_0	r_1	r_k
Tropical	0.95	0.98	1.02
Mid-latitude summer	0.97	0.99	1.02
Sub arctic summer	0.99	0.99	1.01
Mid-latitude winter	1.03	1.01	1.00

After determining the bean transmittance τ_b, the sky diffuse transmittance and ground diffuse transmittance can be determined [Liu and Jordan 1960]

$$\tau_{sd} = 0.271 - 0.294\tau_b \tag{11}$$

$$\tau_{gd} = \tau_b + \tau_{sd} \tag{12}$$

Extraterrestrial normal solar radiation:

$$I_{on} = 1353[1 + 0.033\cos(360\frac{n_d}{365})] \tag{13}$$

Then the beam solar radiation

$$I_b = I_{on}\tau_b \cos\theta \tag{14}$$

The sky diffuse radiation and ground diffuse radiation are respectively,

$$I_{sd} = I_{on}\tau_{sd}\sin\alpha(\frac{1+\cos\beta}{2}) \tag{15}$$

$$I_{gd} = I_{on}\tau_{gd}\sin\alpha(\frac{1-\cos\beta}{2}) \tag{16}$$

So, the total solar energy that passes through a glazing with transmittance τ is,

$$S = \tau \cdot (I_b + I_{sd} + I_{gd}) \tag{17}$$

where τ is the transmittance of glazing, which is also changeable with angle of sunlight incidence θ, is determined by the glazing physical properties n and KL

2 Optical property of glazing

The solar transmittance, reflectance and absorbance are dependent on the sunlight incident angle θ, the glass thickness L, refractive index n, and the extinction coefficient k. The procedure for calculating these properties is given in detail by Athienitis and Santamounris (2002).

Refraction angle θ' is calculated by Snell's law

$$\theta' = a\sin(\frac{\sin(\theta)}{n}) \tag{18}$$

Component reflectivity r

$$r = \frac{1}{2}\cdot\left[\left(\frac{\sin(\theta-\theta')}{\sin(\theta+\theta')}\right)^2 + \left(\frac{\tan(\theta-\theta')}{\tan(\theta+\theta')}\right)^2\right] \tag{19}$$

$$a = \exp\left[-\frac{kL}{\sqrt{1-\left(\frac{\sin(\theta)}{n}\right)^2}}\right] \tag{20}$$

The transmittance and reflectance are respectively,

$$\tau = \frac{(1-r)^2\cdot a}{1-r^2\cdot a^2} \qquad \rho = r + \frac{r\cdot(1-r)^2\cdot a^2}{1-r^2\cdot a^2} \tag{21}$$

From energy conservation, the absorbance is,

$$\alpha = 1-\tau-\rho \tag{22}$$

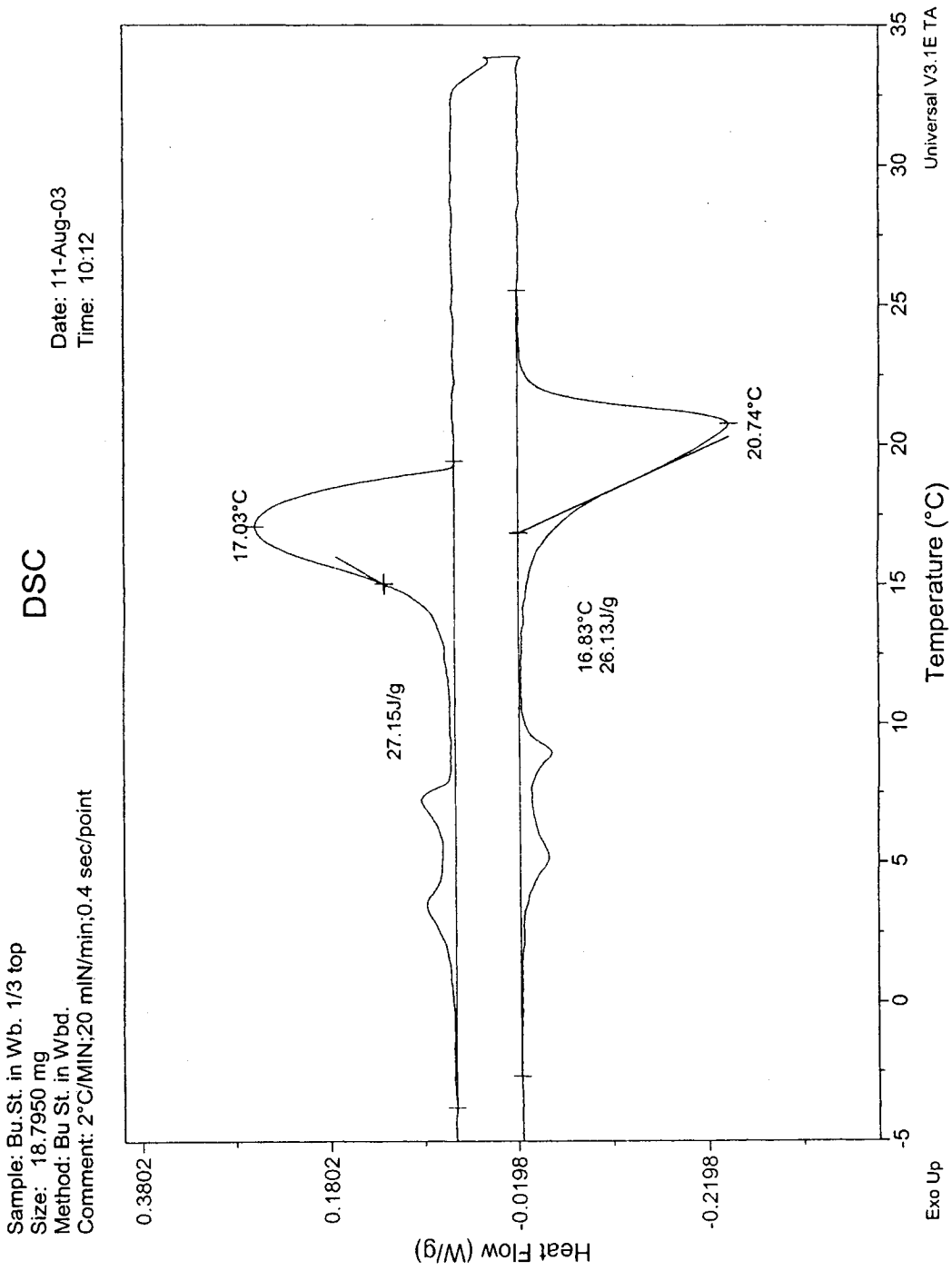

DSC test result of BS-gypsum board in 1/3 top

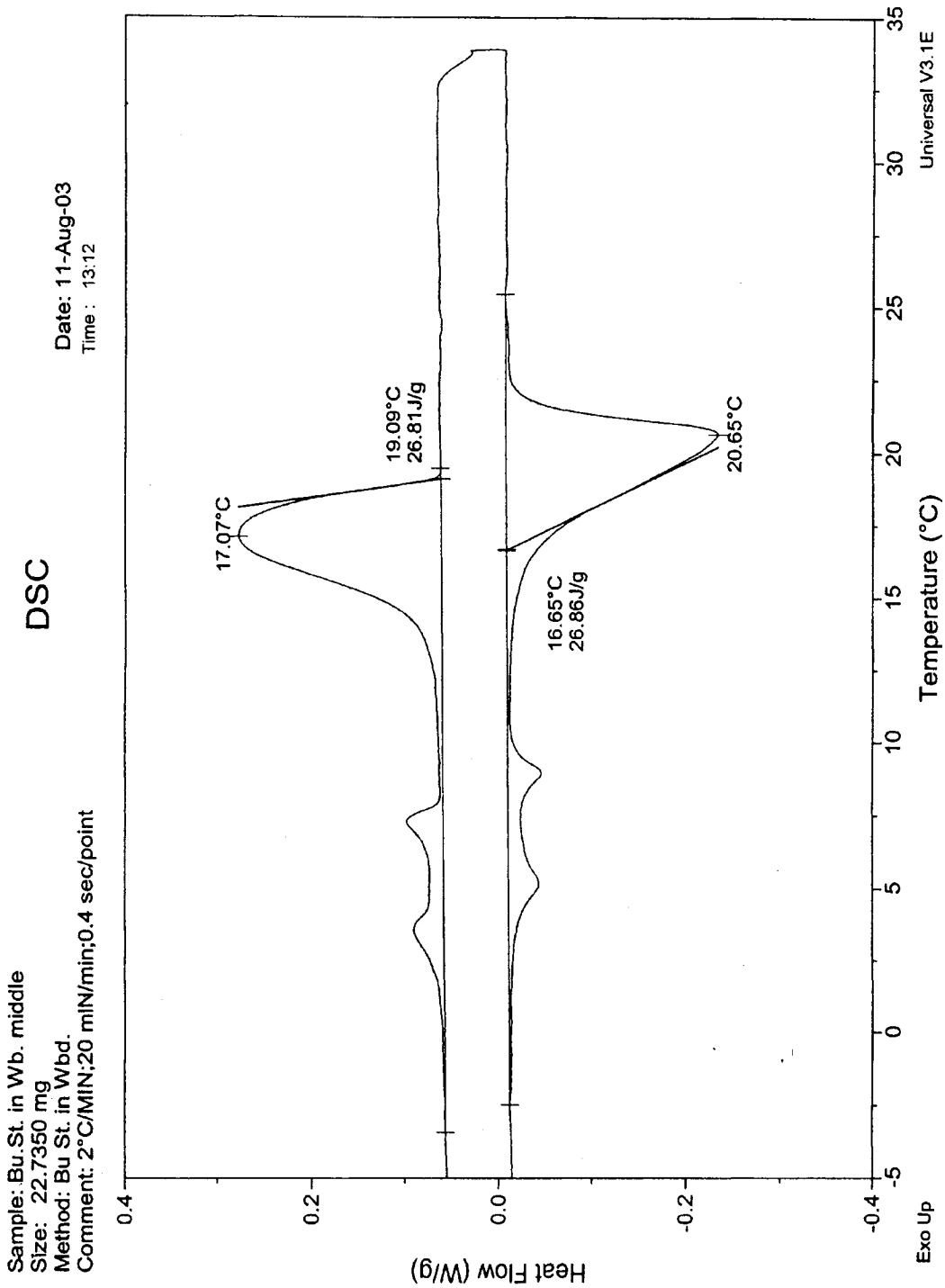

DSC test result of BS-gypsum board in middle

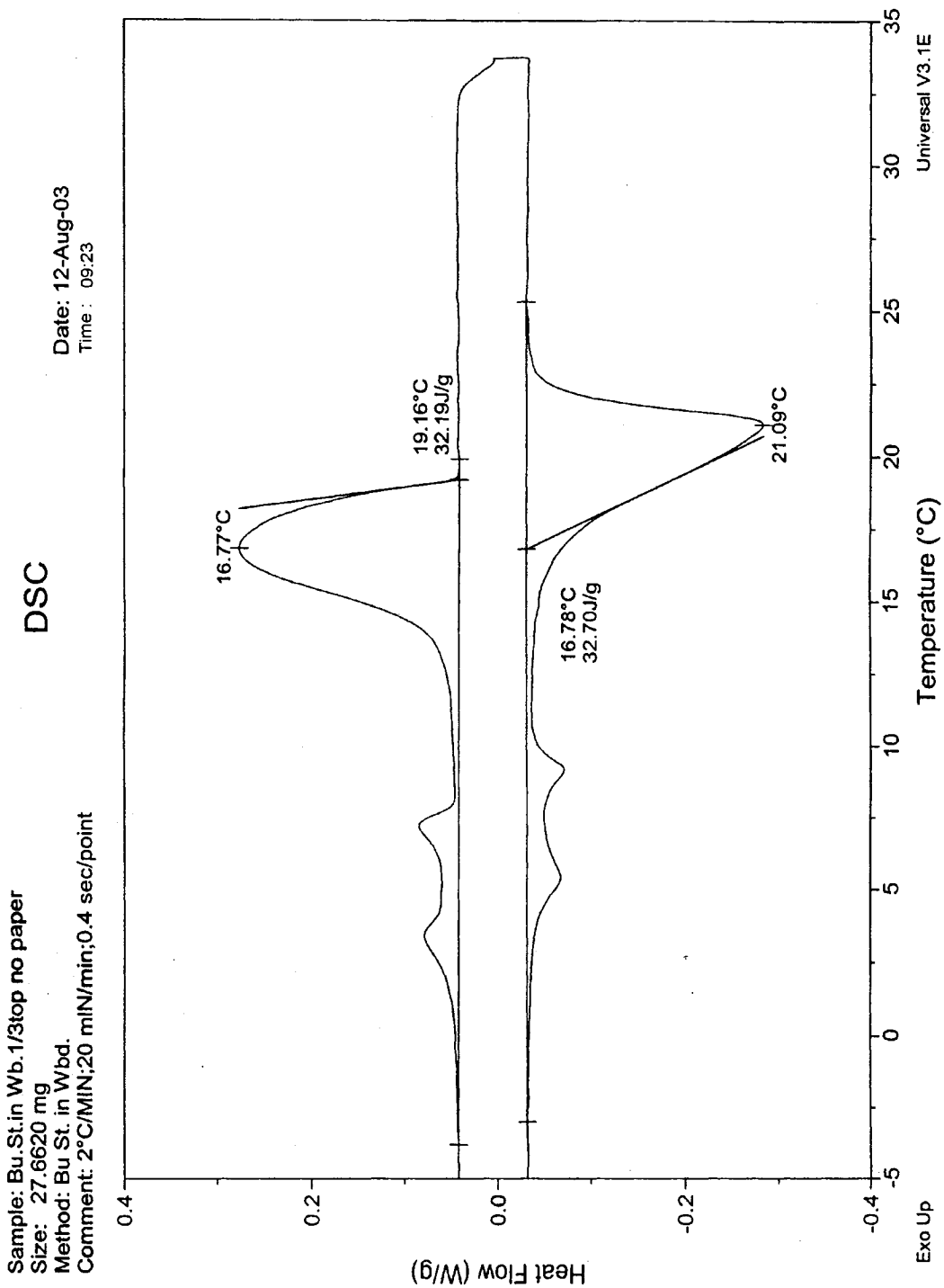

DSC test result of BS-gypsum board in 1/3 top no paper

APPENDIX C

Calculation of natural air velocity by buoyancy.

$$
\begin{aligned}
\text{Vin} = \;& Va \leftarrow 0.1 \cdot \frac{m}{sec} \\
& Re \leftarrow \frac{\rho a \cdot Va \cdot La}{\mu} \\
& D_{it} \leftarrow \frac{W \cdot La \cdot Va \cdot ca \cdot \rho a}{W \cdot h_{it}} \\
& Tfm_{it} \leftarrow \frac{1}{11} \cdot \left[\sum_i \left[\left(\frac{Tb_{it} + T0_{it}}{2} \right) + \left(To_{it} - \frac{Tb_{it} + T0_{it}}{2} \right) \cdot \exp\left(\frac{-X_i \cdot 2}{D_{it}} \right) \right] \right] \\
& f \leftarrow \text{if}\left[Re \le 2500, \frac{64}{Re}, 0.11 \cdot \left(\frac{e}{La} + \frac{68}{Re} \right)^{0.25} \right] \\
& Vin_{it} \leftarrow \sqrt{\frac{2 \cdot g \cdot \left[\rho a \cdot \frac{\left(Tfm_{it} - To_{it} \right)}{Tfm_{it} + 273 \cdot degC} \right] \cdot H}{\rho a \cdot \left(Ci + Co + f \cdot \frac{H}{La} \right)}} \\
& \text{while } \left| Vin_{it} - Va \right| > 0.1 \cdot \frac{m}{sec} \\
& \quad Va \leftarrow Va + 0.1 \cdot \frac{m}{sec} \\
& \quad Re \leftarrow \frac{\rho a \cdot Va \cdot La}{\mu} \\
& \quad D_{it} \leftarrow \frac{W \cdot La \cdot Va \cdot ca \cdot \rho a}{W \cdot h_{it}} \\
& \quad Tfm_{it} \leftarrow \frac{1}{11} \cdot \left[\sum_i \left[\left(\frac{Tb_{it} + T0_{it}}{2} \right) + \left(To_{it} - \frac{Tb_{it} + T0_{it}}{2} \right) \cdot \exp\left(\frac{-X_i \cdot 2}{D_{it}} \right) \right] \right] \\
& \quad f \leftarrow \text{if}\left[Re \le 2500, \frac{64}{Re}, 0.11 \cdot \left(\frac{e}{La} + \frac{68}{Re} \right)^{0.25} \right] \\
& \quad Vin_{it} \leftarrow \sqrt{\frac{2 \cdot g \cdot \left[\rho a \cdot \frac{\left(Tfm_{it} - To_{it} \right)}{Tfm_{it} + 273 \cdot degC} \right] \cdot H}{\rho a \cdot \left(Ci + Co + f \cdot \frac{H}{La} \right)}} \\
& Vin_{it}
\end{aligned}
$$

APPENDIX D

Simulation on Natural airflew that passes through both sides of blinds.

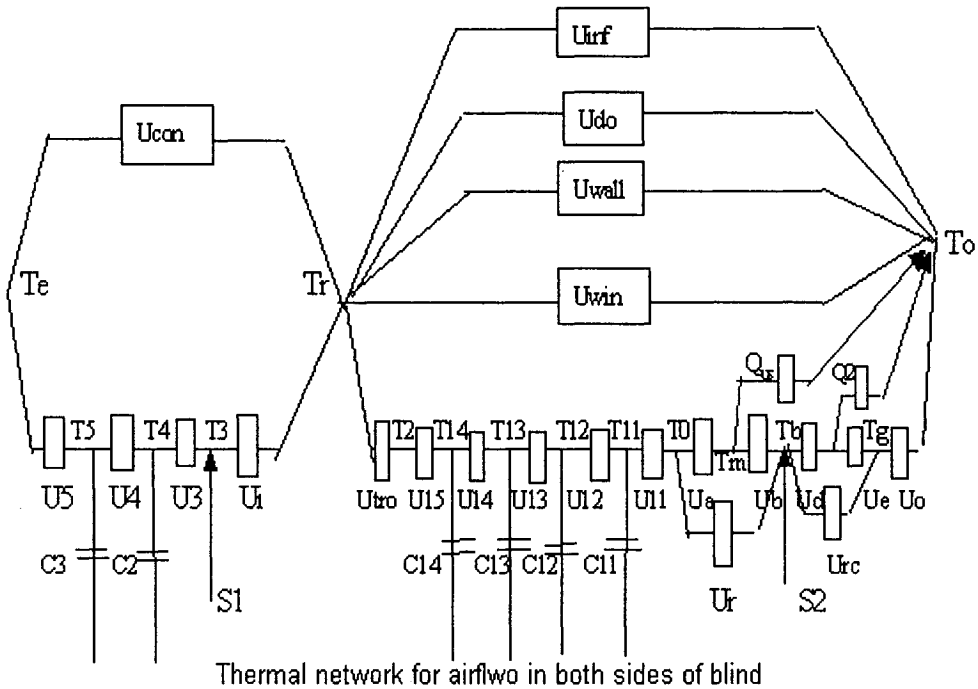

Thermal network for airflwo in both sides of blind

Assume the room to have the following dimensions: 3.5m* 3.5m *3.5m . window 1.5m* 1.5m ;the trombe wall has a equavelent dimension: 3.0m *1.5m ,the gap thickness is 0.5m, the floor consists of 0.2m thickness concrete, the thickness of absorption material in trombe wall is 0.1m (concrete).

degC := 1

assume that convetive coefficient of outside and inside $ho := 20 \cdot \frac{watt}{m^2 \cdot degC}$ $hi := 8 \cdot \frac{watt}{m^2 \cdot degC}$

the floor thickness Lf := 0.2m

the thickness of concrete in gap Lg := 0.35m

emissivity of inner wall and exteroi glazing ε0 := 0.9 εg := 0.8

the properties of concrete $km := 1.7 \cdot \frac{watt}{m \cdot degC}$ $cm := 800 \cdot \frac{J}{kg}$ $\rho m := 2200 \cdot \frac{kg}{m^3}$

$V := 3.5^3 \cdot m^3$

Awin := 1.5m·1.5m Ado := 1.0m·2.0m Atro := 1.5m·3m Acon := 3.5m·3.5m

$Aflo := 3.5^2 \cdot m^2$ $Awall := 3.5^2 \cdot m^2 + 2 \cdot 3.5^2 \cdot m^2 - Ado$ $Awall = 34.75\,m^2$

$$Awall := 3.5^2 \cdot m^2 + 2 \cdot 3.5^2 \cdot m^2 - Ado$$

$$Rwall := 3.0 \cdot \frac{m^2 \cdot degC}{watt} \qquad Rwin := 0.34 \cdot \frac{m^2 \cdot degC}{watt} \qquad Rdo := 1.0 \cdot \frac{m^2 \cdot degC}{watt}$$

$$Uwin := \frac{Awin}{Rwin} \qquad Uwall := \frac{Awall}{Rwall} \qquad Udo := \frac{Ado}{Rdo}$$

$$Ucon := \frac{Acon}{Rwall} \qquad Utro := Atro \cdot hi \qquad Uo := ho \cdot Atro \qquad Ui := Aflo \cdot h$$

$$U11 := Atro \cdot \frac{km \cdot 8}{Lg} \qquad U12 := \frac{U11}{2} \qquad U13 := U12 \qquad U14 := U12$$

$$U15 := U11 \qquad U3 := Aflo \cdot \frac{km}{Lf} \cdot 4 \qquad U4 := \frac{U3}{2} \qquad U5 := U3$$

the time interval

$$Cm1 := \rho m \cdot cm \cdot Atro \cdot \frac{Lg}{4} \qquad \frac{Cm1}{U11 + U12} = 2.642 \times 10^3 \, s$$

$$C12 := \rho m \cdot cm \cdot Atro \cdot \frac{Lg}{4} \qquad \frac{C12}{U12 + U13} = 3.963 \times 10^3 \, s$$

$$Cm2 := \rho m \cdot cm \cdot Aflo \cdot \frac{Lf}{2} \qquad \frac{Cm2}{U3 + U4} = 3.451 \times 10^3 \, s$$

time interval $Dt := 180 \cdot sec$

air properties:

$$ka := 0.0247 \cdot \frac{watt}{m \cdot degC} \qquad \rho a := 1.2 \cdot \frac{kg}{m^3} \qquad ca := 1000 \cdot \frac{J}{kg}$$

$$Cair := V \cdot \rho a \cdot ca \qquad ach := 1$$

air circulation per hour

$$Uinf := \frac{ach \cdot \rho a \cdot ca \cdot V}{3600 \cdot sec}$$

$$Ut := Uinf + Udo + Uwall + Uwin$$

Energy balances on each node

$$Uo \cdot (To_{it} - Tg_{it}) + Ue \cdot (Tn - Tg_{it}) + Urc \cdot (Tb_{it} - Tg_{it}) = 0$$

$$Ue \cdot (Tg_{it} - Tn_{it}) + Ud \cdot (Tb_{it} - Tn_{it}) - Q2_{it} = 0$$

$$Ud \cdot (Tn_{it} - Tb_{it}) + Urc_{it} \cdot (Tg_{it} - Tb_{it}) + Ub \cdot (Tm_{it} - Tb_{it}) + Ur_{it} \cdot (T0_{it} - Tb_{it}) + S_{it} = 0$$

$$Ua \cdot (T0_{it} - Tm_{it}) + Ub \cdot (Tb_{it} - Tm_{it}) - Qu_{it} = 0$$

$$Ua \cdot (Tm_{it} - T0_{it}) + Ur \cdot (Tb_{it} - T0_{it}) + U11 \cdot (T11 - T0_{it}) = 0$$

$$Cm1\cdot\frac{\left(T11_{it+1}-T11_{it}\right)}{Dt}=U12\cdot\left(T12_{it}-T11_{it}\right)+U11\cdot\left(T0_{it}-T11_{it}\right)$$

$$Cm1\cdot\frac{\left(T12_{it+1}-T12_{it}\right)}{Dt}=U13\cdot\left(T13_{it}-T12_{it}\right)+U12\cdot\left(T11_{it}-T12_{it}\right)$$

$$Cm1\cdot\frac{\left(T13_{it+1}-T13_{it}\right)}{Dt}=U14\cdot\left(T14_{it}-T13_{it}\right)+U13\cdot\left(T12_{it}-T13_{it}\right)$$

$$Cm1\cdot\frac{\left(T14_{it+1}-T14_{it}\right)}{Dt}=U15\cdot\left(T2_{it}-T14_{it}\right)+U14\cdot\left(T13_{it}-T14_{it}\right)$$

$$Utro\left(Tr_{it}-T2_{it}\right)=U15\cdot\left(T14_{it}-T2_{it}\right)$$

$$Cair\cdot\frac{Tr_{it+1}-Tr_{it}}{Dt}=Ui\cdot\left(T3_{it}-Tr_{it}\right)+Ucon\cdot\left(Te-Tr_{it}\right)+Ut\cdot\left(To_{it}-Tr_{it}\right)+Utro\cdot\left(T2_{it}-Tr_{it}\right)$$

$$S1+Ui\cdot(Tr-T3)+U3\cdot(T4-T3)=0$$

$$Cm2\cdot\frac{\left(T4_{it\_1}-T4_{it}\right)}{Dt}=U3\cdot\left(T3_{it}-T4_{it}\right)+U4\cdot\left(T5_{it}-T4_{it}\right)$$

$$Cm2\cdot\frac{\left(T5_{it+1}-T5_{it}\right)}{Dt}=U4\cdot\left(T4_{it}-T5_{it}\right)+U5\cdot\left(Te-T5_{it}\right)$$

$$\begin{pmatrix}Tg_0\\Tm_0\\Tb_0\\T0_0\\T11_0\\T12_0\\T13_0\\T14_0\\T2_0\\Tr_0\\T3_0\\T4_0\\T5_0\end{pmatrix}:=\begin{pmatrix}15\\20\\22\\22\\22\\22\\22\\22\\22\\22\\22\\22\\22\end{pmatrix}$$

$K := 1$

$\sigma := 5.67\cdot10^{-8}\cdot\frac{watt}{m^2\cdot K}$

$e := 3.0mm$

$Ra_0 := 30000$

$Tre_0 := 0.5\cdot degC$

$Nudf_0 := 1383$

$h_0 := 3\cdot\frac{watt}{m^2\cdot degC}$

$h2_0 := 3\cdot\frac{watt}{m^2\cdot degC}$

$c := 1.32$

$Ur_0 := 10\cdot watt$

$Urc_0 := 10\cdot watt$

$Tn_0 := 18$

$Ra2_0 := 30000$

$Tre2_0 := 0.5\cdot degC$

$Nufd2_0 := 1400$

$Vcir_0 := 0.1\cdot\frac{m}{sec}$

$Vci2_0 := 0.2\cdot\frac{m}{sec}$

$$g \cdot La^3 \cdot \frac{\left[0.5 \cdot (Tg_{it} + Tb_{it}) - To_{it}\right]}{\left[273 + 0.5 \cdot (Tg_{it} + Tb_{it})\right] \cdot (\alpha 1 \cdot \nu)}$$

$$\text{if}\left(\frac{Tg_{it} - To_{it}}{Tb_{it} - To_{it}} \geq 1, 0, \frac{Tg_{it} - To_{it}}{Tb_{it} - To_{it}}\right)$$

$$\frac{4 \cdot (Tre2_{it})^2 + 7 \cdot Tre2_{it} + 4}{90 \cdot (1 + Tre2_{it})^2} \cdot Ra2_{it}$$

$$\text{if}\left(\frac{ka}{La} \cdot \frac{Ra2_{it}}{24} \leq 2 \cdot \frac{watt}{m^2 \cdot degC}, 2 \cdot \frac{watt}{m^2 \cdot degC}, \frac{ka}{La} \cdot \frac{Ra2_{it}}{24}\right) \quad \text{if} \quad Ra2_{it} < 10$$

$$\text{if}\left[\frac{ka}{La} \cdot c \cdot Ce \cdot (Ra2_{it})^{0.25} \leq 2 \cdot \frac{watt}{m^2 \cdot degC}, 2 \cdot \frac{watt}{m^2 \cdot degC}, \frac{ka}{La} \cdot c \cdot Ce \cdot (Ra2_{it})^{0.25}\right] \quad \text{if} \quad 10 \leq Ra2_{it} \leq 10^5$$

$$\frac{ka}{La} \cdot \left[(Nufd2_{it} + 0.00001)^x + \left[c \cdot Ce \cdot (Ra2_{it})^{0.25}\right]^x\right]^{\frac{1}{x}} \quad \text{if} \quad Ra2_{it} > 10^5$$

$$0 \cdot \frac{m}{sec} \quad \text{if} \quad To_{it} \geq 0.5 \cdot (Tg_{it} + Tb_{it})$$

otherwise

$$Va2 \leftarrow 0.1 \cdot \frac{m}{sec}$$

$$Re2 \leftarrow \frac{\rho a \cdot Va2 \cdot La}{\mu}$$

$$D2_{it} \leftarrow \frac{W \cdot La \cdot Va2 \cdot ca \cdot \rho a}{W \cdot h2_{it}}$$

$$Tfm2_{it} \leftarrow \frac{1}{11} \cdot \left[\sum_i \left[\left(\frac{Tb_{it} + Tg_{it}}{2}\right) + \left(To_{it} - \frac{Tb_{it} + Tg_{it}}{2}\right) \cdot \exp\left(\frac{-X_i \cdot 2}{D2_{it}}\right)\right]\right]$$

$$f2 \leftarrow \text{if}\left[Re2 \leq 2500, \frac{64}{Re2}, 0.11 \cdot \left(\frac{e}{La} + \frac{68}{Re2}\right)^{0.25}\right]$$

$$Vin2_{it} \leftarrow \sqrt{\frac{2 \cdot g \cdot \left[\rho a \cdot \frac{(Tfm2_{it} - To_{it})}{Tfm2_{it} + 273 \cdot degC}\right] \cdot H}{\rho a \cdot \left(Ci + Co + f2 \cdot \frac{H}{La}\right)}}$$

while $\left|Vin2_{it} - Va2\right| > 0.1 \cdot \frac{m}{sec}$

$$
\begin{pmatrix} Ra2_{it} \\ Tre2_{it} \\ Nufd2_{it} \\ h2_{it} \\ Vci2_{it+1} \\ Qu2_{it} \\ Ra_{it} \\ Tre_{it} \\ Nufd_{it} \\ h_{it} \\ Vcir_{it+1} \\ Qu_{it} \\ Ur_{it} \\ Urc_{it} \\ Tg_{it+1} \\ Tn_{it+1} \\ Tb_{it+1} \end{pmatrix} :=
$$

$$
\begin{cases}
\begin{cases}
\begin{cases}
Va2 \leftarrow Va2 + 0.1 \cdot \dfrac{m}{sec} \\
Re2 \leftarrow \dfrac{\rho a \cdot Va2 \cdot La}{\mu} \\
D2_{it} \leftarrow \dfrac{W \cdot La \cdot Va2 \cdot ca \cdot \rho a}{W \cdot h2_{it}} \\
Tfm2_{it} \leftarrow \dfrac{1}{11} \cdot \left[\sum_i \left[\left(\dfrac{Tb_{it} + Tg_{it}}{2} \right) + \left(To_{it} - \dfrac{Tb_{it} + Tg_{it}}{2} \right) \cdot \exp\left(\dfrac{-X_i \cdot 2}{D2_{it}} \right) \right] \right] \\
f2 \leftarrow if\left[Re2 \le 2500, \dfrac{64}{Re2}, 0.11 \cdot \left(\dfrac{e}{La} + \dfrac{68}{Re2} \right)^{0.25} \right] \\
Vin2_{it} \leftarrow \sqrt{\dfrac{2 \cdot g \cdot \left[\rho a \cdot \dfrac{(Tfm2_{it} - To_{it})}{Tfm2_{it} + 273 \cdot degC} \right] \cdot H}{\rho a \cdot \left(Ci + Co + f2 \cdot \dfrac{H}{La} \right)}}
\end{cases} \\
Vin2_{it}
\end{cases} \\
W \cdot La \cdot Vci2_{it} \cdot \rho a \cdot ca \cdot \left[To_{it} - \dfrac{(Tb_{it} + Tg_{it})}{2} \right] \cdot \left[\exp\left[\dfrac{-H \cdot 2}{\left(\dfrac{W \cdot La \cdot Vci2_{it} \cdot ca \cdot \rho a}{W \cdot h2_{it}} + 0.00001 \cdot m \right)} \right] - 1 \right] \\
g \cdot La^3 \cdot \dfrac{\left[0.5 \cdot (T0_{it} + Tb_{it}) - To_{it} \right]}{\left[273 + 0.5 \cdot (T0_{it} + Tb_{it}) \right] \cdot (\alpha 1 \cdot \nu)} \\
if\left(\dfrac{T0_{it} - To_{it}}{Tb_{it} - To_{it}} \ge 1, 0, \dfrac{T0_{it} - To_{it}}{Tb_{it} - To_{it}} \right) \\
\dfrac{4 \cdot (Tre_{it})^2 + 7 \cdot Tre_{it} + 4}{90 \cdot (1 + Tre_{it})^2} \cdot Ra_{it} \\
\begin{cases}
if\left(\dfrac{ka}{La} \cdot \dfrac{Ra_{it}}{24} \le 2 \cdot \dfrac{watt}{m^2 \cdot degC}, 2 \cdot \dfrac{watt}{m^2 \cdot degC}, \dfrac{ka}{La} \cdot \dfrac{Ra_{it}}{24} \right) & \text{if } Ra_{it} < 10 \\
if\left[\dfrac{ka}{La} \cdot c \cdot Ce \cdot (Ra_{it})^{0.25} \le 2 \cdot \dfrac{watt}{m^2 \cdot degC}, 2 \cdot \dfrac{watt}{m^2 \cdot degC}, \dfrac{ka}{La} \cdot c \cdot Ce \cdot (Ra_{it})^{0.25} \right] & \text{if } 10 \le Ra_{it} \le 10^5 \\
\dfrac{ka}{La} \cdot \left[(Nufd_{it} + 0.00001)^z + \left[c \cdot Ce \cdot (Ra_{it})^{0.25} \right]^z \right]^{\frac{1}{z}} & \text{if } Ra_{it} > 10^5
\end{cases} \\
\begin{cases}
0 \cdot \dfrac{m}{sec} & \text{if } To_{it} \ge 0.5 \cdot (T0_{it} + Tb_{it}) \\
\text{otherwise}
\end{cases}
\end{cases}
$$

$$\begin{pmatrix} Tm_{it+1} \\ T0_{it+1} \\ T11_{it+1} \\ T12_{it+1} \\ T13_{it+1} \\ T14_{it+1} \\ T2_{it+1} \\ Tr_{it+1} \\ T3_{it+1} \\ T4_{it+1} \\ T5_{it+1} \end{pmatrix}$$

$$Va \leftarrow 0.1 \cdot \frac{m}{sec}$$

$$Re \leftarrow \frac{\rho a \cdot Va \cdot La}{\mu}$$

$$D_{it} \leftarrow \frac{W \cdot La \cdot Va \cdot ca \cdot \rho a}{W \cdot h_{it}}$$

$$Tfm_{it} \leftarrow \frac{1}{11} \cdot \left[\sum_i \left[\left(\frac{Tb_{it} + T0_{it}}{2} \right) + \left(To_{it} - \frac{Tb_{it} + T0_{it}}{2} \right) \cdot \exp\left(\frac{-X_i \cdot 2}{D_{it}} \right) \right] \right]$$

$$f \leftarrow if\left[Re \le 2500, \frac{64}{Re}, 0.11 \cdot \left(\frac{e}{La} + \frac{68}{Re} \right)^{0.25} \right]$$

$$Vin_{it} \leftarrow \sqrt{\frac{2 \cdot g \cdot \left[\rho a \cdot \frac{(Tfm_{it} - To_{it})}{Tfm_{it} + 273 \cdot degC} \right] \cdot H}{\rho a \cdot \left(Ci + Co + f \cdot \frac{H}{La} \right)}}$$

while $\left| Vin_{it} - Va \right| > 0.1 \cdot \frac{m}{sec}$

$$Va \leftarrow Va + 0.1 \cdot \frac{m}{sec}$$

$$Re \leftarrow \frac{\rho a \cdot Va \cdot La}{\mu}$$

$$D_{it} \leftarrow \frac{W \cdot La \cdot Va \cdot ca \cdot \rho a}{W \cdot h_{it}}$$

$$Tfm_{it} \leftarrow \frac{1}{11} \cdot \left[\sum_i \left[\left(\frac{Tb_{it} + T0_{it}}{2} \right) + \left(To_{it} - \frac{Tb_{it} + T0_{it}}{2} \right) \cdot \exp\left(\frac{-X_i \cdot 2}{D_{it}} \right) \right] \right]$$

$$f \leftarrow if\left[Re \le 2500, \frac{64}{Re}, 0.11 \cdot \left(\frac{e}{La} + \frac{68}{Re} \right)^{0.25} \right]$$

$$Vin_{it} \leftarrow \sqrt{\frac{2 \cdot g \cdot \left[\rho a \cdot \frac{(Tfm_{it} - To_{it})}{Tfm_{it} + 273 \cdot degC} \right] \cdot H}{\rho a \cdot \left(Ci + Co + f \cdot \frac{H}{La} \right)}}$$

Vin_{it}

$$W \cdot La \cdot Vcir_{it} \cdot \rho a \cdot ca \cdot \left[To_{it} - \frac{(Tb_{it} + T0_{it})}{2} \right] \cdot \left[\exp\left[\frac{-H \cdot 2}{\left(\frac{W \cdot La \cdot Vcir_{it} \cdot ca \cdot \rho a}{W \cdot h_{it}} + 0.00001 \cdot m \right)} \right] - 1 \right]$$

$$4 \cdot \sigma \cdot \left[273 + 0.5 \cdot (T0_{it} + Tb_{it}) \right]^3 \cdot Atro$$

$$4 \cdot \sigma \cdot \left[273 + 0.5 \cdot (Tg_{it} + Tb_{it}) \right]^3 \cdot Atro$$

$$\frac{h2_{it}\cdot Atro\cdot Tn_{it} + Uo\cdot To_{it} + Urc_{it}\cdot Tb_{it}}{h2_{it}\cdot Atro + Uo + Urc_{it}}$$

$$\frac{h2_{it}\cdot Atro\cdot (Tg_{it} + Tb_{it}) - Qu2_{it}}{2\cdot h2_{it}\cdot Atro}$$

$$\frac{0.6\cdot S(it)\cdot Atro + h2_{it}\cdot Atro\cdot Tn_{it} + Urc_{it}\cdot Tg_{it} + h_{it}\cdot Atro\cdot Tm_{it} + Ur_{it}\cdot T0_{it}}{h2_{it}\cdot Atro + Urc_{it} + h_{it}\cdot Atro + Ur_{it}}$$

$$\frac{h_{it}\cdot Atro\cdot (Tb_{it} + T0_{it}) - Qu_{it}}{2\cdot h_{it}\cdot Atro}$$

$$\frac{U11\cdot T11_{it} + h_{it}\cdot Atro\cdot Tm_{it} + Ur_{it}\cdot Tb_{it}}{U11 + h_{it}\cdot Atro + Urc_{it}}$$

$$\frac{Dt}{Cm1}\cdot\left[U12\cdot (T12_{it} - T11_{it}) + U11\cdot (T0_{it} - T11_{it})\right] + T11_{it}$$

$$\frac{Dt}{Cm1}\cdot\left[U13\cdot (T13_{it} - T12_{it}) + U12\cdot (T11_{it} - T12_{it})\right] + T12_{it}$$

$$\frac{Dt}{Cm1}\cdot\left[U14\cdot (T14_{it} - T13_{it}) + U13\cdot (T12_{it} - T13_{it})\right] + T13_{it}$$

$$\frac{Dt}{Cm1}\cdot\left[U15\cdot (T2_{it} - T14_{it}) + U14\cdot (T13_{it} - T14_{it})\right] + T14_{it}$$

$$\frac{Utro\cdot Tr_{it} + U15\cdot T14_{it}}{Utro + U15}$$

$$\frac{Dt}{Cair}\cdot\left[Ui\cdot (T3_{it} - Tr_{it}) + Ucon\cdot (Te - Tr_{it}) + Ut\cdot (To_{it} - Tr_{it}) + Utro\cdot (T2_{it} - Tr_{it})\right] + Tr_{it}$$

$$\frac{S(it)\cdot Awin + Ui\cdot Tr_{it} + U3\cdot T4_{it}}{Ui + U3}$$

$$\frac{Dt}{Cm2}\cdot\left[U3\cdot (T3_{it} - T4_{it}) + U4\cdot (T5_{it} - T4_{it})\right] + T4_{it}$$

$$\frac{Dt}{Cm2}\cdot\left[U4\cdot (T4_{it} - T5_{it}) + U5\cdot (Te - T5_{it})\right] + T5_{it}$$